UNIVERSITY OF LIVERPOOL

Study on the properties of plasma activated water for bio-decontamination: generation, characterisation, and scale-up

Thesis submitted in accordance with the requirements of the University of

Liverpool for the degree of Doctor in Philosophy

by

Stéphane Florent Joël Simon

April 2023

Abstract

Plasma activated water (PAW) is part of the new non-thermal technologies, and is under active investigation for its bactericidal properties and application in the food and medical sector. PAW is commonly formed through plasma exposure of water samples; in such treatment, the chemistry of the water exposed is modified and enhanced in reactive species formed within the plasma and transferred to the samples. In this work, various plasma reactors were developed to generate PAW which was characterised and tested for its efficiency in biological applications; those tests aim to define a standard method able to produce up to 1 L.min^{-1} of PAW with concentration of species compatible for bio-decontamination. The study consisted of three topics: (i) a comparison between direct and indirect formation of PAW for bacterial inactivation, (ii) a study on the initial chemical influence of regional water and their impact on the generation of PAW, and (iii) a proof of concept to generate high volumes of PAW through cavitation.

Plasma-liquid interaction has been widely studied by the community with a plethora of reactors designed for this purpose. However, the chemical properties of the PAW can drastically differ from a configuration to another. The first part of this work aims to explore the generation of PAW by either direct or indirect plasma treatment. In the first case, the water sample is used as a ground electrode and plasma

streamers are formed between the tip of the excited electrode and the water sample surface. Whereas in the second case, the plasma formed is confined at the surface of the excited electrode without interaction with the water sample. For the purpose of the work, similar power and treatment time were kept constant; the results showed that both PAW formed by direct or indirect contact had great potential for bio-decontamination. When looking at their chemistry, the PAW obtained by direct treatment had higher concentration of hydrogen peroxide which is known to be a strong oxidiser commonly employed in healthcare settings. However, its efficiency was found to be less significant compared the PAW obtained by indirect treatment. Additionally, the PAW obtained through indirect treatment contained higher concentration of NO_2^- and NO_3^- which combined with a low pH could lead to the formation of HNO_2. This suggested that the PAW with higher concentration of nitrous acid could potentially lead to better bacterial inactivation, giving preference for the indirect discharge configuration.

These results were also confirmed by the second part of the research, where five tap water were selected (France, Norway, Palestine, Slovenia, and United Kingdom) and plasma treated. All water samples had an initial pH in the range of 7.9 to 8.2, following plasma activation samples from the UK and Norway reached a pH below 3, whereas water from France and Palestine remained stable at 8. It was found these water contained higher concentration of bicarbonate encountering the acidification due by the plasma treatment. The concentration of NO_3^- increased in all samples, reaching a maximum concentration of 3 mM after a plasma exposure of 25 minutes; whereas the concentration of NO_2^- showed a non-linear dependence with exposure

time, reaching between 10 and 25 µM after 25 minutes exposure. To demonstrate the impact of water origin on the antimicrobial potential of each solution, the inactivation of *Staphylococcus aureus* and *Escherichia coli* was considered. It was found that activated water from the UK was capable of achieving > 6 log reduction, whereas water from Palestine was only able to achieve a 0.4 log reduction despite both liquids receiving an identical plasma exposure. The study demonstrate the importance of initial water composition on the level of plasma activation, indicating that additional purification steps prior to activation may be necessary to ensure efficacy and repeatability.

Nevertheless, industrialisation of this technology is highly dependent on the possibility to produce high volumes of PAW. In plasma-liquid interaction, one of the main challenge is to increase the mass transfer during the process; it is commonly accepted that increasing the surface-to-volume ratio could effectively enhance the reactive species into the liquid. In the lasts section of this work, conducted as a proof of concept, a plasma reactor designed on venturi tubes was developed. Venturi tubes are often use to generate cavitation, allowing the formation of microbubbles. The reactor was design with a plasma device placed on its aperture, the species formed were then mixed where the cavitation occur allowing a fast dissolution of the species into water. It was found that the reactor was capable to produce 1 L of PAW in 10 min with concentrations of species in appropriate range for bio-decontamination. Therefore, the research presented here provide significant result in terms of PAW chemistry, with possible future development and integration into industrial settings.

Acknowledgements

Declaration

I hereby declare that this thesis is my own work and no further sources of information have been used other than the references cites. Experiments and data presented in this work were carried out and collected at the center of plasma microbiology, at the University of Liverpool. Biological assessment and data interpretation were conducted by Dr Breno Salgado, where the computational modeling was conducted by Dr Mohammad I. Hasan. Both worked at the Department of Electrical Engineering & Electronics at the University of Liverpool.

S F J Simon

April 2023

List of Publications

Results produced during this thesis resulted in one publication as first author and two publications as second author, another paper was under review when the thesis was submitted. The work was also presented in a conference in Slovenia and in from of the different partners involved in the iNOBOX project.

Peer-reviewed Journal Publications

- Efficient endoscope inner channel surface disinfection using a two-step atmospheric pressure plasma treatment - N. Northage, **S. Simon**, V. Shvalya, M. Modic, T. Juergens, S. Eschborn, M. J. Horsburgh, J. L. Walsh - Applied Surface Science, March 2023. https://doi.org/10.1016/j.apsusc.2023.156936

- Influence of Potable Water Origin on the Physicochemical and Antimicrobial Properties of Plasma Activated Water - **S. Simon**, B. Salgado, M. I. Hasan, M. Sivertsvik, E. Noriega Fernandez, J. L. Walsh - Plasma Chemistry and Plasma Processing, December 2021. https://doi.org/10.1007/s11090-021-10221-3

- The Influence of Gas-Liquid Interfacial Transport Theory on Numerical Mod-

elling of Plasma Activation of Water – J. A. Silsby, **S. Simon**, J. L. Walsh, M. I. Hasan – Plasma Chemistry and Plasma Processing. 41, 1363-1380, May 2021. https://doi.org/10.1007/s11090-021-10182-7

Publication under review

- Nebulized plasma activated water for effective viral disinfection of common healthcare surfaces - B. A. Salgado, **S. Simon**, A. Dickenson, M. Modic, A. Heather, J. L. Walsh - Environmental Science & Technology - Submitted in August 2022.

Conferences and project workshops

- iNOBox Project Workshop, 26th November 2021 (online).

- CA19110 " Plasma applications for smart and sustainable agriculture", 17th - 19th March 2021, Jahorina, Bosnia Herzegovina (online)

- iNOBox Project Workshop, October 21st 2020 (online).

- Plasma Activated Tap Water: Impact of the water hardness on liquid chemistry – GES3 2020, 3rd – 6th February 2020, Ljubljana, Slovenia.

- Agritech Catalyst Round 8 Briefing – Innovate UK, 22nd March 2019, Birmingham, United-Kingdom.

- iNOBox Project Workshop, 12th - 13th March 2019, Nofima, As, Norway.

Abbreviations

AC	-	Alternating current
APPJ	-	Atmospheric pressure plasma jet
CFU	-	Colony forming units
DC	-	Direct current
DBD	-	Dielectric barrier discharge
ESR	-	Electron spin resonance
EMR	-	Electron magnetic resonance
FTIR	-	Fourier transform infrared
HAI	-	Healthcare associated infection
HV	-	High voltage
IC	-	Ion chromatography
IR	-	Infrared radiation
MDR	-	Multi-drug resistant
NTP	-	Non-thermal plasma
OES	-	Optical emission spectroscopy
PAW	-	Plasma activated water
RNS	-	Reactive nitrogen species
ROS	-	Reactive oxygen species
RONS	-	Reactive oxygen and nitrogen species
SBD	-	Surface barrier discharge
UV	-	Ultraviolet radiation

Contents

CONTENTS

List of Tables

List of Figures

Chapter 1

Introduction

The present chapter aims to provide a brief introduction on general plasma physics concepts with an emphasis on cold plasma at atmospheric pressure (section 1.1). The chapter continues by a description on the aims of the work in section 1.2 and, the outline of the thesis are presented in section 1.3 of the same chapter.

1.1 Cold plasma at atmospheric pressure

"Physics" is by definition the science "describing the world surrounding us under all its forms". It became a synonym of technological and social progress over centuries, with the discovery of electricity and electronics for example. Plasma physics is another discipline of Physics which remain less well-known by the public even though its potential and importance is as strong as the two previous examples. Irving Langmuir (1881-1957) was the first one to introduce the word *plasma* in 1927 to described an ionised gas formed in a low pressure discharge tube at his work in General Electric Co. [1]. However, the generation of luminous discharges between two copper electrode was already reported by two French physicists, Hippolyte Fizeau and Leon

Foucault in 1844 [2]. Since then, the discipline never stopped to evolve and complexify, splitting into different research axes and application fields. In laboratories, cold plasma are generally formed using devices powered by electricity and under various pressure conditions. Those devices can use various electrical input (AC, DC, pulse) at frequencies going from hundreds Hertz to several kilo Hertz. Thus, extending strongly the chemical composition and properties of the plasma formed from one setup to another. Cold plasma technologies have been widely used in several applications such as the modification of surfaces at low pressure, as thruster for space propulsion, plasma cutting and treatment of gas. More recently, the technology gathered an increasing interest for its potential in medical and biological applications due to its highly reactive chemistry notably in cancer treatment. Finally, the plasma exposure of various liquids (such as biological solutions and water) in order to form "plasma activated liquids" is also under active investigation; with plasma activated water being the most studied for its capabilities in decontamination of medical devices to the decontamination of food products.

Plasma physics is a complex topic combining different physics subjects such as quantum physics, electromagnetism, fluid dynamics, particle physics and statistical physics [3]. Plasma is commonly described as an ionised gas but *electrically neutral* and where the the *charged particles* present a *collective behaviour*. In common literature, plasma is also referred as the *fourth state* of the matter in contrast to the three dominant states found on Earth: solid, liquid and gaseous. Thus, plasma is an ionised gas principally constituted of electrons, ions, neutrals (atomes, molecules), radicals, but also photons. In term of increasing entropy, the relation between the

different "states of matter" can be illustrated by:

$$\text{Solid} \xrightarrow{E} \text{Liquid} \xrightarrow{E} \text{Gas} \xrightarrow{E} \text{Plasma}$$
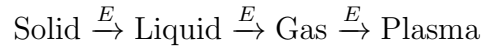
Where E, represent the energy required to change the state of the matter. Similar analogy can be done with the case of water, when heating up a block of ice to turn it into liquid and by continuing the heating to turn it into water vapour. In space, plasma represent 99 % of the universe under the form of stars and nebulae, on Earth plasma are generally under the form of lightning, flames and aurora borealis. Following the recent progress in the field, plasmas are now commonly present in homes and can be found in various devices such as plasma screen, lights and decorative objects.

Due to the different conditions to obtain a plasma, the community developed various criterion to categorize them. Figure 1.1 is an example of this representation.
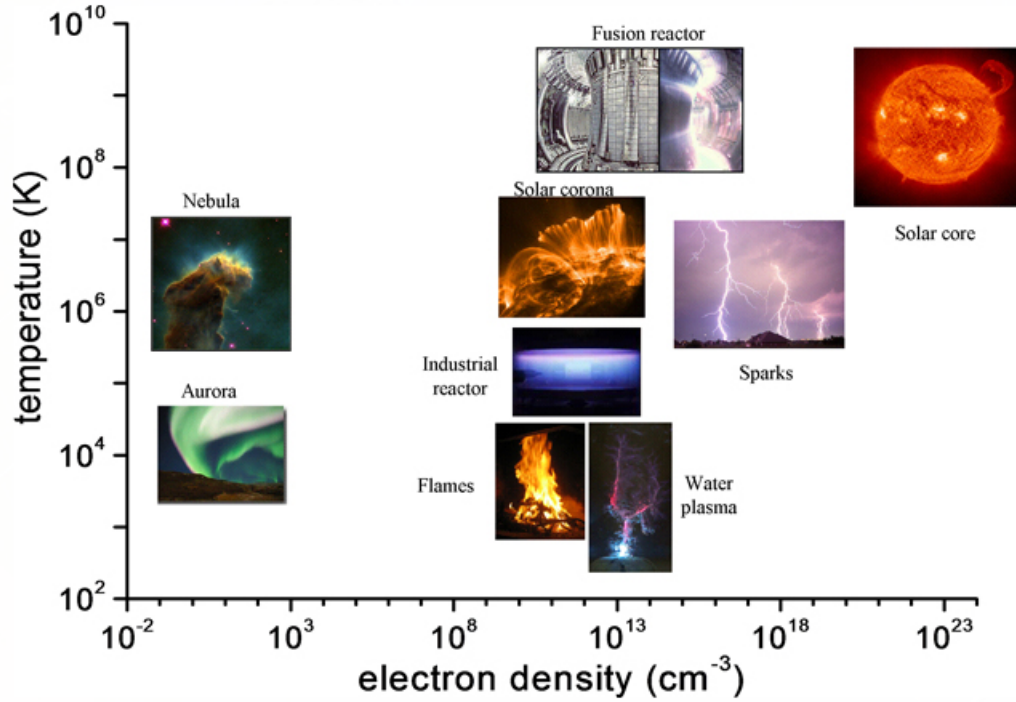
Figure 1.1: Classification of natural and laboratory plasmas in a logarithmic diagram charges density/temperature

The first criteria concerns the degree of ionization α (1.1) which compare the density of ions n_i to the density of electrons n_e and neutrals n_0 [4].

$$\alpha = \frac{n_i}{n_e + n_0} \tag{1.1}$$

In general, plasma properties are mainly governed by the charged particles. However, the neutrals play an important role in the discharge through ionization and diffusion processes. The degree of ionization can be found at different values from 10^{-8} for really weakly plasma such as nebulae and interstellar plasma to 1 for completely ionised plasma in stellar core or plasma formed in nuclear fusion. Secondly, the

plasma temperature can also be used as another criterion to categorize them. However, this parameter can be complex as both single and various temperatures can be found for all the species present in the plasma. From a thermodynamic point of view, the energy can be associated to a temperature following $E \approx K_B T$ where K_B is the Boltzmann constant, E the energy density and T the associated temperature. Thus, the categorization will be divided into two categories: plasma at thermodynamic equilibrium where the particles present an identical temperature $T = T_e = T_i = T_n$ (with T_e, T_i and T_n respectively the temperatures of the electrons, ions and neutrals); and plasma in non-thermodynamic equilibrium, in this case the electric field provided allows a thermal distribution where the electronic temperature is strongly higher than the ionic and neutral temperatures. Cold plasma are part of this second category and are generally weakly ionised, this property increases their versatility for biological applications as their apparent temperature is close to room temperature. Thirdly, the pressure is another criteria used to compare plasma types. However, instead of being a property of the plasma, the pressure will be a parameter conditioning the type of plasma obtained. At low pressure, collisions happening within the plasma are low resulting in a low transfer of momentum between electrons and heavy species. Thus, the plasma is in a non-equilibrium state with an electron temperature higher than the temperature of ions and neutrals. By increasing the pressure, the mean free path between the particles within the plasma decreases inducing an increase of the collisions. Differences between T_e, T_i and T_n are reduced leading the plasma to a closer state of thermal equilibrium. In biological applications, plasma at thermodynamic equilibrium is not recommended as it will lead to high temperatures which

are non suitable with biological medium and treatments of liquids. The use of low pressure plasma devices could find beneficial interests for decontamination of medical devices but not in the case of chemical modification of water [5], [6]. Furthermore, the complexity and cost of those system make them non-competitive to conventional technologies. That's why most of the reactors developed for the activation of water are designed to work at atmospheric pressure and room temperature.

1.2 Scope of the thesis

1.2.1 Comparison between direct and indirect formation of PAW for bacterial inactivation

A plethora of reactors, using both direct and indirect treatment of water samples, are currently used to generate PAW in laboratories. The description of the plasma-liquid interaction remains difficult and still under active investigation. The aim of this work is to compare both direct and indirect formation of PAW by investigating the transfer of chemical species from the gaseous to the liquid phase. This investigation will result in a better understanding of the PAW properties for bacterial inactivation. For this, two plasma reactors reproducing both interactions were developed and tested. Optical emission spectroscopy (OES) and Fourier-transform infrared spectroscopy (FTIR) were chosen as diagnostics of the gas phase where the liquid phase was diagnosed using the protocol developed in chapter 3, section 3.3. It should be emphasised that the research focus in understanding the pathways of the PAW formation and its potential for decontamination rather than describing the

physicochemical properties of the plasma-liquid interaction.

1.2.2 Study on the uniformity of PAW: influence of the initial water chemistry

In most studies, purified or distilled samples of water are commonly used to form PAW. The project was developed with the ability of PAW to be incorporated into an industrial prototype suitable for the decontamination of fresh food products. In this scenario, PAW generated from tap water appears to be the favourite candidate. The research aims to investigate the plasma activation of various tap water samples collected from different regions of the world, and possibly underline a uniformity of the plasma treatment over those samples. Thus, five waters were plasma exposed, analysed and compared for the inactivation of two bacteria stains (Gram-positive and -negative). The activation was performed using an SBD; the discharge was modeled and compared to ozone measurement performed during the treatment. The chemistry of the PAW was quantified using the protocols developed in chapter 3, section 3.3.

1.2.3 Generation of large volumes of PAW: scale-up using venturi

In most studies, generation of PAW remains restricted to small volumes usually under 100 mL. Limitations are mostly dependent on the size of the plasma reactor, as well as the difficulty to reach high concentration of chemical species for a short treatment

time. In this section, the aim was to develop an reactor based on a venturi design connected to a plasma reactor. The cavitation formed will enhance the transfer of the chemical species from the plasma phase to the liquid phase. Various design were developed based on fluid dynamic principles and tested to at different pressure and flow rate to reach the observe the cavitation phenomenon. The bubbles formed were tracked using a high speed camera and measured by computer; the chemistry of the PAW was quantified using the protocols in chapter 3, section 3.3. The research topic investigated the use of several venturi as well as different plasma reactors to optimise the production of PAW.

1.3 Outline

The outline of the thesis is as following:

- **Chapter 2** reports a review of the relevant background literature for the research topic. Focusing on the actual context of the study with actual concerns in healthcare environment and food products. The review continues by describing the generation and mechanisms leading to the formation of PAW, and the diagnostic tools to characterise both gaseous and liquid phase. Finally, the review reports common applications of PAW for bio-decontamination.

- **Chapter 3** reports the different plasma reactors designed for this work, and the different techniques employed for the diagnostic of both gas and liquid phase. The chapter reports as well the chemical protocol developed for this work and used to analyse the PAW. Details on the procedure to follow, chemical

interactions and calculus of the uncertainties are also explained. The chapter will also details the main conditions of operation of the plasma devices.

- **Chapter 4** reports the results obtained from the comparison between direct and indirect treatment of water samples. Their efficiency for bacterial inactivation is also presented.

- **Chapter 5** reports the results and discussions obtained from the plasma exposure of different regional tap waters. This chapter extend the work done in chapter 4 by investigating the influence of the initial chemistry of the tap waters and their impact on the PAW formed.

- **Chapter 6** reports the results and discussions obtained in up-scaling the production of PAW using a venturi. Several configuration were done with various outcomes to generate high-volumes of PAW with suitable chemistry for bacterial inactivation.

- **Chapter 7** concludes the work achieved in this thesis by providing a summary of the research topics, conclusions and future outlook.

Chapter 2

Literature review

The chapter goal is to provide a context of the research topic and to motivate the research objectives presented in chapter 1. The literature review starts with an actual context of the research topic, followed by three sections: generation and properties of the PAW; diagnostics of both gaseous and liquid phase; and, applications of PAW and comparison to other non-thermal technologies.

2.1 Context of the study

2.1.1 Contamination in healthcare environment and food products

Contamination of medical devices and food products remains one of the main concerns of public health worldwide. Following the recent pandemic situation of the COVID19 and the global warming crisis combined with the emergence of new multidrug resistant microorganisms; new techniques and technologies are more than required to ensure a good level of sanitisation and disinfection. In Europe, over

4 million people get a healthcare-associated infection (HAI) every year and around 37000 die as a direct result of the infection [7],[8]. HAI are defined as infections developed following a medical intervention or contact in a healthcare setting. The death toll from HAI is comparable to the number of people who die each year in road traffic accidents. In the United Kingdom, HAI are estimated to cost the NHS about £2.1 billion per year and healthcare organisations have a legal responsibility to reduce their impact [9]. They are influenced by a complex combination of factors including mainly gaps in policies and/ or infrastructure, knowledge, defects by health-care workers' behaviour and patient antecedents. In standard conditions, classic sterilisation and decontamination protocols of medical devices can easily prevent them and ensure a good conduct of the health care services [10]. In a medical environment, every equipment is divided into three categories depending on its interaction with human tissues (i.e., skin, mucous, etc) as described in Table 2.1.

Categories	Description	Disinfection strategy
Non-critical devices	Items in contact with intact or normal skin (i.e., stethoscope)	Cleaning and/or low-level of disinfection
Semi-critical devices	Items in contact with mucous membrane or non-intact skin (i.e., flexible endoscope)	Cleaning and high-level of disinfection
Critical devices	Items that penetrate skin or mucous membrane and enter normally sterile tissue (i.e., needles, vascular catheters)	Must be sterile at all times

Table 2.1: Spaulding classification and disinfection strategy [11]

These categories are not restrictive, and a medical device declared as non-critical can become contaminated during patient care and must be correctly classified after use

[12]. The equipment is then cleaned and sterilised following the appropriate strategies ensuring elimination of any viable microbiota. The classification was originally developed by Spaulding and based on microbial resistance to various disinfection processes. However, microbes evolved to resist human approaches to their elimination forcing an actualisation of the processes by governmental policies. One significant concern is the lack of guidance concerning multi-drug resistance (MDR) bacteria and the possible formation of MDR biofilms [13]. MDR is major threat of both patient safety and public health; MDR develops through evolution of microbiota exposed to sub-lethal levels of antibiotics without proper elimination of the whole population [14], [15]. Devices with flexible element or mechanics which interact with microbiome of the gastrointestinal (GI) system, bronchioles or urogenital system carry a high-risk infecting patient when disinfection procedure are not correctly followed [10], [16]. For example, GI endoscope or duodenoscope may promote the growth of MDR pathogens due to the complexity of their structures and the difficulties encountered for proper sterilisation. In Germany, a double-blind study of 14 different hospitals reported that 57 % of the working staff hasn't completed the basic sterilisation qualification, 50 % of the sterilisers and 57 % of the washer disinfectors were either obsolete or not suitable to perform a validated process [17]. Various improvements were done in this area over the last decade; nonetheless, the safety and applicability to reprocess medical devices such as endoscope or duodenoscope remain heavily questioned especially when looking at new MDR outbreaks [18], [19].

The need for a better training of health care staff and a control of disinfection processes has never been as urgently required than now when looking at the recent

outbreak of the coronavirus disease (COVID-19). The COVID-19 turned into a global pandemic in March 2020 and remained a major concern when this work was produced. Aside the requirement for new sterilisation processes to counterbalance this new disease, there is an increase demand in medical and personal protective equipment (PPE). However, as supplies may take a long time to meet the demand, reuse of PPEs appeared as a first response to the COVID-19 [20]. In medical environment, classic disinfection processes include steam sterilisation, gamma or X-ray irradiation, ultraviolet light [21], [22]. Yet, the most common approach remains the use of chemicals such as hydrogen peroxide combined with peracetic acid or ethylene oxide which can be used with all instruments (metal and non-metal) [23], [24]. Recent studies demonstrated a good efficiency on adapting actual sterilisation processes to the pandemic situation notably with N95 respirators, though further studies are still required to ensure their viability [25]. Lastly, studies reported high numbers of bronchoscope contamination mainly due by deficient reprocessing [26]. Knowing the intricate complexity of the situation, possible transmission of COVID-19 or other pathogens due by bronchoscope apparatus must be considered and treated with appropriate disinfection strategies [27], [28]. Studies reported possible faecal-oral transmission of the COVID-19 from endoscopic apparatus; endoscopy department over the world were forced to adapt and set new procedures and techniques to avoid any cross-contamination between patients and healthcare workers [29], [30]. Those points in a time of pandemic situation, underline the urge to develop and standardise new disinfection procedures with appropriate training of medical staff and health care workers.

Comparable to reprocessing of medical equipment, food safety is also a public health priority where unsafe food poses global health threats. Especially for vulnerable people including infants, young children, pregnant women, elderly and those with medical conditions or illness. For example, every year 220 million children contract diarrhoeal diseases and 96000 die. [31] In the last century, policies and regulations have been taken to reduce the possible risks of food contamination which are detailed in three categories: physical contamination, chemical contamination and biological contamination as described in Table 2.2 [32],[33].

Contamination	Description
Physical	Foreign bodies interacting with food products (hair, pests, metal, plastics)
Chemical	Food in contact with natural or artificial chemical substances
Biological	Food products in contact with microorganisms (bacteria, viruses and parasites) transferred through saliva, pest dropping, blood or fecal matter

Table 2.2: Classification of contaminated food materials

Pesticides in environmental sources (air, water, soil) are part of the most common chemical contaminants [34], with the development of new techniques in food safety, cross-contamination have been reported due to the use of hazardous chemicals as well as unapproved food additives and adulterants [35]. However in term of statistics, bacterial contamination represents the most common cause of food poisoning worldwide [36]. Agricultural raw products correspond to the production of fruits and vegetables, their contamination will be mainly caused by fertilisers and/or pesticides. Studies reported residues of pesticides in fruits and vegetables as well as the

presence of derivatives, which can be harmful for the human health [37],[38], [39]. The European Food Safety Authority (EFSA) published in 2019 a report examining pesticides residue levels in foods on the European market. Over 96302 samples were analysed with 96.1 % of them falling below the maximum residue level (MRL), 3.9 % exceed this level of which 2.3 % were non-compliant [40]. Compared to a previous report, those results indicate that products following European guidance are unlikely to pose any concern for consumer health. However, part of the samples (25.3 %) came from third countries with 7.8 % found to have a higher MRL exceedance rate and a higher non-compliance level (5.6 %) compared to food produce within the EU. Pesticides residues can also be found in animal product such as milk, animal fat, eggs. On the same report, over 16090 samples were analysed, 91.2 % were free of quantifiable residues while 8.8 % contained one or several pesticides in quantifiable concentrations. Another contaminant is under intense investigation and concern directly raw animal product. Within the meat industry, contaminations are commonly due by residues of antibiotics used in excess and without control [41], [42]. Knowing the importance of the food market and the actual state of the globalisation, vigilance and international policies as well as new pesticides alternative are more than required to avoid controverse situations like the one concerning the use of glyphosate (withdraw from commercial use due to strong evidence of its toxicity and possible carcinogenicity) [43],[44].

Even if chemical contamination of food products represents a huge part of the governmental vigilance, most part of the contamination and their negative impact on human health result from biological contamination. The world population is cur-

rently around 7.8 billion, 7.69 % of people experience foodborne diseases and 7.5 % (56 million) as a consequence of those diseases [45]. Majority of the patients are affected by norovirus, Campylobacter and Listeria monocytogenes being the most fatal. In the United States, cases of foodborne diseases did not decrease between 1997 and 2017 (except for the case of Campylobacter) and the percentage of illness caused by animal product increased from 10.4 to 14.1 % over this period. In Europe, 23 million of people are affected every year with approximatively 5000 deaths. Foodborne disease affect countries unequally with more cases of Campylobacter and Salmonella in European countries compared to the rest of the regions. Australia reported higher case of Campylobacter followed by Salmonella. In Asia, Korea had more cases of Escherichia coli followed by norovirus where Japan reported similar number of cases of Campylobacter and Clostridium perfringens. The study described by Lee and Yoon, concluded that foodborne illness and outbreaks in the world are due by the presence of Campylobacter, Salmonella, L. monocytogenes and E. Coli in animal-source products [45]. Agricultural products are also subject to biological contamination, recent studies reported the case of rice contamination by fungi, bacteria, nematodes and viruses [46]. Countries in Africa and Asia which are high producer of rice appear to be the most susceptible to fungal and nematode contamination, due to the hot and humid climate of those regions. Furthermore, Bacillus cereusthat are commonly detected in cooked rice suggesting a default on the storage and hygienic conditions after cooking [47]. To conclude, chemical and/or bacterial contamination of food product remain a priority to avoid undesirable consequences on human health. Even more knowing that some disease linked with foodborne pathogen are

not, yet well understood and require further investigation as mentioned in the work of Trevisan et al., about foodborne parasites [48]. With the increase of the world population and the change in term of food consumption and habits, new measures and techniques are required to ensure a good quality of the food products and reduce the development of MDR microorganisms in the future.

2.1.2   Actual technological responses and their drawbacks

As described previously, medical devices and food safety are highly sensitive to external contamination resulting in severe affection to human health. Fortunately, international policies and regulations are now well-defined and regroup several available techniques combining physical treatments (i.e., high temperature/ high pressure processes, ultraviolet light) and chemical treatments (i.e., chemical oxidisers) to ensure an adequate disinfection. Nevertheless, developments in those areas are still required due either to the emergence of new diseases or the resistivity of some bacteria strain to disinfectant processes. Furthermore, some techniques used to treat contaminated food products or medical devices appear to have a negative impact on human health as well as degrading the quality of the products itself. For examples, decontamination of endoscope is done in washer disinfectors using chlorine dioxide as high-level disinfectant. Martin et al., investigated bacteria isolated from those washers and exposed them to peracetic acid, chlorine dioxide and hydrogen peroxide to study their resistance to these highly reactive oxidising biocides [49]. They compared their results with two standard suspensions (Bacillus subtilis and Micrococcus luteus) and noted that the techniques mentioned were not always effective to

provide a required disinfection efficacy within recommended exposure time. Ultra-violet radiation is also used as a rapid disinfection process for surfaces in medical environment [50], [51], the maximum bactericidal effect occurs at 240 – 280 nm with inactivation of bacteria and viruses. However, it remains inefficient against bacterial spores [52]. Even if several applications are used based on this technology, its germicidal properties are influenced by several parameters which reduce its effectiveness (i.e., organic matter, UV intensity, temperature, distance with target) [53]. Apart from the possible risks for bacterial resistance, studies reported alterations and degradations of medical devices after sterilisation processes. Residues from chemical decontamination agents have been found in manufactured devices where disinfectants may be absorbed by plastics and leach out when used, resulting in chemical burns or risk of sensitisation of the patient or user [54], [55]. Cleaning agents and chemical sterilant may cause corrosion and/or changes in the material of the device as well as mechanical stress during high temperature/pressure treatments reducing the shelf life of the equipment/ food and the generalisation of a process suitable for any applications.

Recent studies also reported negative impact on health after using strong oxidisers as disinfectant. Casey et al., investigated the possible health hazard reported after hospital staff members expressed health concerned following the implementation of a surface disinfectant product containing hydrogen peroxide, peracetic acid and acetic acid [56]. Their study revealed that the product was associated with mucous membrane and respiratory health effect increasing potential risks of mucous membrane irritation and asthma in healthcare workers. Within the emergence of the pandemic

Cleaning strategies	Drawbacks
Chemical oxidisers	Lack of efficiency and bacterial residues still present after reprocessing, presence of chemical residues which can affect human health (membrane irritation or asthma for example), deterioration of medical devices
UV sterilisation	Inefficient against bacterial spores, highly dependent on UV intensity, temperature, distance with target
Hand-sanitizers	Possible carcinogene, extensive use can increase bacterial resistance

Table 2.3: Summary on drawbacks of conventional cleaning strategies

situation due to the COVID-19 and the absence of therapies, health professionals recommended frequent washing of hands using soap or common chemical sanitisers such as alcohol or hypochlorite solutions [57]. Even if those compounds are affordable, have a low toxicity and easy to use, they remain a health hazard if frequently used in healthcare centres for example. Studies reported tendency of ethanol causing skin cancer by absorption and carcinogenicity [57], [58]. Common hand-sanitizers are associated to minimal systemic toxicity which could lead to potential risks for children becoming poisoned [59]. Furthermore, it has been reported that extensive use of alcohol-based hand sanitizers enhances bacterial resistance [59], [60].

As described earlier, both healthcare and food industry are highly sensitive to external contamination and possible residues generated during the cleaning processes. Even if those techniques are suitable for now and well-studied, some of the chemical compounds used have a severe impact on the environment with recent studies observing a link between new foodborne pathogens and climate change [61], [62]. In brief, effects of temperature, rainfall, wind, and dust events have been examined and demonstrated variable impacts depending on geographic locations on the transport

of pathogens into crops and livestock. These studies revealed that proper management of water sources, soils, wildlife intrusion, combined with an awarness of the effect of climate change on these elements, will be paramount to food safety over the coming century.

During the pandemic, the increased need of disinfectant caused direct discharge of high concentrations of chemicals into the wastewater system affecting the water resources [63]. The use of such strong oxidisers and disinfectant processes which are, for most of them, toxic for the environment have to be reconsidered. Considering the objectives defined by the policies signed in the last United Nations Climate Change Conferences, investigations for new eco-friendly technologies are urgently required in order to maintain high quality and safety disinfection standards combined with a better respect of the environment. In that way, non-thermal disinfection technologies appear to have great potential for efficient and effective microbial inactivation, without many of the drawbacks associated with conventional methods [64], [65].

2.2 Non-thermal technologies: Plasma Activated Water

A plethora of plasma systems have been developed by the community for the generation of PAW. In this section, the literature review is organised as follows: (1) description of the plasma-liquid interactions; (2) a basic introduction on DBD; (3) an overview of the chemistry generated by DBD in air at atmospheric pressure; and finally, (4) explanation of the mechanisms and pathways at the interface.

2.2.1 Plasma-liquid interactions

As explained previously, "cold plasma" and more precisely the processes performed at atmospheric pressure have been widely investigated for their potential in biological applications. A sub-topic of this field concerns the interactions of non-thermal plasma with liquids; the first report involving plasma-liquid interaction came from Cavendish's work, "experiments on air" in 1785, where he investigated the production of nitric oxide using an electric spark [66]. Over the last 30 years, this topic has been an active field of research with various configurations and designs tested leading to numerous applications notably in environmental remediation and health care. As a consequence, an extended number of chemical mechanisms and pathways exist increasing the complexity of the process and the resultant chemistry of the PAW obtained. From the literature, the plasma reactors used in those processes can be reported into three main categories:

- Direct discharges within the liquid phase,

- Discharge in the gas phase over a liquid,

- Discharge in a multiphase environment.

Figure 2.1 illustrates the different categories of plasma-liquid interaction listed previously.
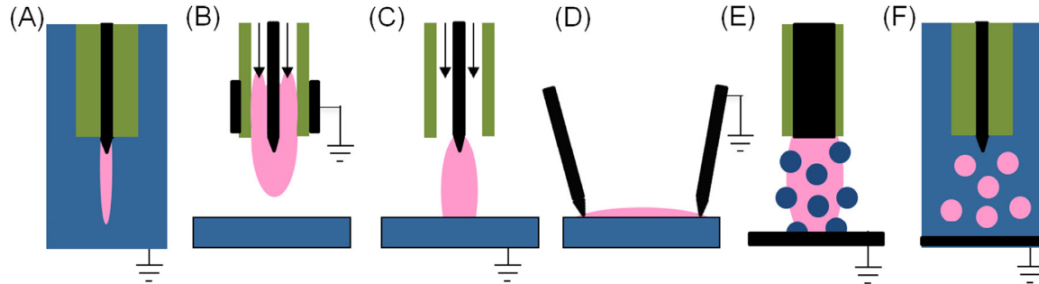
Figure 2.1: Schematic of different discharges used in plasma–liquid interactions: (A) direct discharge in liquid, (B)–(D) gas phase discharges and (E) and (F) multiphase discharges. [67]

The first category is quite straightforward and concerns the generation of plasma directly in the liquid phase. The second category can be divided into two sub-category where the liquid exposed can be either used as an electrode or not. In the last category, the plasma is generated in both gas and liquid phases to increase the surface contact of the interaction through bubbles or fine mist.

2.2.1.1 Direct discharge in liquids

Direct discharges in liquids are limited by the considerable amount of energy they require to achieved electrical breakdown. Figure 2.2 shows an example of two discharges in water.
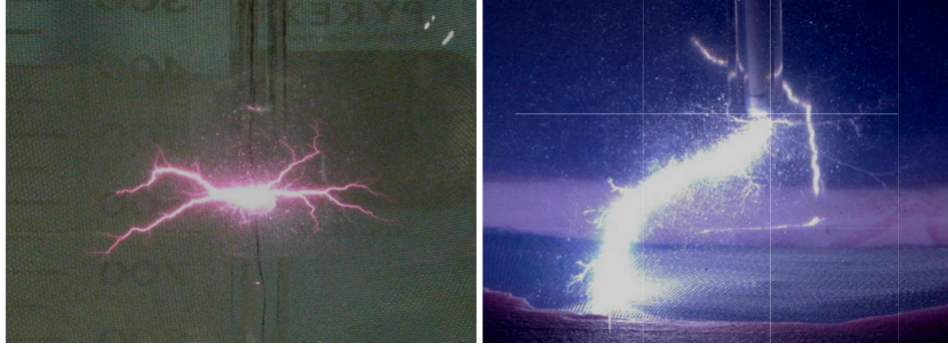
Figure 2.2: Image of plasma discharge in water: (a) pulsed corona, (b) pulsed arc [68]

Most atmospheric plasmas follow the Paschen curve which states the breakdown voltage required to start an electric discharge; however, due to the high density and the short mean free path of electron, breakdowns in liquids required an extremely high electric fields E/n_0. Nevertheless, this problem can be solved by using electric field slightly exceeding the ones employed in atmospheric pressure gases. The electric field produced will generate the formation of microvoids and quasi-"cracks" in the liquids allowing the discharge to happen [68]. The discharges are usually sustained using high voltage pulses forming streamers or corona discharges starting from a sharp electrode immersed into liquid. If the streamer does not reach the second electrode, the discharge is categorized as a pulsed corona. Where if the streamer reach the second electrode the plasma will be categorized as a pulsed arc. Numerous geometry have been developed to realise those discharge with the most common being point-to-plane and point-to-point geometry. In a point-to-plane geometry, the streamer formed usually does not reach the second electrode leading to the formation of a pulsed corona where the point-to-point will lead to the formation of

a pulsed arc. The mechanisms of breakdown for those discharges are reported into two categories:

- In the first scenario, the breakdown is initiate through a sequence of a bubble process followed by an electronic process. The bubble process starts from the generation of microbubbles formed by the vaporisation of liquid induced by the local heating of the intense electric field. The cavitation is not only dependent on the intensity of the electric field but also on the pressure with time to form the bubbles going from 3 to 15 ns [69]. Concerns could be raised about the conductivity of the liquid which may influence the formation of the bubbles, however this parameter has been reported to be minimum [69]. The evaporation process can be estimated using the velocity, size of the streamer as well as the heat of vaporization [70],[71]. When using a streamer radius of 31.6 µm, a power of 2.17 kW was estimated to be released into a single streamer allowing its propagation in the form of vapor channels [72]. If multiple streamers are observed, the power required can be estimated by multiplying their number with the power calculated for a single streamer. In the electronic process, two main observations were done depending on the electrode considered. At the cathode, electrons are injected and drifted into the liquid where hole injections through a resonance tunneling mechanisms occurs at the anode [73]. Breakdown occurs when an electron makes suitable ionizing collisions during its transit across the gap region.

- The second scenario divides the process into a partial discharge and a fully developed discharge (arc or spark) [74], [75], [76] . In the partial discharge, the

current is mostly transferred by ions, intrinsically the conductivity will play a key role for the breakdown to occur. For high-conductive liquids, a large current flows is observed resulting in a shortening of the streamer length due to the fast compensation of the space charge electric fields. Consequently, a high power density occurs in the channel leading to higher plasma temperature and UV radiation combined to the generation of acoustic waves (weak for the case of corona discharges). In the case of spark or arc discharges, the current is transferred by electrons. The heating produced by the high current between the two electrodes generate a quasi-thermal plasma and most of the energy is consumed to form the thermal plasma channel. The channel emits strong UV radiation combined with the generation of intense shock waves within the surrounding liquid [77].

As demonstrated previously, most of the discharges achieved in liquids are generated using intense electric fields produced through pulsed power supplies. However, some groups reported the formation of microplasma in liquids through sonoluminescent bubble implosion [78],[79]; De Giacomo et al., also reported the generation of plasma through ns-pulse lasers [80]. The plasma generated by these configurations has a small area and is restricted to the geometry of the bubble with temperatures over several thousands of Kelvin.

2.2.1.2 Discharge in the gas phase over a liquid

Here, the plasma reactivity is formed in the gas phase surrounding the liquid surface. Figure 2.3 shows a discharge performed in air over a liquid done at the University of
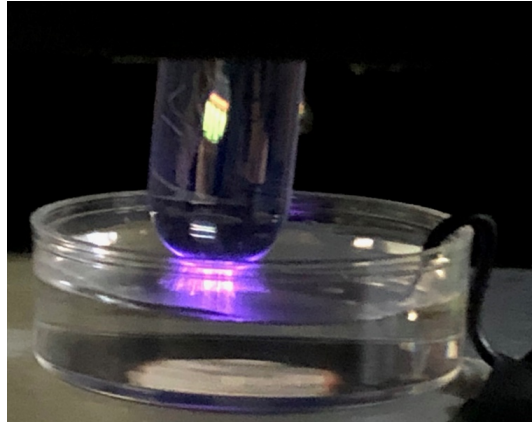
Liverpool.

Figure 2.3: Example of plasma discharge in air over a liquid achieved at the University of Liverpool

Depending on the configuration employed and if the liquid exposed is part of the system as an electrode, the final chemistry of the solution will differ strongly. Two main configurations are reported:

- The liquid exposed acts as an electrode and complete the plasma system allowing the electrical conduction. Either corona, glow discharge or sparks can be observed between the metallic pin to the water surface (depending on the applied voltage and gap distance), this geometry is usually referred as a "pin-to-water" configuration [81], [82]. When the pin is covered with a dielectric material, the discharge produces streamers emitted from the dielectric and reaching the surface of the liquid [83].

- Consequently, the second category concerns liquids which are not grounded and set as floating potential. Generally, groups used atmospheric pressure plasma jets (APPJs) fed with air or various gas mixture to form plasma activated

water. The device can be either placed above the water surface forming a gap between the plume and the water bulk [84] or directly immersed in the liquid [85]. Knowing that plasma jet can be costly due to the use of noble gas (such as Helium), groups replaced them by surface barrier discharge (SBD) which acts as remote discharge diffusing the species generated within the gas phase to the liquid phase through diffusion/dissolution mechanisms [86], [87].

In the first category, the liquid exposed can be either set as the cathode or anode. For both, the liquid electrode stabilize the discharge preventing its contraction. The glow discharge formed is usually powered by a DC excitation in atmospheric pressure air ([88], [89]), operating conditions require a voltage around 1kV with current in a range of 5 to 50 mA and gaps of few mm. Due to the resistivity of such systems, a fraction of the discharge power is dissipated within the liquid leading to an evaporation of the last. The electron energy distribution is non-Maxwellian and the mean electron temperature can reach 1 eV in the positive column, the gas temperature can exceed 3000K with an electron density around 10^{-19}m^{-3} [90]. Used as an anode, self-organised pattern are commonly observed on the surface of the liquid electrode [91]. The type of discharge will depend on the input power; when using a low power a corona discharge is observed where the increase of power will lead to the formation of a spark in the gas phase. The large electric field generated at the cathode sheath leads to the formation of instabilities at the plasma-liquid interface which enhanced the transport of species from the gas to liquid phases [92]. In most corona discharge, generation of ionic wind has been reported inducing a deformation of the liquid interface [93], [94], however studies are still in progress to determine the possible outcomes

for the mass transfer of species between phases. Another interesting configuration concerns the use of metallic pin (respectively cathode and anode) in contact with the water surface and separated by a gap; this geometry produces streamer discharges on the surface of the liquid within the gap with propagation velocities from 1 to 10 $km.s^{-1}$. This type of surface discharges was reported for enhancing the rate transfer of the species from the gas phase to the liquid phase due to the generation of the streamers directly at the interface.

When exposing a liquid to an atmospheric pressure plasma jet (APPJ), the species generated within the jet are transported by the gas flow to the liquid surface. Convection processes were reported which might enhance the transfer and generation of reactive species [95]. A recent review on plasma-jet interacting with liquids can be found in [96], most of those system are AC or DC powered or using pulse power supplies at frequencies in range of kHz to MHz. Two main setups are reported with variation on the electric field observed; when the anode is part of the jet, the electric field appears perpendicular to the gas flow whereas it was observed to be parallel with the gas flow when the anode used is the liquid bulk. This variation induce strong variations on the final chemistry obtained for the liquid exposed; the species produced are mainly ionic and neutrals which dominates the chemical processes. Studies also reported the presence of photolysis mechanisms induced by the UV photons produced by the plasma and absorbed by the liquid phase. Those mechanisms have been widely studied and modeled by simulations as reported in [67],[97]. Finally, recent studies reported the use of surface barrier discharge where the plasma is formed remotely in the gas phase over a liquid bulk [98], [99]. The characteristics

of such interactions are close to the APPJs with a transfer of the chemical species following Henry's Law and photolysis mechanisms dependent on the gap separating gas and liquid phase.

2.2.1.3   Mixed phase discharge

As detailed previously, plasma-liquid interactions are highly dependent on several parameters such as the strength of the electric field, the type of discharge produced (corona, sparks or streamers) as well as the gap separating the gas and liquid phase. Numbers of studies investigated approaches to increase the surface-to-volume ratio between plasma and liquid to enhance the transfer of the plasma species into the liquid bulk. One of this approach is to reduce the water into a thin mist and inject it into a gas discharge also referred as an electrospay [100], [101]; electrostatic spray are widely studied and used in several applications (i.e., electrospinning, electrospray ionisation mass spectrometry). They can be used in continuous or pulsed mode depending on the gas flow rate, the liquid surface tension, conductivity and viscosity. Due to the size of the droplets (usually micrometers), the mass transfer of the species generated in the plasma is increased by the large surface-to-volume ratio. Most of those systems use sparks or arcs in noble gas or air. Another approach concerns the injection of gas into the liquid, the resulting bubbles are drifted into the surface near the interface which will see the formation of plasma. With sufficiently high voltage, a plasma can be performed in the bubbles before reaching the interface. Figure 2.4 shows an example of discharge in bubbles.

Figure 2.4: Example of a plasma discharge in bubbles [102]

The general properties of the plasma are close to the one performed at atmospheric pressure, but the resultant chemistry is enhanced due to the direct dissolution of the chemical species formed within the liquid phase [103], [104]. However, the size of the bubbles is a paramount parameter leading to strong variation of the liquid chemistry.

2.2.2   Dielectric barrier discharge

DBD are commonly employed for the generation of plasma in air at atmospheric pressure. In this type of systems, the use of a dielectric material in the discharge gap avoids the formation of sparks and current growth in the channels formed by

streamers. The first introduction of DBD was done by Siemens in 1857 to produce ozone [105], form this application several studies investigated this type of discharge with descriptions of its physical nature done by Buss in 1932 [106] and Klemenc et al. in 1937 [107]. They showed that the discharge occurs in a number of individual small breakdown channels referred as microdischarge. From a physical point of view, these microdischarges are actually self-organized streamers due to the accumulation of charges on the dielectric surface. Classic parameters of the microdischarge can be found in Table 2.4.

Lifetime	1-20 ns	Filament radius	50 / 100 µm
Peak current	0.1 A	Current density	0.1 / 1 kA cm^{-2}
Electron density	10^{14} / 10^{15} cm^{-3}	Electron energy	1-10 eV
Total transported charge	0.1-1 nC	Total dissipated energy	5 µJ
Gas temperature	$\approx 300K$	Overheating	5 K

Table 2.4: Parameters of a microdischarge [108]

The charge accumulation on the surface of the dielectric barrier reduces the electric field at the location of a microdischarge, furthermore their extinguishing voltage is close to their ignition voltage; resulting in a very short lifetime of few nanoseconds as reported in Table 2.1. Due to this short lifetime, the overheating of the streamers channel and the general temperature of the device remains low. Studies reported that the formation of new streamers were set at new locations due to the presence of residual charges on the dielectric surface. This result in a reduction of the electric field at the location where previous streamers were formed. For the same reason, when the voltage is reversed, microdischarge are formed at the exact same position. In AC-powered DBD, this memory phenomenon of the charge position is used

to spread microdischarge over the dielectric surface. This is observed in DBD at high voltage low frequency whereas the low voltage and high frequency DBD tend to reignite the old microdischarge channels every half-period [109],[110],[111]. Microdischarge properties for most frequencies are not dependent on the characteristics of the external circuit, but will be dependent on the pressure, composition and configuration of the electrode. An increase of power will result in the generation of a large number of microdischarge per unit time which ease their scale-up [108].

DBDs are categorised in two main classes: "volume discharge" [112] and "surface discharge" [113]. In volume discharge, the streamers are formed in the gap between two conductors (plates or cylinders) filled with gas, with one or both being covered by a dielectric. This type of configuration and discharge is commonly reported for the case of plasma jets. Figure 2.5 reports the main configuration found in literature for both volume and surface discharge.
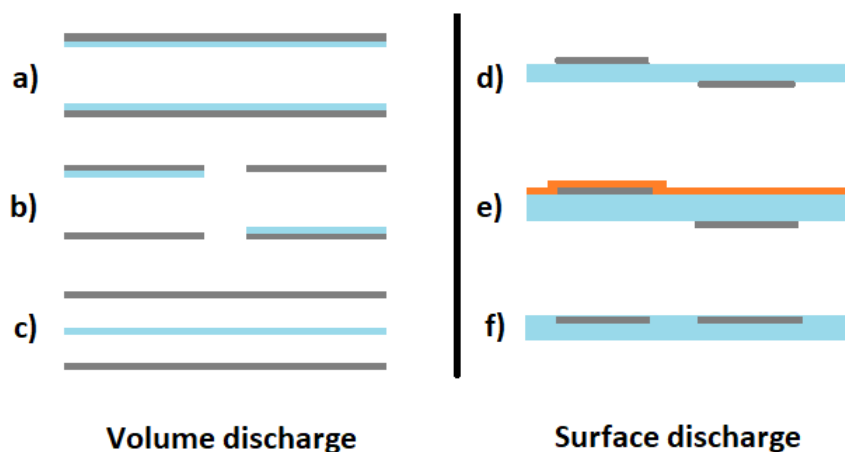
Figure 2.5: Common electrode configuration for DBD

Looking closer at the surface discharge, the classic arrangement consists of two electrodes separated by a dielectric. The main differences between them is not only the removal of the gap between the electrode but also the geometry of the electric field formed. The electric field appears to be perpendicular to the gas flow for volume discharge where its along on or above the electrode plates for surface discharge. This parameter plays a crucial role in the treatment of surfaces as volume discharge will lead to electrons crossing the substrate which could result in an increase of the local heating and deterioration of the substrate exposed. In the case of surface discharge, the gap separating the reactor and the medium exposed will play a paramount role in the final chemistry transferred to the medium [114].

2.2.3 Gas phase chemistry of DBD in air

When generating a plasma in air, complex chemical mechanisms occur leading to the formation of charged and excited species, dissociated molecules, and neutral species. The electrons generated by the breakdown induced by the electric field have been reported with a mean energy on the order of 1 to 3 eV. Knowing that air is mainly constituted of nitrogen and oxygen with some rare elements, this electron energy is sufficient for oxygen molecules to dissociate. Thus, leading mostly to the production of reactive oxygen species (such as ozone and excited oxygen molecules) as well as nitrogen species (under the form of nitrogen oxides for the most) [115], [116].

The mixture of the species formed varies spatially and temporally during the plasma process. Short lifespans species (under 10 µs) are confined to the visible domain of the plasma, where long-lived species will be able to diffuse and reach the water bulk. As reported in Table 2.5.

	Short lived species	Long lived species
Neutral species	$N(^2D), N_2(A^3\Sigma), N_2(B^3\Pi)$ $O(^1D), H, N, O$	$O_2(A^1\Delta), O_3, NO, N_2O, NO_2$ $NO_3, N_2O_3, N_2O_4, N_2O_5$ $H_2, HO, HO_2, H_2O_2, HNO$ $HNO_2, HNO_3, N_2, O_2, H_2O$
Positively charged species	$N^+, N_2^+, N_3^+, N_4^+, O^+$ $O_2^+, O_4^+, NO^+, N_2O^+, NO_2^+$	
Negatively charged species	e-, $O^-, O_2^-, O_3^-, O_4^-, NO^-$ $N_2O^-, NO_2^-, NO_3^-, H^-, HO^-$	

Table 2.5: Short- and long-lived species formed in a DBD in air [115]

The long-lived species will interact at the interface separating gaseous and liquid

phase and recombined in the first layers of the water bulk. Resulting in a specific chemistry with bactericidal properties for the PAW formed.

SBD in air and in confined environment have another property characteristic of this discharge known as "ozone poisoning". This type of reactor is known for the ease of production of ozone; however, while increasing the power, the ozone generation rise up to a maximum followed by a sudden decrease and disappearance. The mechanisms under this phenomenon remains unclear; however, hypothesis stated that the transition may occur by the reaction between vibrationally excited nitrogen molecules and singlet oxygen enhancing the formation of nitric oxide. Nitric oxide is known for being a major quencher of ozone by producing by-products such as NO_2 which further reacts with ozone to form NO_3 [117]. Furthermore, Pekàrek et al., reported that the increase of temperature in such devices could also accelerate ozone quenching, favouring the production of RNS species [118]. This hypothesis can be validate by the considerable increase of nitrogen species referred as a transition from an ROS mode to a RNS mode. Chapter 4 and 5, will investigate further this transition and see its impact on the PAW generated through those regimes.

2.2.4 Mass transfer at the interface: from the gas phase to the liquid phase

The plasma-liquid interaction results in a consequent number of interactions occurring in the first layers of the liquid, and affecting the final chemistry of the treated samples. The different mechanisms are complex to explain and remain under active

investigation; however, thanks to numerical models, its description begins to be more accessible. Figure 2.6 reports the main mechanisms observed in numerical models and experiments [67], [119].
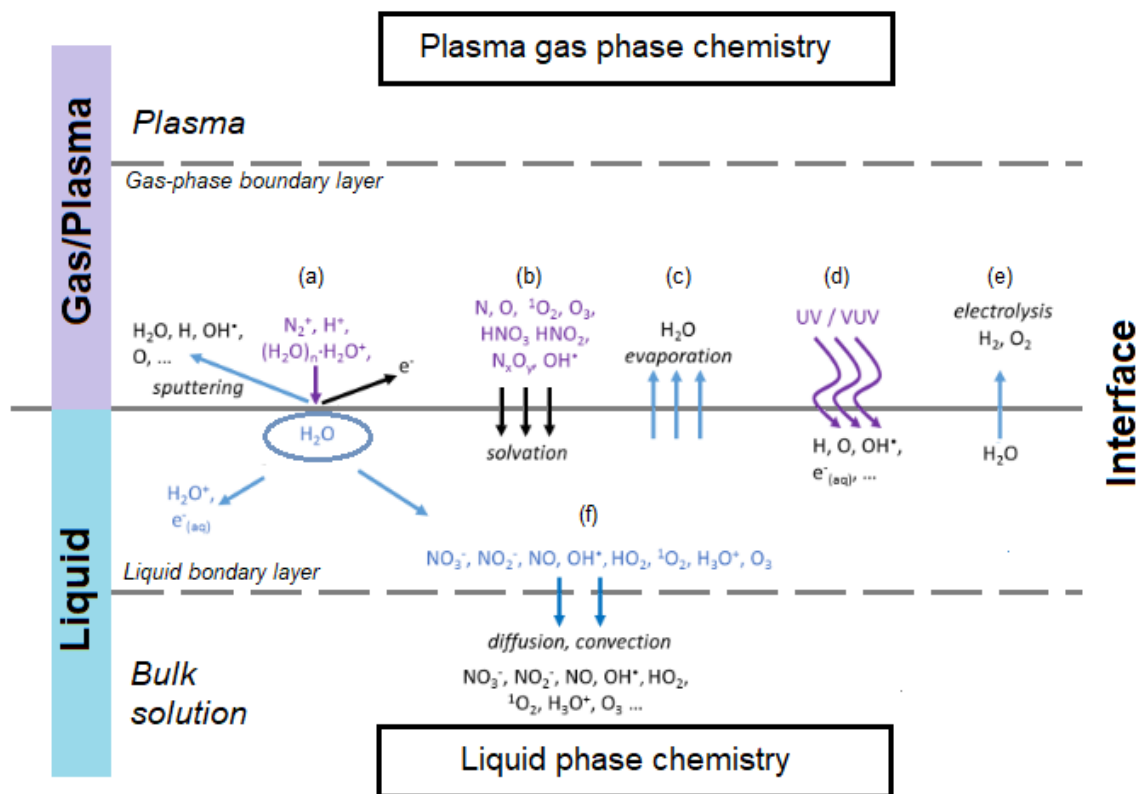
Figure 2.6: Mechanisms and pathways occurring between the gaseous and liquid phase [67]

Previous section described the chemistry generated during an air discharge; here, the section will focus on the transport of the RONS across the liquid boundary layers and the interface as reported in [120]. In most plasma formed over a liquid, the species will be transferred by diffusion and convection process. From Figure 2.6, the dominant mechanisms occurring at the interface and in the first boundary layer of

the liquid are reported in a, b, c, d, and e; where the one in the bulk solution are reported in (f):

- (a) In the scenario where the plasma is in contact with the liquid, the excited species are mixed at the interface with H_2O which recombine into long-lived molecules. Through this interaction, sputtering phenomenon are observed combined with emission of photo-electrons.

- (b) The long-lived species formed in the gas phase reach the interface and are transferred to the liquid layers by solvation.

- (c) Due to the heat generated during plasma treatment, a local elevation of the temperature from the water bulk is observed; this leads to an evaporation of the solution and enhance the concentration of water vapour in the gas phase.

- (d) UV emission generated by the discharge can reach the interface inducing a decomposition of H_2O.

- (e) Similar to the scenario described in (a), the plasma in contact with the liquid can induce an electrolysis of the water solution at the interface.

- (f) The species transported within the first layer of the liquid are then recombined in the bulk by diffusion and convection process.

2.3 Analysis of the gas and liquid phase

The analysis of the gas and liquid phase has been widely investigated by the community with consequent development of suitable techniques. In this section, the literature review reports the most common techniques employed to measure the species formed in the gas phase and, the species dissolved in the PAW.

2.3.1 Gas phase diagnostics

As explained previously, a discharge in air lead to the formation of short- and long-lived species. However, due to their short lifespans, short-lived species are dominantly studied in numerical simulations. Long-lived species formed in the afterglow are more accessible and can be easily compared to numerical simulations; the species of interest includes O_3, NO, NO_2, N_2O, N_2O_5, HNO_2, HNO_3, HO, and H_2O_2 [115]. FTIR spectroscopy is used to characterise and determine the concentration of IR active species present in the gas phase during the discharge. The absorbed wavelength is specific to the vibrational bonds of the molecule detected giving access to the composition of the gas sample [121], [122]. Even though, the technique is widely accepted; its efficiency is limited to discharge in a confined environment. In the case of discharge in an open air environment, OES techniques are favored. OES techniques scan the emissions generated in a discharge which refer to the emission of excited states nitrogen and oxygen species [123], [124]. The technique provides only qualitative information about excited states.

2.3.2   Liquid phase diagnostics

Due to the extensive number of interactions occurring at the interface and in the first layers of the liquid phase; mostly long-lived species can be detected and quantified such as HNO_2, NO_2^-, HNO_3, NO_3^-, H_2O_2, O_3. Most common techniques are adapted from colourimetric assays used for biological medium. Their efficiency has been widely approved by the community with consequent publications [67],[83],[125]. For the case of dissolved ozone, three main approaches were developed:

- Oxidation-Reduction Potential probe (ORP probe), when immersed into the desired solution the probe measures the voltage generated by the oxidation of ozone to a platinum electrode. The measurement taken is relative to a standard reference electrode,

- Iodometric titration, the dissolved ozone reacts with a solution of potassium iodide KI to form iodine I_2 which is then titrated with thiosulfate in buffered solution (pH = 2) [126],

- UV absorbance at 260 nm, the solution can be exposed to a UV light which will interact with the molecule of ozone leading to a drop of intensity [127], [128].

ORP probe are usually less employed due to the presence of other oxidative compounds able to interfere with the measure. Iodometric titration and UV-spectroscopy are commonly employed in laboratories for the quantification of ozone, with the lastest being favoured.

Regarding the presence of short lived-species such as peroxynitrite, fluorometric techniques could be potentially used [129]. HO radicals can be also detected using UV-spectroscopy in presence of terephthalic acid [130],[131]. Some groups have also employed IC for the characterisation of the PAW; however, Tarabova et al., reported no major differences between colourimetric assay and IC when using enzyme catalase in the presence of H_2O_2 [125]. Recent studies reported the use of UV-spectroscopy to quantify the species dissolved in the PAW; this techniques is non-invasive compared to colourimetric assays or IC [127], [132], [133]. Nevertheless, this techniques still under investigation to asset its efficiency.

For readers interested in analysis of short-lived species, electron spin resonance (ESR) or electron magnetic resonance (EMR) spectroscopy is the most commonly used technique for the determination of radicals densities; providing both qualitative and quantitative data. However, direct measurement of many radicals can prove difficult due to their short lifetimes [134]. ESR measurements can be enhanced by performing spin trapping techniques in which the radicals are conjugated to specific spin trap compounds to extend their lifetime [135]. As an example, 5,5-dimethyl-1-pyrroline-N-oxide (DMPO) is a common spin trap used notably for oxygen radicals [136], [137]. Nevertheless, care should be taken in the analysis since the spin trap could potentially interact with media or facing instabilities when prepared [138]. The technique is known to be complex with several variables required to be controlled beforehand. Lastly, only the averaged concentration can be determined as both spatially and temporally resolved measurement cannot be performed.

For the work presented in this thesis, colourimetric assays are used to measure the

species dissolved in the PAW. In chapter 3, a standard operating protocol will be designed combining previous publications in the field as well as techniques developed in [139].

2.4 PAW applications for bio-decontamination

The particular chemistry of the PAW provides its incredible potential for bacterial inactivation; due to the combination of high concentration of oxidisers with a low pH. Groups across the world employed it for decontamination of various bacteria and biofilms both in medical environment and food products.

In healthcare environment, various studies reported its bactericidal properties notably against bacteria, fungus, and viruses. Studies reported its efficiency in the disinfection of medical devices such as duodenoscope [140]; furthermore it has been reported its efficiency in the removal of biofilms which are a dominant issue in healthcare environments [102]. PAW find also application in dentistry for disinfection of apparatus as well as surfaces [141]. PAW can also be employed in cancer treatment [142] and used as hand sanitizer [143]. Most recently, studies reported its efficiency against COVID-19 [87]. Thus, its versatility and potential for this sector makes it a perfect candidate for further investigation and industrial application.

In the food industry sector, PAW find also many applications going from the preservation of food products when conditioned as ice [144] to the disinfection of various vegetable and meat products [145], [146]. It has also been reported positive results on the inactivation of fungal spores on food products [147]. Even if other non-thermal

technologies such as as electrical pulses [148], UV radiation [149] and ultrasounds [150] are already well adapted in this area; PAW has the ability to reproduce most part of those techniques with more eco-friendly outcome.

2.5   Summary

The brief literature review presented here reported some of the main challenges that both healthcare and food industry are facing. With the recent outbreak of the COVID-19 and the lack of resources to face it; the urge for new non-thermal solutions are more than required.

Recent advances in both experiment and numerical models provide a better understanding on the generation of PAW. Notably on the mass transfer occurring between the gaseous and liquid phase; although, due to the consequent number of mechanisms and pathways at the interface further investigations are required to ensure a complete characterisation. A standardisation of the PAW generation appears difficult due to the consequent number of PAW reactors. However, the generation of PAW through DBD reactors appears to be more convenient, and suitable for future up-scaling of the technology and integration into industrial applications.

Chemical analysis of both gaseous and liquid phase have earned considerable progress over the last 30 years; leading to fast and reliable quality control of the PAW formed. Those techniques are accessible for most laboratories across the world which lead to various applications with positive outcomes. Thanks to those progress, PAW technology appears as a suitable candidate for the concerns reported previously as

part of the new non-thermal technologies.

Chapter 3

Materials and Methods

This chapter aims to detail the experimental setup (conception and experimental conditions) employed for the generation of PAW. The diagnostics tools employed for the characterisation of the species present in both gaseous and liquid phase are also described. For the purpose of the work presented in this thesis, a standard operating protocol was designed allowing the detection and quantification of the main long-lived species present in the PAW. Finally, the biological culture of microbial content is also described.

The systems developed were defined by the requirements of the industrial partner (Nofima) who desired to generate high-volumes of PAW for their activities (1 L.min^{-1} of PAW). To achieve this goal, several system were built and tested based on discharge in the gas phase over a liquid through SBDs or DBDs. In the case of a SBD, the water bulk was not part of the plasma system; where in the DBD pin-to-plane configuration the water bulk was part of the plasma system and act as an electrode (floating or grounded). Large SBD were initially designed allowing the treatment of hundreds milliliters of water. However, they were limited by the capacities of the gen-

erator. In the last stages of the project a venturi device was developed and combined to a plasma reactor which succeed in generating high-volumes of PAW.

3.1 Conception of SBD, DBD and plasma venturi for the generation of PAW

This section is divided into three parts: (1) Conception of SBD; (2) Conception of DBD over water; and (3) conception of a venturi plasma reactor. The characteristics of the power supply employed is also described in part (1).

3.1.1 Surface barrier discharges

In this project several SBD were developed going from small reactors (50×50 mm) for the characterization of small volumes of PAW to large setup (300×300 mm) for biological applications in Nofima facilities.

Starting witht the small reactor, the design was made using a CAD software (Fusion 360 from Autodesk) and printed using a 3D printer Ultimaker 2+. The conception by 3D printing allowed an easy and fast maintenance of the device. In this configuration, the SBD electrode was constructed using a quartz glass dielectric with a surface area of 250 mm^2 and a thickness of 2 mm. A thin metallic film made of copper was placed on the top part of the electrode where metallic mesh was placed on the other side of the quartz plate as shown in Figure 3.1.
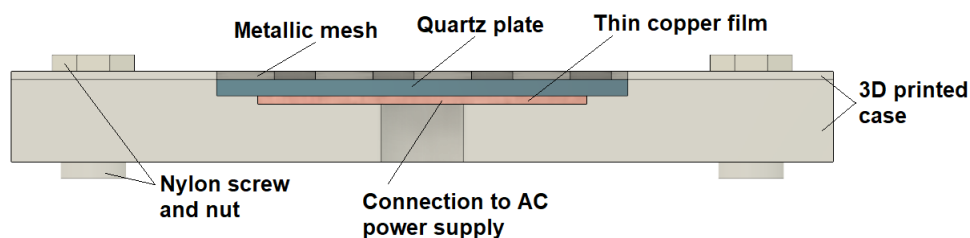
Figure 3.1: Design of the small SBD used for quick generation of PAW for chemical analysis.

The copper film electrode was connected to an AC power generator built using a custom-made step-up transformer developed in-house by Dr Aaron Dickenson; powered with a DC power supply (RS PRO Bench Power Supply, 200W, IPS 405) and a signal generator (TTi TG200). The voltage and current waveforms were measured using a high voltage probe (TTP HVP 15HF) and a wide bandwith current probe monitor (Pearson model 2877), and recorded using a digital storage oscilloscope (Keysight EDUX 1002A). To monitor the discharge power in real-time, the current and voltage signals were multiplied using the oscilloscope to obtain the instantaneous power which was averaged over multiple cycles to obtain the mean power. Figure 3.2 describes a schematic of the power generator and its connection to the surface barrier discharge.
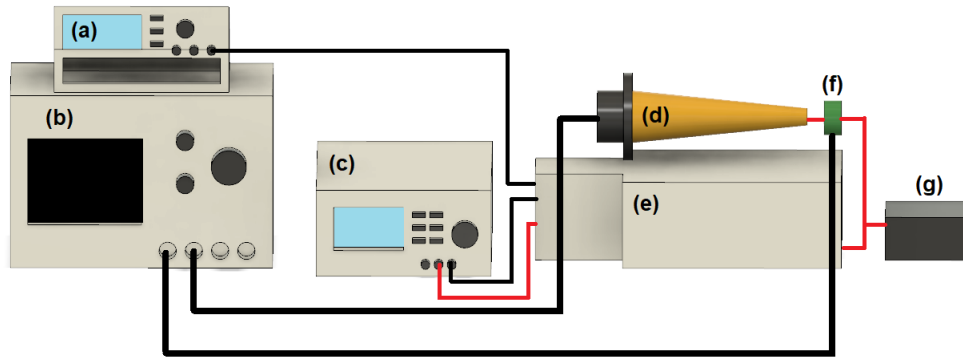
Figure 3.2: AC power generator with a) signal generator, b) oscilloscope, c) DC power supply, d) voltage probe, e) custom-made transformer, f) current monitor, g) SBD.

The conception of large SBD follows the same pattern as described previously. However, heating and oxidation damages were observed with the small device which could be replaced easily by printing new parts. The large device was supposed to be used in Nofima facilities without the presence of a qualified technician or equipment to replace any damaged parts. The case containing the SBD was replaced by clear laser cut acrylic plates able to resist to temperature up to 160∘ and resistant to oxidation, two quartz plate (150 × 150 mm) were use to form the dielectric layer forming a total surface of 90000 mm^2 with a thickness of 2 mm. The dielectric was covered with a thin film of copper placed on its top part, Kapton tape (Tesa 51408, RS Components Ltd) was also added on the edges of the electrode to ensure a good isolation of the copper film from the oxidation generated during plasma deposition and for heating prevention. On the other part of the electrode, a metallic mesh was placed and connected to the ground, the whole case was then secure by several screws and nuts

as show in picture 3.3.
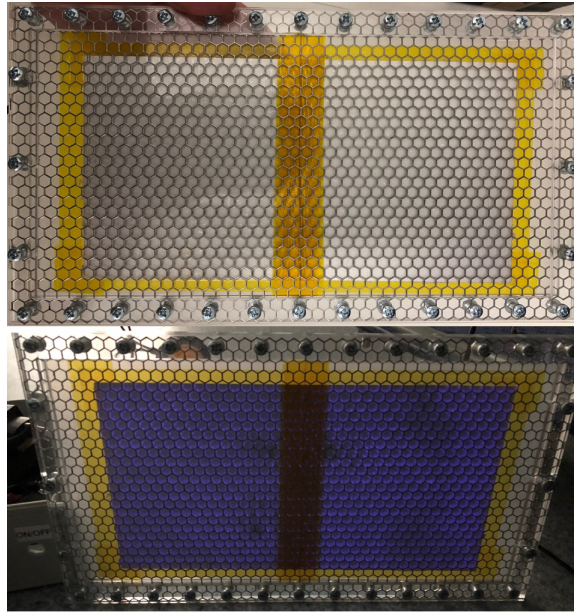
Figure 3.3: Picure of the large SBD with and without plasma.

3.1.2 Pin DBD over water

Another configuration was developed in which the plasma generated will be in direct contact with the water. As shown in Figure 3.4, a holder was 3D printed containing nine holes in which the electrodes will be inserted. The configuration presented here only contained one electrode made with a borosilicate glass tube (playing the role of dielectric) in which is inserted a metallic rod or wire. When running the system in this state, a plasma was formed inside the tube, it was observed that a corona discharge was formed at the extremity of the rod/wire. To avoid this effect, water was added into the tube to ensure a complete conduction of the charges leading to the formation of the discharge at the extremity of the borosilicate tube.
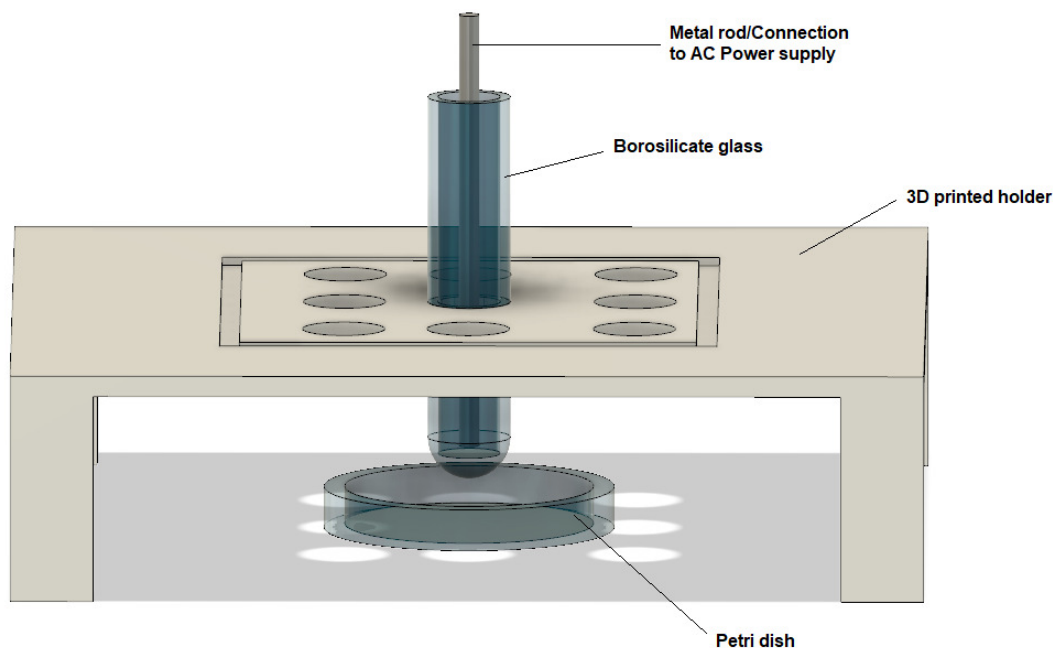
Figure 3.4: Design of a pin DBD over a Petri dish containing water

Different solutions with various conductivity values were used to evaluate the conductivity effect on the efficiency of the device. The solution conductivity was set using NaCl in the concentration range from 0.1 to 1 mol.L^{-1}. All the experiments achieved with this system were done by using tap water as the conductive liquid. Finally, the water contained in the Petri dish can be either grounded or not depending on the tests done using solid tinned copper wire with PVC sheath. For the tests performed in this work the grounded option was opted since it enhanced the formation of hydrogen peroxide (H_2O_2). The discharge resulted in the formation of streamers going from the bottom of the electrode to the surface of the water as

shown in Figure 3.5.
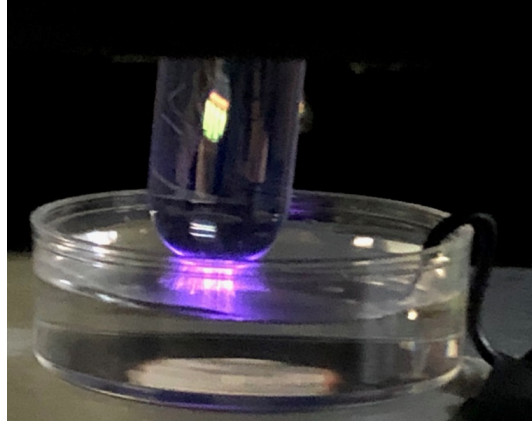
Figure 3.5: Picture of a plasma formed with the pin DBD over water at 30kHz / 15kV.

3.1.3   Venturi plasma device

Due to the requirement of producing large volume of PAW, a last system has been developed consisting of a venturi tube with a cavity chamber as shown in Figure 3.6. The design was achieved using a CAD software (Fusion 360) and 3D printed by stereolithography (SLA, UV Photopolymer Resin from XYZprinting) printing (Nobel Superfine from XYZprinting). Different resolutions were accessible (25, 50 and 100 microns), the best results and quality was obtained using a resolution of 50 microns. The system consists of a venturi constriction in a tube with a cavity chamber surrounding it and containing an aperture. Following the laws of fluid dynamics, when water flows through the venturi, a depression is observed at the constriction leading to a suction of the air present in the cavity chamber. In the aperture, a quartz tube was inserted and covered with a thin copper film on its

surface. When a wire was inserted into the tube, the configuration acted as a DBD where the copper film was connected to an AC power supply and the wire to the ground.
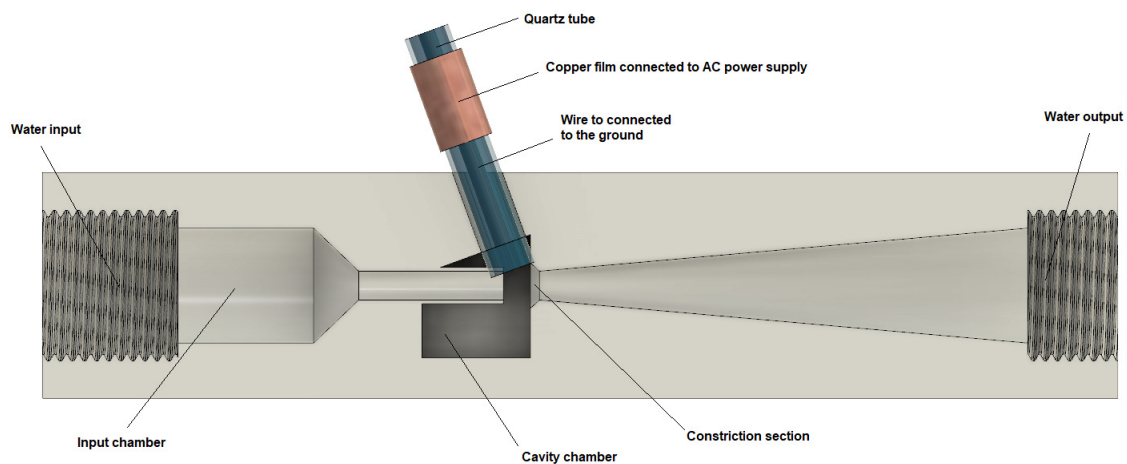
Figure 3.6: Design of a venturi plasma system used for the generation of 1L of PAW.

As the tube was left opened to the surrounding environment (air), a plasma was formed inside the tube which was sucked into the venturi device and interacted with the water. Another configuration was also tested using an SBD enclosed into a box and connected to the venturi using peristaltic tubing. This configuration is widely used for fast dissolution of chemicals product into water, here it has been adapted for the requirement set by Nofima. Further details on the design and its efficiency are detailed in chapter 6.

3.2 Diagnostic tools for the characterisation of the gaseous phase

This section is split into four parts: (1) optical emission spectroscopy; (2) Fourier transform infrared spectroscopy; (3) spectrophotometry; and (4) numerical simulation of both gas and liquid phase.

3.2.1 Optical Emission Spectroscopy

OES measurements were done by recording the spectrum generated by the plasma using a Ocean Optics spectrometer (USB 200+) connected to a computer. The spectrometer has a 2 MHz analog-to-digital (A/D) converter and a Sony ILX511 2048-element linear silicon CCD array detector. It allows measurements from 200 nm to 1100 nm with an optical resolution of 0.1 nm (FWHM) and integration times from 1 ms to over 60 seconds. The data were recorded using OceanView software, a Java-based spectroscopy software developed by Ocean Optics. An optical fiber (400 µm diameter) was placed in front of the device where the plasma is formed. To ensure a repeatability of the measure, a background was first recorded then subtracted to the emission generated by the plasma.

3.2.2 Fourier Transform Infrared Spectroscopy

FTIR measurements were done using a Jasco FT/IR-400. The device has a mid-IR optical bench from 500 cm^{-1} to 7800 cm^{-1} with an optical resolution of 8 cm^{-1}.

A diagram of the setup is shown in Figure 3.7, tubing were placed close to the plasma discharge and connected to an external pump filling the gas cell placed into the spectrometer. The gas cell consists of a 100 mm long Pyrex tube with at its end two IR-transmitting windows (KBr) of 25 mm diameter sealed by Viton O-rings (Pike 162-2100).
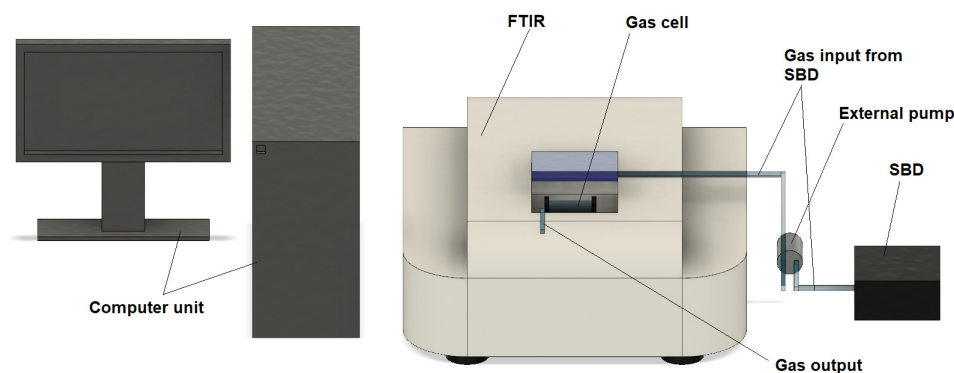
Figure 3.7: Setup for the measurement of the gas phase by FTIR using a gas cell.

The data were averaged over 10 consecutive scans and subtracted to a background recorded prior measurement. Between each acquisition the chamber was flushed with ambient air for 15 seconds and another scan was performed to ensure the absence of any species produced by the plasma. The data were analysed using the software developed by Jasco and the peaks analysed using the library provided by the National Institute of Standards and Technology (NIST) https://doi.org/10.18434/T4D303.

3.2.3 Spectrophotometry

The chemical species dissolved into the PAW were analysed using the chemical assays described in section 3.3. The colourimetric assays were analyzed using two spectrophotometers (SPECTROstar Nano from BMG LABTECH and Jenway 7200 from Cole-Parmer Ltd) at specific wavelength. Prior measurements, the standard curves were plotted following the absorbance measured for each reagent and using the Beer-Lambert law, A = f(C). Where A is the measured absorbance of the reagent investigated at a specific wavelength and C the concentration of the sample tested (NO_2^-, NO_3^-, etc.). The colourimetric assays used in this work are reported in section 3.3 based on the work reported in chapter 2, section 2.3.2.

3.2.4 Numerical simulation

Numerical simulations of the plasma phase generated by an SBD were preformed by Dr. Mohammad I. Hasan at the University of Liverpool. The model used here is similar to the one reported in a previous work presented by Hasan and Walsh [151]. Description of the model can be found in the Appendix A, and the results obtained are reported in chapter 5.

3.3 Characterisation of chemical species in PAW

This section describes the different methods used to determine and quantify the chemical species present in the PAW after plasma exposure. Chapter 2 presented the different mechanisms occurring in the formation of short- and long-lived species

between the plasma-liquid interaction (section 2.2.4). This "Standard Operating Protocol" based on previous studies (section 2.3.2), can be used to measure the long-lived species relevant for biological applications. Stock solutions were prepared and analysed to produce standard curves used to confirm the accuracy of the techniques. Depending on the assay, the uncertainties are either calculated by triplicate or using the derivative method.

3.3.1 Physical parameters of the PAW

3.3.1.1 pH measurement, concentration of hydronium and hydroxide ions, and temperature

The pH was measured using a pH probe from Hanna Instruments (HI 9813-6 with the probe HI-1285-6) right after the plasma exposure; the measure was provided with an accuracy of $\pm$ 0.1. The concentration of hydronium ions H^+ was directly calculated from the measure of the pH using the equation $[H^+] = 10^{-pH}$. The concentration of hydroxide ions HO^- are typically calculated from the concentration of the hydrogen ions and the ionic product of the water, K_W. However, in the setups described in sections 3.1.1 and 3.1.2 the plasma reactors induced a local elevation of the temperature of the water exposed, impacting the value of the ionic product. To avoid any errors in the measurement of the ionic product, a modified equation developed by Harned and Owen was used which consider the thermal response of K_W [152]:

$$HO^- = 10^{pH+0.0335\times T-14.88} \tag{3.1}$$

With T [°C], the in-situ temperature of the liquid treated in Celsius and pH, the value recorded by the pH probe. The standard deviation is obtained by applying the derivative method to equation 3.1, leading to the following expression:

$$\Delta[\text{HO}^-] = \left|0.0335 \times \ln(10) \times 10^{\text{pH}+0.0335\times\text{T}-14.88}\right|\Delta\text{T}$$
$$+ \left|\ln(10) \times 10^{\text{pH}+0.0335\times\text{T}-14.88}\right|\Delta\text{pH} \quad (3.2)$$

Where, ΔT and ΔpH are respectively the accuracy of the thermocouple and pH meter. The temperature was monitored using a thermocouple immersed in the water (SIGNSTEK, ST300 Dual Channel Digital Thermometer) with an accuracy of $\pm$ 0.2°C. The measures were taken depending on the parameters of the experiment, usually before and during plasma exposure every 5 min.

3.3.2 Chemical parameters of the PAW

3.3.2.1 Measurement of the concentration of nitrites and nitrous acid

The concentration of nitrites NO_2^- was evaluated using a colorimetric assay using Griess reagent (Supelco Ltd, MFCD01866819). The reagent has two compounds which interact with the nitrites following two main reactions as described in Figure 3.8:
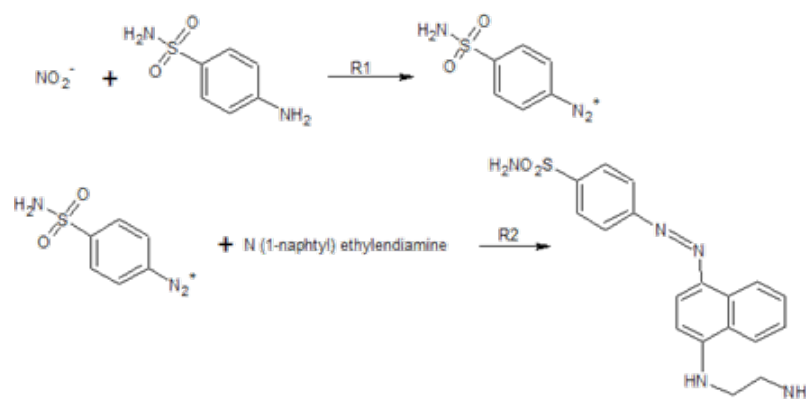
Figure 3.8: Interaction of the Griess reagent with nitrites following two mechanisms

Under acidic condition, the nitrites interact with a solution of sulphanilamide to form a complex (R1), this complex will then react with a solution of N (1-naphtyl) ethylenediamine (R2) giving a pink purple coloration to the final product.

The method is valid for samples with concentration from 1 to 200 µM, dilution are required for solutions with higher concentrations of nitrites. To obtain the standard curve, a stock solution of nitrites sodium (0.2 mM) was prepared by dissolving 13.8 mg of so sodium nitrites salt (Sigma Aldrich Ltd, CAS 7632-00-0) in 1L of distilled water. Eight diluted solutions were prepared using $F = \frac{C}{C'}$ where F is the dilution factor, C the concentration of the stock solution and C' the concentration of the diluted solutions, as described in the Table 3.1

Solution	1	2	3	4	5	6	7	8
Concentration [µM]	5	10	15	20	25	50	100	200

Table 3.1: Standard solution of nitrites

For the analysis, 100 µL of the diluted solutions are placed into a micro-plate with 50 µL of reagent, the solution were then left for a stabilization period of 15 min. The

blank was performed with either distilled or tap water with 50 µL of Griess reagent. The complex formed was then detected by spectrophotometry at a wavelength of 548 nm.

The couple nitrous acid HNO_2 and nitrites NO_2^- are linked by an acid-base relation which combines their respective concentration, the pH of the solution and their acidic constant ($pK_{a1} = 3.39$), as defined in equation 3.3. Knowing that pK_a is the negative value of the logarithm of the acid dissociation constant (Ka) and $pH = -\log([H^+])$, the previous equation can be rearranged to express the concentration of the nitrous acid HNO_2, equation 3.6.

$$[h]Ka \ = \ \frac{[NO_2^-][H^+]}{[HNO_2]} \tag{3.3}$$

$$pKa \ = \ -\log(Ka) \tag{3.4}$$

$$pKa \ = \ -\log\left(\frac{[NO_2^-]}{[HNO_2]}\right) - \log([H^+]) \tag{3.5}$$

$$[HNO_2] = \frac{[NO_2^-]}{10^{(pH-pKa_1)}} \tag{3.6}$$

3.3.2.2   Measurement of the concentration of nitrates and nitric acid

The concentration of nitrates NO_3^- was also measured using a colorimetric assay where the nitrates ions interact with a solution of sodium salicylate in a sulfuric medium. The mechanism, described in Figure 3.9, starts with a first fixation of the sulfuric acid to the salicylate ions (R1). The fixation will attract the nitrates ions and fix them by substitution to form a nitrosalicylate ion complex (R2). The reaction is instantaneous and no stabilization period is required.
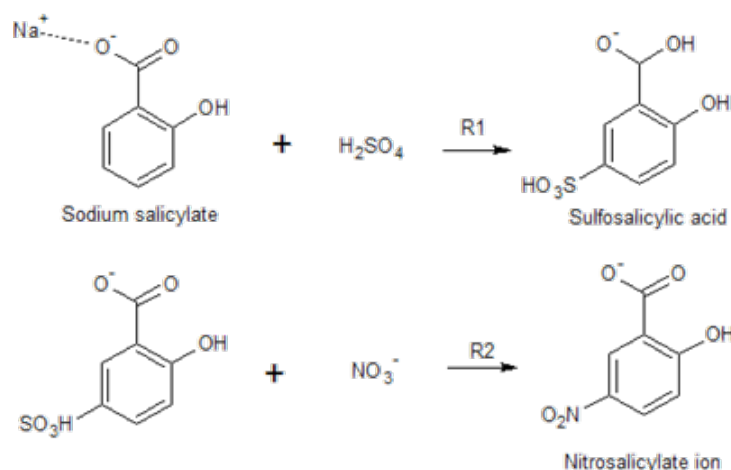
Figure 3.9: Interaction of the salicylate reagent with nitrates ions following two mechanisms

The procedure requires three stock solutions:

- A solution of nitrate potassium prepared using 81.5 mg of nitrates potassium salt (Sigma Aldrich Ltd, CAS 7757-79-1) into 1L of distilled water (S_0),

- A solution of sodium hydroxide and sodium tartrate prepared by dissolving 40g oh hydroxide sodium pallet (Sigma Aldrich Ltd, CAS 1310-73-2) into 100 mL of distilled water and then adding 6g of tartrate double salt (Sigma Aldrich Ltd, CAS 6381-59-5) (S_1),

- A solution of sodium salicylate prepared by dissolving 0.5 g of sodium salicylate salt (Sigma Aldrich Ltd, CAS 54-21-7) into 100 mL of distilled water (S_2).

For the standard curve, the nitrates stock solution was diluted five times and combined with a blank of distilled (see Table 3.2).

Diluted solution	1	2	3	4	5
Volume of S_0 (mL)	2	4	6	8	10
Volume of distilled water (mL)	8	6	4	6	8
Volume of S_2 (mL)			1		
$[NO_3^-]$ (mg/L)	10	20	30	40	50

Table 3.2: Standard solution of nitrates

Each diluted solution are then evaporated in a water bath or a stove at around 80°C until a white crystal appeared. After cooling down, 400 µL of sulfuric acid is added to the crystals and left for 10 min. The solution was mixed with 4 mL of the stock solution S_1, the nitrosalicylate ions formed have a yellow coloration observable by spectrophotometry at 420 nm.

The concentration of nitric acid HNO_3 was also calculated with an acid-base relation using the acidic constant of the couple HNO_3/NO_3^- ($pK_{a2} = -1.37$). The demonstration has been explained previously (3.6), the final equation is:

$$[HNO_3] = \frac{[NO_3^-]}{10^{(pH - pKa_2)}} \tag{3.7}$$

3.3.2.3 Measurement of the concentration of hydrogen peroxide

Hydrogen peroxide are detected and measured using a solution of titanium sulfonate, the reaction will produce pertitanic acid which has a yellow coloration once formed.

$$Ti^{4+} + H_2O_2 = H_2TiO_4 + 4\,H^+$$
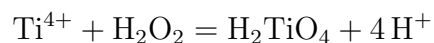
A stock solution of hydrogen peroxide was prepared by diluting 10 mL of hydrogen peroxide bought from a supplier (Sigma Aldrich Ltd, CAS 7722-84-1) into 1L of distilled water. From this stock solution, several diluted ones were prepared to make to build the standard curve as detailed in Table 3.3.

Blank	S_1 (mM)	S_2 (mM)	S_3 (mM)	S_4 (mM)	S_5 (mM)	S_6 (mM)	S_7 (mM)
0	0.25	0.5	0.75	1	1.5	2	2.5

Table 3.3: Standard solution of hydrogen peroxide

100 µL of the diluted solutions are then placed into a micro-plate reader and combined with 100 µL of titanium sulfate reagent, forming a yellow complex detectable by spectrophotometry at 410 nm. For smaller concentration of hydrogen peroxide, two other techniques were also used:

- The FOX reagent or ferrous oxidation-xylenol orange, is a colorimetric technique assay used to measure the concentration of hydrogen peroxide in biological systems. The methods relies on the oxidation of Fe^{2+} to Fe^{3+} in acidic conditions (*i.e.*, sulfuric acid). After the intitial oxydation, the xylenol orange within the assay is also oxidized, producing a complex detectable by spectrophotometry at 560 nm,

- As a complementary option, the FOX reagent method was combined with test strips suitable for small concentration (Single Parameter Peroxide test Strip 0-100 ppm, RS Components).

For the FOX method, several stock solutions were prepared and preserved in the lab:

- A stock solution of sulfuric acid (Sigma Aldrich Ltd, CAS 7664-93-9)with a concentration of 25 mM which is used to prepare the other stock solution S_0,

- A solution of xylenol orange made by dissolving 152 mg of xylenol orange salt (Sigma Aldrich Ltd, CAS 3618-43-7) into 100 mL of the solution S_0 kept in a dark bottle,

- A solution of sorbitol (Sigma Aldrich Ltd, CAS 50-70-4) with a concentration of 1 M made by dissolving 182.2 mg of salt per mL of S_0. The solution is then diluted (1:100) with S_0 to reach a final concentration of 10 mM. The final product is then kept at 4°C,

- A solution of hydrogen peroxide with a concentration of 0.5 mM.

The iron sulfate reagent was prepared on the day by dissolving 1.112 mg of sulfate iron salt (Sigma Aldrich Ltd, CAS 7782-63-0) into 1 mL of S_0.

The standard curve was prepared with the following dilutions of hydrogen peroxide and sulfuric acid (Table 3.4):

Concentration (µM)	µL of H_2O_2	µL of H_2SO_4
0	0	10
25	0.5	9.5
50	1.0	9
75	1.5	8.5
100	2.0	8
150	3.0	7
200	4.0	6
250	5.0	5

Table 3.4: Diluted solution of hydrogen peroxide in sulfuric acid

10 µL of the diluted solutions were then added into a micro-plate and mixed with 0.195 mL of the working reagent. The solutions were left for incubation for 45 min and read by spectrophotometry at 560 nm.

3.3.2.4 Measurement of the carbonic compounds: carbonic acid, bicarbonates and carbonates

Carbonic compounds are present in tap water under the form of bicarbonates HCO_3^-, their concentration was measured by classic titration of the water using a strong base [NaOH] = 0.1mM (Sigma Aldrich Ltd, CAS 1310-73-2) or acid [HCl] = 0.1mM (Sigma Aldrich Ltd, CAS 7647-01-0) depending on the pH of the solution. The base or acid were slowly introduced into the solution which induced a modification of the pH until reaching a plateau (titration curve), the curve was then derivated to obtain the equivalence point where both conjugate acid and base are in equilibrium. This value was then used to obtained the concentration of the total carbonic compounds (C_{total}) dissolved in the water, equation 3.8.

$$C_{total} = \frac{C \times V_{eq}}{V_{sample}} \qquad (3.8)$$

Where C, V_{eq} are respectively the concentration and volume at equivalence of the added acid/base and V_{sample}, the initial volume of the sample. As explained previously, the bicarbonates HCO_3^- are the dominant species dissolved into water and considered as an amphoteric compound able to provide and capture protons. The acid/base relations are then expressed with the bicarbonate being a base for the cou-

ple ($[H_2CO_3]/[HCO_3^-]$) and an acid for the couple ($[HCO_3^-]/[CO_3^{2-}]$), equations 3.9 and 3.10.

$$K_{a3} = \frac{[HCO_3^-][H^+]}{[H_2CO_3]} \tag{3.9}$$

$$K_{a4} = \frac{[CO_3^{2-}][H^+]}{[HCO_3^-]} \tag{3.10}$$

Equation 3.10 can be rearranged as following:

$$\frac{[CO_3^{2-}]}{[HCO_3^-]} = 10^{(pH-pKa_4)} \tag{3.11}$$

Knowing that the C_{total} can be expressed as the sum of the different carbonic species dissolved into water $[C_{Total}] = [H_2CO_3] + [CO_3^{2-}] + [HCO_3^-]$. The concentration of bicarbonates HCO_3^-, carbonates CO_3^{2-}, and carbonic acid H_2CO_3 are respectively:

$$[HCO_3^-] = [C_{total}] - [CO_3^{2-}] - [H_2CO_3] \tag{3.12}$$

$$[H_2CO_3] = \frac{[HCO_3^-]}{10^{(pKa_3-pH)}} \tag{3.13}$$

$$[CO_3^{2-}] = \frac{[HCO_3^-]}{10^{(pH-pKa_4)}} \tag{3.14}$$

Where, $pKa_3 = 6.37$ and $pKa_4 = 10.32$. Their uncertainties are expressed as following:

$$\Delta[\text{C}_{\text{Total}}] = \left|\frac{\text{V}_{\text{eq}}}{\text{V}_{\text{sample}}}\right|\Delta[\text{C}] + \left|\frac{[\text{C}_{\text{Total}}]}{\text{V}_{\text{solution}}}\right|\Delta\text{V}_{\text{eq}} \tag{3.15}$$

$$\Delta[\text{CO}_3{}^{2-}] = \left|\frac{1}{10^{\text{pH}-\text{pKa}_4}}\right|\Delta[\text{HCO}_3{}^-] + \left|\frac{-[\text{HCO}_3{}^-] \times \ln(10) \times 10^{\text{pH}-\text{pKa}_4}}{(10^{\text{pH}-\text{pKa}_4})^2}\right|\Delta\text{pH}$$
$$\tag{3.16}$$

$$\Delta[\text{HCO}_3{}^-] = \Delta[\text{C}_{\text{Total}}] + \Delta[\text{CO}_3{}^{2-}] + \Delta[\text{H}_2\text{CO}_3] \tag{3.17}$$

$$\Delta[\text{H}_2\text{CO}_3] = \left|\frac{1}{10^{\text{pKa}_3-\text{pH}}}\right|\Delta[\text{HCO}_3{}^-] + \left|\frac{-[\text{HCO}_3{}^-] \times \ln(10) \times 10^{\text{pKa}_3-\text{pH}}}{(10^{\text{pKa}_3-\text{pH}})^2}\right|\Delta\text{pH}$$
$$\tag{3.18}$$

3.3.2.5 Measurement of the concentration of ammonia and ammonium

Ammonia and ammonium were measured in a previous work [83]. However, it was found that the concentrations did not change with plasma activation. In this work, the technique was also used to confirm this point. Readers interested in this technique can find the description in the Appendix B.

3.3.2.6 Measurement of dissolved ozone

Dissolved ozone O_3 was measured by UV absorbance at 260 nm, the solution can be exposed to a UV light which will interact with the molecule of ozone leading to a drop of intensity [127], [128]. The freshly prepared PAW, is directly placed into a dwell and exposed to an Ocean Optics Deuterium lamp (DH-2000-CAL) as light source. An Ocean Optics spectrometer (USB2000 +) was used to monitor the light intensity at 260 nm. Alternatively, the concentration was also measure using test strips (RS stock no 261-8619, from Rs Components Ltd).

3.4 Biological assessment

The bacteria used in this work were cultivated in the centre of plasma microbiology by Dr. Breno Salgado. Two bacteria strains were selected: *Escherichia coli* BW25113, and *Staphylococcus aureus* USA300 JE2. To prepare the bacterial inoculum, single colonies of *E. coli* and *S. aureus* were inoculated, respectively, into 10 ml of either Luria-Bertani broth (LB, Sigma-Aldrich Company Ltd, Gillingham, United Kingdom) or Tryptone Soya broth (TSB, Sigma-Aldrich), and incubated for 24 hours at 37 $^\circ C$ at 160 rpm (SI500; Stuart Equipment, Staffordshire, United Kingdom). 0.1 ml aliquots of the stationary-phase cultures were added to 10 ml of fresh culture media and incubated until the cell population reached 5.0 $\times 10^{10}$ CFU/mL. 1 mL of the stationary-phase culture was centrifuged (C2500-230V, Labnet International Inc, United States) for 10 minutes at 13000 rpm at room temperature and the cell pellet (agglomeration of cells found at the bottom of the test tube) was resuspended in freshly prepared PAW alongside an un-activated filtered water sample as a control. Depending on the experiment, the mixtures were incubated for different period of time at room temperature; the bacterial cells were recovered by centrifugation (13000 rpm for 10 min at room temperature) and resuspended in Phosphate Buffered Saline (PBS, Sigma-Aldrich). Serial decimal dilutions were then prepared in PBS and 0.1 mL aliquots from appropriate dilutions were inoculated on LB agar and TSA plates (Sigma-Aldrich) for the determination of E. coli and S. aureus, respectively, and incubated for 24 hours at 37 $^\circ C$. A colony forming unit (CFU) count was performed and reported as log CFU/mL. Experiments were performed in triplicates across multiple

days and room temperatures.

The protocol was employed in chapter 4 and 5 to form the colony, the efficiency of the PAW formed in those chapter were then tested.

Chapter 4

Comparison between direct and indirect formation of PAW for bacterial inactivation

4.1 Introduction

The present chapter explores two plasma systems designed for the activation of water, both reactors are based on dielectric barrier discharge (chapter 3) with one set in a pin-to-plane geometry as already described in section 3.1.2; the second reactor consists in a surface barrier discharge and follow a plane-to-plane geometry (section 3.1.1). As explained previously in chapter 2, there is different ways on how a plasma can interact with liquids either by having a plasma entering in contact with the liquid or by remote exposure. The pin-to-plane geometry allow the formation of streamers from the bottom of the electrode to the surface of the liquid exposed. Whereas, the surface barrier discharge will form a plasma on the surface of the dielectric, the chemical species formed are then diffused within the gap separating plasma and liquid.

In this chapter, the aim is to investigate the impact of both reactors on the final

chemistry of the PAW obtained, and to compare its bactericidal properties. This
chapter is organised as follows: (1) a description of the discharge conditions, the di-
agnostic tools employed, and bacterial inoculation. (2) The results obtained through
the activation from both reactors; with discussion on the analysis performed for both
gas and liquid phase, as well as the biological results obtained. (3) conclusion on the
study. It should be emphasis that the chapter focuses in understanding the pathways
of the PAW formation and its potential for decontamination rather than describing
the physicochemical properties of the plasma-liquid interaction.

4.2 Material and methodology

The conception of the plasma systems used in this chapter can be found in section
3.1.1 and 3.1.2 of chapter 3. Characteristics on the power supply can be found in
Figure 3.3, section 3.1.1 of the same chapter. The relevant background theory and
interpretation of the experimental data are presented in chapter 2. The diagnostic
tools details are found in chapter 3. The specific details related to this study are
described below.

4.2.1 Plasma systems and experimental conditions

4.2.1.1 Direct formation of PAW

For the direct formation of PAW, a volume of 5 mL of purified water was placed into
a petri dish in which a wire was immersed and grounded. As previously reported
in chapter 3 (section 3.1.2), different solutions with various conductivity values were

used to evaluate the conductivity effect on the efficiency of the device. The solution
conductivity was set using NaCl in the concentration range from 0.1 to 1 mol.L^{-1}.
When increasing the conductivity no major differences were observed in comparison
to classic tap water; however, when decreasing the conductivity of the solution by
using distilled water, an increase of the heat generated by the discharge was observed
which damaged drastically the structure. Due to the difficulties to stabilize the
discharge only a power of 12 W was accessible at a frequency of 30 kHz, and a voltage
AC peak to peak of 22 kV. In this scenario, multiple streamers were observable going
from the bottom of the electrode to the surface of the water. When decreasing the
voltage, the streamers formed are weaker and unstable which result in an overall
weak and inefficient plasma. Inversely, increasing the power did not lead to a more
powerful plasma but increased the heat resistance of the system and the temperature
of the water in the tube which started to boil. Thus, stopping the plasma to work
correctly by damaging the system and contaminating the water exposed by drops of
boiling water. In addition, when variating the voltage, the water exposed is attracted
by the electrode forming a Taylor cone on the water surface due to its conductivity
and the electric field in place in the system. This phenomenon has already been
observed and reported by Bruggeman et al., [67]; and will decrease the space between
the water and the electrode to the point where the water is completely touching the
electrode. In this scenario, the plasma is formed at the surface of the water as
detailed by the geometry (f) of Figure 2.1 (section 2.2.2 of chapter 2), leading to
a weaker plasma. For the purpose of this chapter and the resultant chemistry of
the PAW formed, the power will be kept constant at 12 W. Depending if the water

exposed contained bacteria or not, a thermocouple electrode was immersed into the water to control the temperature of the water during plasma exposure. In all cases, all waters (purified or containing bacteria) were treated for a period of time going from 0 to 16 minutes.

4.2.1.2 Indirect formation of PAW

For the indirect formation of PAW, a volume of 5 mL of purified water was placed into a petri dish. For this plasma system, two power modes were selected: a "low" power mode set at 6W for a voltage of 9kV and a "high" power mode set at 12 W for a voltage of 13 kV, both modes were ran at a frequency of 19 kHz. The device and water formed a gap of 0.5 cm and the plasma occurs on the surface of the SBD. Comparably to the experiment described in chapter 5, a coupled thermocouple was immersed into the water to measure the variation of the water temperature during the plasma treatment. For this device, only purified waters were exposed for a period of time going from 0 to 16 minutes. However, the gas phase was studied for a period of time up to 25 minutes.

4.2.2 Characterization of the gaseous phase

The gas phase was characterized OES and FTIR techniques. Detailed description of the techniques setup can be found respectively in chapter 3, section 3.2.1 for the OES and section 3.2.2 for the FTIR. Due to the process and environment in which the discharge were performed, OES technique was used for the direct discharge where the indirect discharge was analysed using FTIR.

4.2.3 Characterization of the liquid phase

The chemical composition of the PAW formed was quantified using the protocols developed in chapter 3, section 3.3. The samples of purified water were plasma exposed and analysed right after the exposition, a non-treated sample of purified water was used as a blank. For the purpose of this chapter, only the main chemical compounds found in literature were measured to link the interaction described in chapter 2 (section 2.2) i.e, HNO_2/NO_2^- (nitrous acid/nitrites), HNO_3/NO_3^- (nitric acid/nitrates), H_2O_2 (hydrogen peroxide) and O_3 (ozone).

4.2.4 Bacterial inoculation

The bacterial inoculation follows the same protocol as the one described in chapter 3, section 3.4. This part was performed with the help of Dr Breno Salgado who is also one of the authors of the publication referred in chapter 5. Dr Breno Salgado granted permission to use the biological results to support the work presented in this chapter.

4.3   Results and discussions

4.3.1   Comparison of the plasma-liquid interactions

4.3.1.1   Direct treatment of PAW

As explained in section 4.2.1, the plasma-liquid interaction will be affected by the position of electrode over the water. When the electrode is immersed into the solution, the plasma is formed on the surface between the water and the electrode. Instead of the formation of streamers going from the bottom of the electrode and reaching the surface of the water, a weak surface plasma is formed. This configuration lead to an important generation of ozone in the surrounding atmosphere combined with weak concentration of nitrogen species in the water bulk. When increasing the gap between the plasma and the water, several streamers can be observed. The picture reported in Figure 4.1 shows this phenomenon.

Figure 4.1: Comparison between immersed and non-immersed electrode

To ensure a good exposure of the water samples, the gap is kept constant to 0.5 cm allowing a correct "activation" of the samples with adequate concentration of the

chemical species of interest. Figure 4.2 report the OES spectrum obtained during
the treatment.
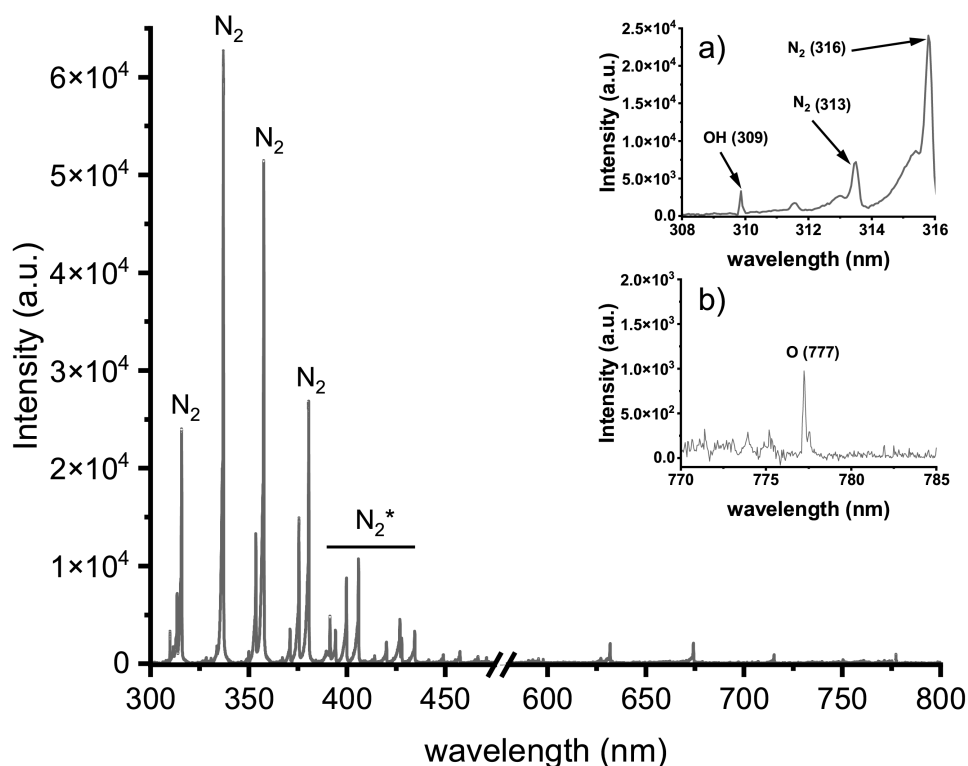
Figure 4.2: Optical emission spectroscopy spectrum of the pin to water interaction

As the plasma generated here is in air, the dominant species reported in the Figure are
mainly nitrogen species (N_2 (C-B)). Similar observation were done in previous work
as reported in [123], [153]. Singlet oxygen (777 nm) is also commonly found in OES
spectrum as reported in [124]. In air plasma ozone is formed by the recombination of
atomic oxygen with molecular oxygen through a tertiary molecule (M) as described

by (R1):

$$O + O_2 + M \rightarrow O_3 + M \quad (R1)$$
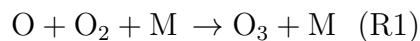
Finally, the presence of OH was also detected at 309 nm, formed by dissociation of water molecule by UV photons produced within the plasma (R2) [154] and sputtering affect [67]:

$$H_2O + UV \rightarrow H^\bullet + OH^\bullet \quad (R2)$$
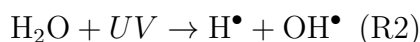
Formation of OH classically occurs in similar configuration and in plasma jet and are reported to be a key element leading to the formation of hydrogen peroxide.

4.3.1.2 Indirect treatment of PAW

As already presented in chapter 2, the plasma in a SBD is formed on the surface of the dielectric in close contact with the grounded electrode (i.e., the metal mesh covering the quartz glass). This configuration has not been reported to have any issues to generate the plasma. However, the gas chemistry in those systems are dependent on various conditions such as the input gas, working power and heat of the system. Knowing that the system was operated in air at atmospheric pressure and room temperature, only the power will play a major difference. Figure 4.3 reports the measurement of the chemical species generated in the gaseous phase depending on the power mode (low power "LP" and high power "HP") at different time points. Figure 4.3 a) reports the FTIR measurements for the low power mode. Measurements were taken at specific time points: 4, 15 and 25 minutes.
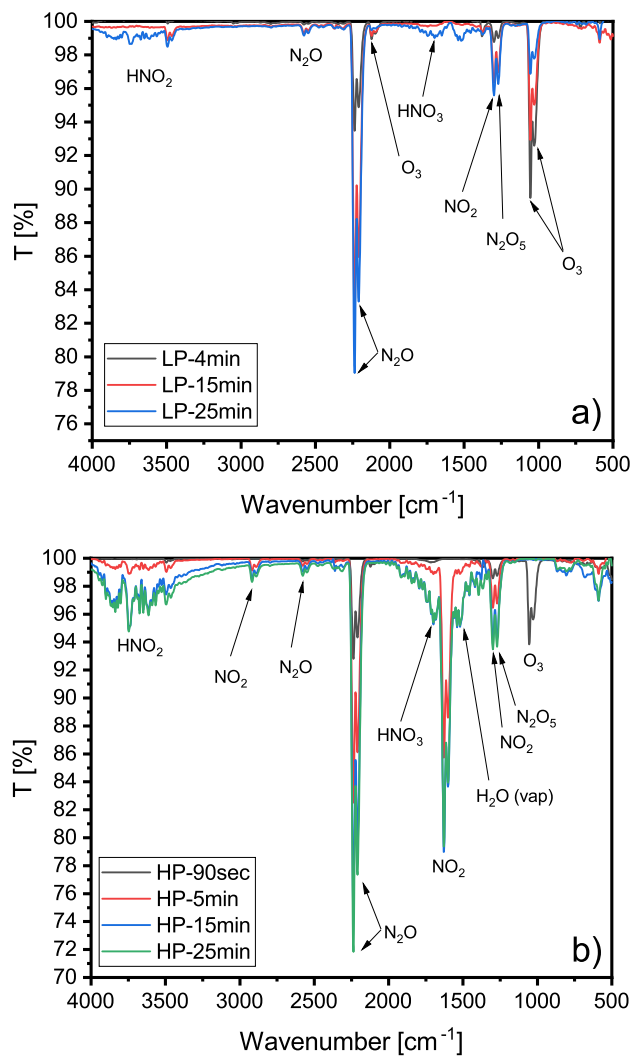
Figure 4.3: FTIR measurement of the gas phase generated at different power modes:
a) low power and b) high power at different time points

In an air plasma, several studies reported the production of high concentration of excited nitrogen N_2 $(A^3\Sigma_u^+)$ [121], [122] & [155]; which recombined with O_2 present in the gas environment to form N_2O (R3). From the Figure, the concentration of N_2O increases with the time treatment which is linked to the higher production of molecular nitrogen.

$$N_2(A^3\Sigma_u^+) + O_2 \rightarrow N_2O + O \quad (R3)$$
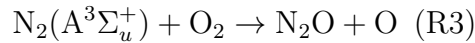
From the Figure, peaks of O_3 are also reported with its intensity decreasing with exposure time. The intensity decrease of ozone can be explained by its role in the formation of NO_2 and N_2O_5. Vibrationally excited N_2 and O enhance the formation of nitrogen oxide (NO, (R4)) which reacts with O_3 to form NO_2 (R5).

$$N_2\left(\nu\right) + O \rightarrow NO + N \quad (R4)$$

$$O_3 + NO \rightarrow NO_2 + O_2 \quad (R5)$$
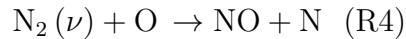
The mechanisms of formation of N_2O_5 is relatively complex and can be found in [156]. From this study, they demonstrate that the presence of ozone combined with nitrogen oxide at temperatures around 60 °C to 80 °C favour the formation of N_2O_5 and NO_2. In this study, the temperature of the electrode was measured and reached a maximum of 75 ± 2 °C after 25 minutes treatment, corroborating with previous description. Peaks of HNO_3 were also detected associated to the recombination of N_2O_5 with water vapor molecule present in the gas environment (R6).

$$N_2O_5 + H_2O\,(vap) \rightarrow 2HNO3 \quad (R6)$$
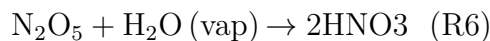
Figure 4.3 b) reports the peak intensities for the high power mode. Similar to the low power mode, peaks of N_2O, NO_2, N_2O_5, HNO_3 and O_3 are shown. Compare to the low power mode, peaks of N_2O and NO_2 are stronger due to a stronger generation of nitrogen oxide and the fast quenching of ozone leading to a plasma mainly dominated by nitrogen reactive species. Furthermore, the temperature of the electrode is close to 100 - 110 °C which enhance the ozone quenching as it has been reported in [157]. Peak of water vapour are also shown which can be linked by the rise of the temperature from the water bulk exposed enhancing the relative humidity of the gas phase. Thus, enhancing the formation of HNO_3 and HNO_2.

4.3.2   Chemical comparison on the PAW chemistry

Following previous section, the final chemistry of the PAW through direct and indirect plasma exposure will be drastically impacted. Figure 4.4 reports the PAW chemistry obtained by both plasma systems. When looking at the pH, both devices are able to decrease the pH of the purified water from 6.5 to below 2 after 16 minutes treatment. The decrease is sharper for the indirect treatment which could be explained by a higher plasma surface area in the indirect treatment compare to the direct treatment.
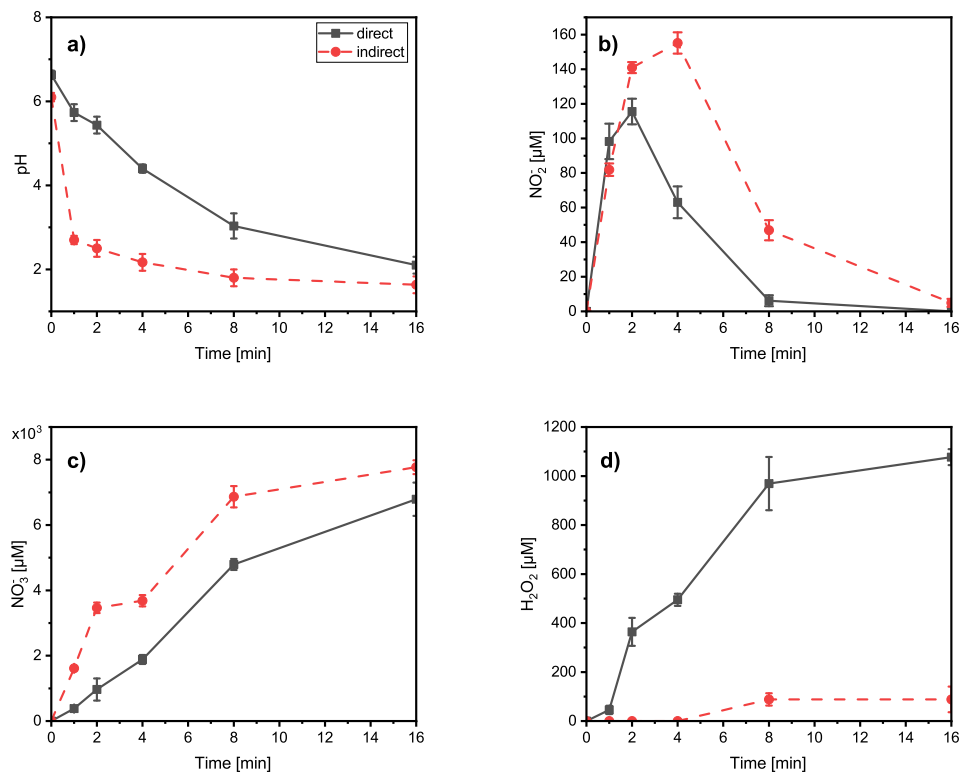
Figure 4.4: Kinetic evolution of: a) pH, b) nitrite concentration, c) nitrate concentration, and d) hydrogen peroxide from direct and indirect plasma treatment

In a SBD at high power, the reactor enters in a reactive nitrogen mode which enhance the formation of nitrogen species such as NO_2 and HNO_3, those species dissolved into the liquid phase affecting the acidity of the final concentration (also observed in chapter 5). Whereas, in the direct contact the pH is mostly dominated by the streamers reaching the surface of the solution and enhancing the dissociation of the water molecules.

Figure 4.4 a) shows higher concentration of nitrate for the indirect treatment with

a maximum peak obtained at 155 ± 2 µM after 4 minutes. The direct treatment reaches a maximum after 2 minutes treatment with a concentration at 115 ± 7 µM. For both reactors, the concentration of NO_2^- increase drastically in the first 2 minutes of exposure then decrease slowly until the end of the process. This trend has been widely reported in other works as well in the work presented in chapter 5; briefly, through oxidoreduction and recombination, NO_2^- are recombined into NO_3^- by the presence of ozone in the environment (R7) as well as used to form nitrous acid (R8).

$$NO_2^- + O_3 \rightarrow NO_3^- + O_2 \quad (R7)$$

$$NO_2^- + H^+ \rightarrow HNO_2 \quad (R8)$$
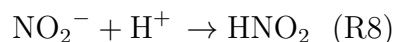
Figure 4.4 b) shows the kinetic evolution of the nitrates concentration increasing gradually to reach a maximum after 16 minutes treatment, respectively 7 ± 0.5 mM for the direct treatment and 7.7 ± 0.2 mM for the indirect treatment. The concentration of hydrogen peroxide (Figure 4.4 d)) is drastically different with the direct contact being the most efficient in its production. Concentrations reached a maximum of 1 ± 0.3 mM after 16 minutes treatment for the indirect treatment, where the concentration stayed stable at 88 ± 10 µM for the indirect treatment for the same exposure time. This observation is in agreement with the dissociation of the water molecule which recombined into H_2O_2 directly into the water bulk instead of generation into the gaseous phase followed by a dissolution process (R9).

$$OH^\bullet + OH^\bullet \rightarrow H_2O_2 \quad (R9)$$
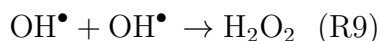
Comparatively, in a SBD the formation of hydrogen peroxide is lead by the re-combination of OH$^\bullet$ radicals formed directly into the gas phase. However, further experiment on SBD interactions with water samples indicated that those species were unable to reach the water bulk. Chapter 5 provide further details on this observation. Finally, from the Figure, both waters treated by direct and indirect contact have their chemistry modified by plasma exposure which make them suitable for bio-decontamination. Strong concentration of $NO_2{}^-$ and $NO_3{}^-$ combined with low pH can lead to the presence of nitrous and nitric acid. The direct contact will also paramount this parameter by the presence of H_2O_2 which is renown for being a strong oxidiser notably used in medical environment [158].

4.3.3   Potential for bacterial inactivation
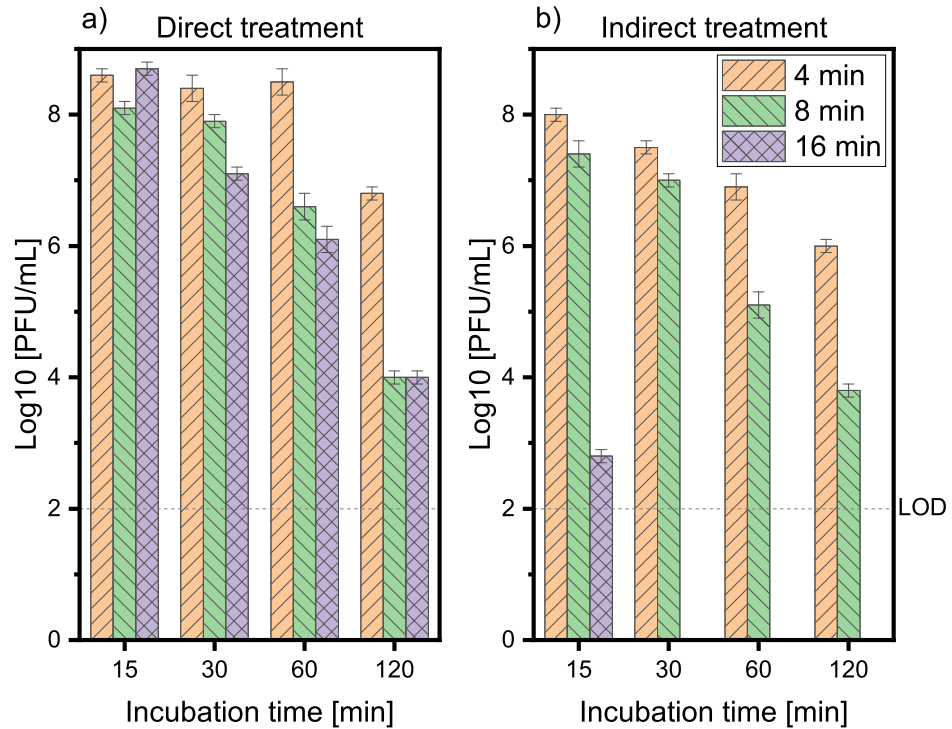
Figure 4.5: Bacterial inactivation by a) PAW formed by direct treatment and b)
PAW formed by indirect treatment

Figure 4.5 a) shows the inactivation obtained through direct plasma treatment of

the water. PAW were obtained after 4, 8 and 16 minutes of exposure and directly

added in contact with the contaminated pallets; the pallets and water were then

incubated for period of time going from 15 min to 120 minutes. For the 4 min-PAW,

the log-reduction goes from 8.9 ± 0.1 to 6.8 ± 0.1 log after an incubation of 120 min.

Whereas, PAW formed after 8 and 16 min goes from 8.9 ± 0.1 log to 4 ± 0.2 log

after an incubation of 120 min. The results suggest that a longer period incubation

time favour the bacterial inactivation. In terms of chemistry, the results suggest than
the hydrogen peroxide combined with the low pH are the main responsible of those
results which can be related to observation done in [159]. Comparatively, Figure
4.5 b) shows a drastically better inactivation. The 4 min- and 8 min- PAW remain
similar to the results obtained with the direct treatment (respectively 8 ± 0.1 log
to 6 ± 0.1 log and 7.4 ± 0.2 log to 3.8 ± 0.1 log after an incubation time of 120
minutes). The 16 min-PAW shows the best results out of the others with 2.8 ± 0.1
log reduction after an incubation of 15 minutes and below the limit of detection for
longer period (LOD: limit of detection). Those results can be linked by the strong
concentration of oxidisers in a strong acidic environment (pH $= 1.6 \pm 0.2$), this can
be underline with the high concentration of nitrous acid present in the 16 min-PAW
solution (around 280 ± 2 µM). Chapter 5 confirms those results with similar results
obtained during the activation of different tap waters.

4.4   Conclusion

In this chapter both direct and indirect plasma treatment were used to form plasma activated water. The gaseous phase analysis indicated the variation between those two reactors impacted the final chemistry of the PAW. The FTIR results obtained for the indirect treatment indicated the presence of two working modes with a low power mode leading to the formation of more reactive oxygen species where the high power mode enhanced the generation of nitrogen species with a quenching of the ozone molecules. The OES spectrum obtained from the direct treatment observed the presence of common excited nitrogen molecules combined with oxygen species under the form of O, OH and O_3. The direct system showed interesting results for the generation of hydrogen peroxide where the indirect treatment was unable to provide equivalent concentration. Both PAW formed with direct or indirect treatment showed great potential for the inactivation of bacterial samples. However, the indirect treatment remained more efficient indicating that strong concentration of hydrogen peroxide combined with low pH was inefficient towards acidic PAW with strong concentration of nitrogen species such as NO_2^- and NO_3^-. Due to the possible recombination of NO_2^- into HNO_2 in an acidic environment, this suggest that PAW with high concentration of nitrous acid could potentially lead to better bacterial inactivation. Chapter 5 will investigate further the indirect treatment of water samples with the use of tap waters from different regions. This will show the capabilities of the reactors to provide a standard PAW suitable for bio-decontamination applications, as well as confirming the initial results obtained in this chapter.

Chapter 5

Study on the uniformity of PAW: influence of the initial water chemistry

Results and discussions detailed in this chapter were reported in: Simon, S., Salgado, B., Hasan, M. I., Sivertsvik, M., Fernández, E. N., Walsh, J. L. (2022). Influence of Potable Water Origin on the Physicochemical and Antimicrobial Properties of Plasma Activated Water. Plasma Chemistry and Plasma Processing, 1-17.

5.1   Introduction

Despite the growing body of evidence demonstrating the benefits of PAW, its translation into a useable technology at the industrial scale remains fraught with difficulties. It is well-known that the choice of plasma reactor has a dramatic impact on the reactivity of the generated PAW [67], yet the most effective reactor is not necessarily the easiest to scale. Furthermore, the operating gas plays a crucial role in dictating the level of PAW reactivity, with several studies demonstrating the benefits of operating in a noble gas environment with small oxygen admixtures [160],[161]. Despite

this, most real-world applications are inevitably restricted to operation in ambient air for economic reasons [162]. A third vital point, which is often overlooked in laboratory-based studies of PAW, is the quality of the initial water source. Most studies reported in the scientific literature employ purified water (e.g., distilled or reverse osmosis filtered) or local tap water for PAW generation, with little consideration as to how the composition of the water may influence the ability of plasma to activate it. Certainly, for widespread adoption of PAW technology the use of local potable water sources, with minimal additional filtration, will be of paramount importance for cost effective operation.

In this chapter, to investigate the impact of water origin on PAW generation, potable water samples were acquired from five countries including France (Paris), Norway (Stavenger), Palestine (West Bank), Slovenia (Vipava Valley) and the United-Kingdom (Liverpool). All water samples were subjected to an identical air plasma treatment and the formation kinetics of various aqueous phase species were probed. The buffer capacity of the plasma-exposed water samples was also investigated and compared to a chemical model. Finally, to highlight the impact of initial water composition on the effectiveness of PAW, water samples from the UK and Palestine were plasma activated and used to inactivate *Staphylococcus aureus* and *Escherichia coli*.

5.2 Materials and methods

The conception of the plasma reactor, and characteristics of the power supply used for this study can be found in section 3.1.1 of chapter 3. Similar to chapter 4, the relevant background theory, data interpretation, and diagnostic tools are presented respectively in chapter 2 and chapter 3.

5.2.1 Plasma system and exposure conditions

The plasma reactor was slightly modified for the study as reported in Figure 5.1. A sinusoidal voltage up to 12 kVpp at a frequency of 27 kHz was used. To monitor the discharge power in real-time, the current and voltage signals were multiplied in the oscilloscope to obtain the instantaneous power which was averaged over multiple cycles to obtain the mean power. For all experiments, a constant operating power of 12 W was maintained for a maximum exposure of 25 minutes. During the plasma treatments, the SBD electrode was positioned above 5 mm a petri dish containing 20 mL of the water sample which was stirred at 200 rpm using a stir plate. During plasma operation the concentration of O_3 within the reactor was monitored in real-time using UV absorption at a light intensity of 253.6 nm. The Beer-Lambert law was used to determine absolute O_3 density using an absorption pathlength of 10 mm and an absorption cross-section of 1.1329×10^{-17} cm^2.molecule^{-1}.
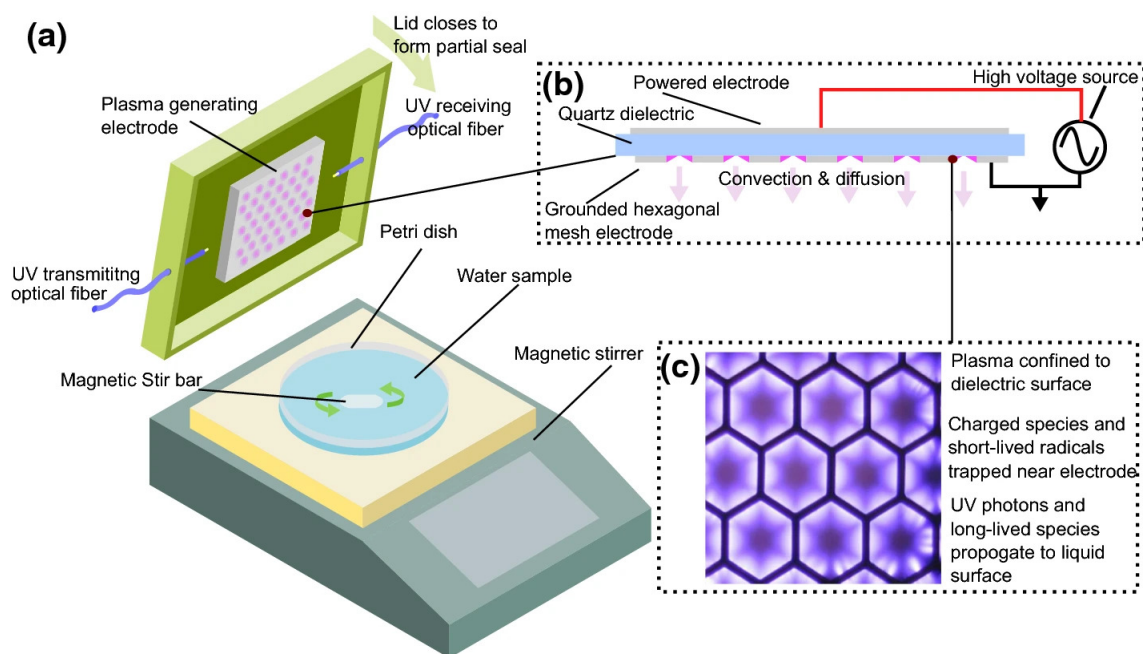
Figure 5.1: Experimental setup used for plasma activation of water samples; (a) experimental configuration showing surface barrier discharge, water sample and optical fibers for in-situ absorption measurements, (b) schematic of surface barrier discharge electrode, and (c) photograph of the discharge operating in ambient air at an average power of 12 W.

5.2.2 Numerical model of reactive species transport

The numerical model used in the study is similar to that reported previously by Hasan & Walsh [151]. A description of the model can be found in chapter 3, section 3.2.4. The model was run for an applied power of 12 W until the long-lived species filled the gap between the electrode and the surface of the water. All geometrical parameters of the model were set to match those used in the experiment.

5.2.3 Chemical analysis of the PAW samples

The chemical composition of the PAW formed was quantified using the protocol described in chapter 3, section 3.3. The calibration curves were created using filtered water generated with a Select Analyst water purification system (SUEZ Water Technologies & Solutions) including carbon pre-treatment, reverse osmosis, and deionisation. All experiments were conducted in triplicate and at different times and room temperature. In each case, filtered water was used as blank. Measurements were taken before plasma exposure and every 5 min during the exposure.

5.2.4 Assessment of microbial inactivation efficacy

The bacterial inoculation follows the protocol described in chapter 3, section 3.4. Based on the liquid characterisation results, two water samples were selected that showed the greatest divergence in chemical composition following plasma exposure and their antimicrobial efficacy was explored. Water from the UK and Palestine, alongside a control sample of filtered water, were plasma activated and tested against *Escherichia coli* BW25113 and *Staphylococcus aureus* USA300 JE2, as representative Gram-negative and Gram-positive species. The culture were incubated for 1 hour at room temperature and resuspended in PBS solution. Several dilutions were prepared and inoculated in LB agar and TSA plates for the determination of E. coli and S. aureus, respectively, and incubated for 24 hours at 37 °C. A colony forming unit (CFU) count was performed and reported as log CFU/mL. Experiments were performed in triplicates across multiple days and room temperatures.

5.2.5 Potable water samples

To investigate the impact of plasma exposure on water sourced from different geological locations, potable water samples were obtained from five different countries, the characteristics of their origin are detailed in Table 5.1.

Geographical origin	Water sources
France, Paris	Aquifers (Ile-de-France, Bourgogne, and Normandie) and rivers (Seine and Marnes) [163]
Norway, Stavanger	Lakes Romsvatn and Stølsvatn in Bjerkreim and lake Storavatnet in Gjesdal [164]
Palestine, West Bank	Mountain Aquifer (Western Aquifer Basin, North-Eastern and Eastern Aquifer Basin) [165]
Slovenia, Vipava Valley	Vipava river basin (springs and rivers from the region) and groundwater from the Vipava valley [95]
United-Kingdom, Liverpool	Deer river and Vynwy Lake [166]

Table 5.1: Origin of the potable water samples

All the potable water samples detailed in Table 5.1 are assumed to be processed in a similar fashion; following collection from the source they are subjected to different processing stages: pre-treatment, coagulation/flocculation/sedimentation, and filtration [167]. The pre-treatment removes the first traces of biological contamination (i.e., microorganisms, algae, etc.); coagulation/flocculation/sedimentation are used in conjunction, in which small particles are removed. The filtration stage consists of passing the water through different layers of sand, gravel, and charcoal to achieve chemical filtration. During this last stage, a small amount of chlorine (in a range of 0.2 to 1 mg.L^{-1}) or ozone (maximum of 0.02 mg.min.L^{-1} at 5 °C, pH 6-7) is added to the water for microbial disinfection purposes [168],[169]. Despite the

considerable efforts of potable water providers, it is inevitable that the final water
chemistry is impacted by the soil characteristics of the source (e.g., porosity, miner-
als, etc.) and localised human activity (e.g., agriculture, industry). Consequently,
a significant variation in the chemical composition of water samples collected from
different geographical locations is inevitable. Table 5.2 shows the chemical compo-
sition (average and standard deviation in triplicates) of the five water samples used
in this study.

Country	pH		NO_3^- (uM)		HCO_3^- (mM)	
	Mean	SD	Mean	SD	Mean	SD
France (FR)	8.2	0.1	148	6.6	2.96	0.05
Norway(FR)	8.2	0.1	ND	ND	0.89	0.00
Palestine (PAL)	8.0	0.1	300.4	38.7	5.11	0.07
Slovenia (SLO)	8.1	0.1	88.1	12.4	2.17	0.04
United-Kingdom (UK)	7.9	0.1	46.4	13	0.56	0.05

Table 5.2: Initial chemical composition of tap water from the different countries
included in this study

No water samples were found to contain nitrites and the concentration of dissolved
carbon dioxide and carbonates are not presented as they were found to be signifi-
cantly lower than that of the bicarbonates due to the pH of the samples.

5.3 Results and discussions

5.3.1 Plasma and gas phase chemistry

In a low temperature plasma, ionisation, excitation, and dissociation reactions of O_2,
N_2 and H_2O, result in a plethora of both short- and long-lived reactive species, such
as O, OH, NO, O_3, H_2O_2. Specifically, in a surface barrier discharge, the powered
and grounded electrode are separated by a thin dielectric material which changes the
shape of the electric field. This characteristic reduces the breakdown voltage and
promotes plasma formation along the edges of the electrode, where the electric field
is the greatest. Short-lived species are primarily created by electron driven reactions
involving energetic electrons within the plasma, such as those highlighted in R1 –
R5:

$$H_2O + e^- \rightarrow H^\bullet + OH^\bullet + e^- \quad (R \cdot 1.)$$

$$e^- + O_2 \rightarrow O^\bullet + O^\bullet \quad (R \cdot 2.)$$

$$e^- + N_2 \rightarrow N^\bullet + N^\bullet \quad (R \cdot 3.)$$

$$O^\bullet + N_2 \rightarrow NO + N^\bullet \quad (R \cdot 4.)$$

$$N^\bullet + O_2 \rightarrow NO + O^\bullet \quad (R \cdot 5.)$$
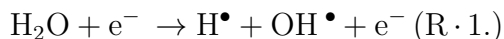
Beyond the discharge region, where the electric field is low, electrons rapidly cool
below the energy threshold required for excitation, dissociation, and ionisation reac-
tions to occur. Consequently, many of the production pathways of short-lived species

are inhibited and their density drops rapidly as they react to form long-lived species. As the SBD electrode used in this study was confined within a sealed volume, quantification of species densities was limited to the measurement of ozone using optical absorption, a process that required no gas to be drawn from the enclosure. Figure 5.2(a) shows the temporal evolution of ozone within the reactor as a function of plasma generation time. Notably, an increasing discharge power led to a higher ozone density peak followed by accelerated quenching. Ozone quenching in an air fed atmospheric pressure SBD has been widely studied [157], and it has been posited that the rapid formation of NO is attributed to the reaction between vibrationally excited N_2 and O within the discharge region, which subsequently reacts with O_3 to form NO_2, R6 – 8 [117].

$$O + O_2 + M \rightarrow O_3 + M \, (R \cdot 6.)$$

$$N_2(\nu) + O \rightarrow NO + N \, (R \cdot 7.)$$

$$O_2 + NO \rightarrow NO_2 + O_2 \, (R \cdot 8.)$$
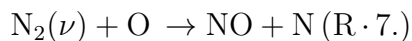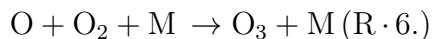
Using the computational model described in section 2.2, the space resolved density of key RONS was calculated, Figure 5.2(b). As the model only captured the first few seconds of discharge operation, ozone quenching was not captured. It is clear from the Figure that many of the short-lived RONS, including OH and HO_2 were unable to reach the liquid surface, situated at a position 5 mm from the discharge. All charged species and various other short-lived species, such as O and N, were restricted to the discharge region (40 µm) as they were rapidly converted into more stable long-lived

species. Therefore, they played no direct role in activation of the liquid sample. Downstream of the SBD electrode, the calculated ozone density is overestimated by approximately 15 % compared to the measured value; this is a likely result of the spatial averaging associated with the UV absorption measurement technique. Critically, these results indicate that the only plasma generated species able to reach the liquid surface are O_3, N_2O, NO, and NO_2; therefore, these species must act as precursors for liquid phase reactions.
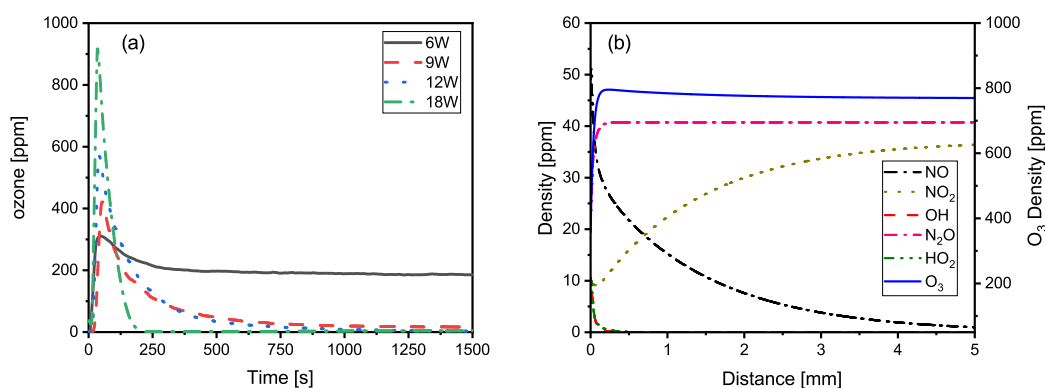
Figure 5.2: (a) Evolution of Ozone concentration measured in-stiu at a constant dissipated plasma power of 6, 9, 12 and 18 W, and (b) calculated species densities as a function of distance downstream of the SBD electrode at a dissipated plasma power of 12 W.

5.3.2 Kinetic evolution of the pH, nitrite, nitrate, and nitrous acid

It is well established that water exposed to air plasma experiences a drop in pH; in the case of purified water (i.e., distilled or deionized) the decrease can occur very rapidly and reach very low pH values (e.g., 1–2) [170]. Figure 5.3(a) shows the

evolution of pH for the five samples with increasing plasma exposure time. From
the Figure, it can be observed that the water samples did not respond equally to the
plasma treatment. Water from the United Kingdom and Norway showed a significant
drop in pH, decreasing from pH 8 ± 0.1 to below 3 ± 0.2. The pH of water sourced
from France and Palestine was not affected by plasma exposure, remaining stable
at 8 ± 0.1. Finally, water sourced from Slovenia initially had a pH of 8.1 ± 0.1
and was observed to linearly decrease to a pH of 7.5 ± 0.0 after 20 minutes of
exposure. Subsequent plasma exposure resulted in a drop of pH to a final value of
6.7 ± 0.1.
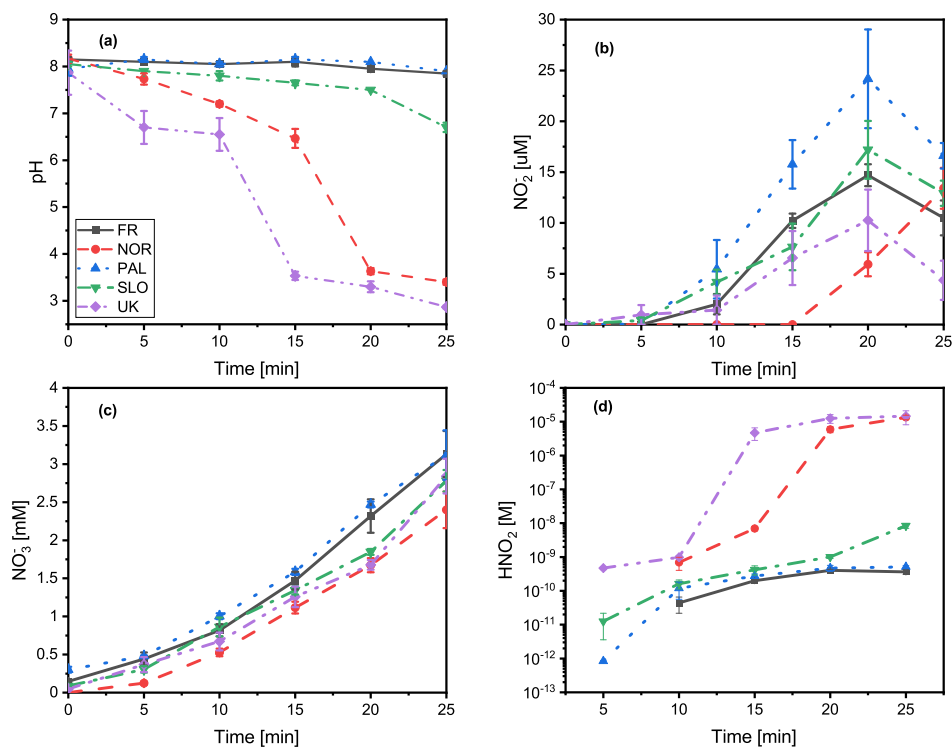
Figure 5.3: Kinetic evolution of: (a) pH, (b) nitrite concentration, (c) nitrate concentration, and (d) nitrous acid concentration.

Figure 5.3(b) shows the kinetics of nitrite formation during plasma exposure. All water samples followed a similar trend, with an initial lag phase, followed by a sharp increase and, with the exception of the Norwegian water, a subsequent drop in concentration. Similar trends have been reported previously for nitrite formation in plasma-activated water [171]. Despite showing the same trend, the absolute values were found to differ, with water from Palestine showing the highest concentration (24.1 ± 4.8 µM), and water from the UK (10.2 ± 3.0 µM) showing the lowest peak concentration. The rapid rise in nitrite concentration can be attributed to the conversion of nitric oxide from the plasma into nitrogen dioxide through reactions 7 and 8. Nitrogen dioxide is readily dissolved into the aqueous phase, leading to the formation of nitrites, nitrates, and hydronium ions through the reaction $2\,NO_2 + H_2O \rightarrow NO_2\,(aq)^- + NO_3\,(aq)^- + O_2\,(R \cdot 9.)$ [172]. The observed reduction in nitrite concentration has been linked to an oxidoreduction reaction that can occur leading to the conversion of nitrites into nitrates due to the presence of ozone: $NO_2^- + O_3 \rightarrow NO_3^- + O_2\,(R \cdot 10.)$ and the recombination of nitrites into nitrous acid with hydronium ions $NO_2^- + H^+ \rightarrow HNO_2\,(R \cdot 11.)$ [173]. Figure 5.3(c) shows the kinetics of nitrate formation in the five water samples during plasma exposure. In all cases, nitrate concentration was observed to increases almost linearly, reaching a maximum after a plasma exposure of 25 minutes. Only minor differences were found in the final concentration, with the highest levels obtained for the French and Palestinian water, with both reaching 3.1 ± 0.3 mM. The evolution of nitrous acid formation is shown in Figure 5.3(d). From the Figure, it is clear that plasma exposure generates nitrous acid which increases in concentration with exposure time and

coincides with the measured decrease in the pH. This is attributed to the accumulation of hydronium ions in the samples through reaction R. 9. and the conversion of nitrites into nitrous acid through reaction R. 11. Critically, the final concentration of nitrous acid was found to vary over four orders of magnitude depending on the origin of the water sample. As nitrous acid is known to be a major antimicrobial component of PAW [174], these results indicate that the five water samples may differ significantly in their antimicrobial properties.

5.3.3 Carbonic acid, bicarbonates and carbonates

In all untreated water samples, the dominant form of carbonic compounds was found to be HCO_3^- and was present in different concentrations; the Palestinian and UK tap water were found to contain, respectively, the highest (5.10 ± 0.06 mM) and lowest (0.55 ± 0.04 mM) concentrations. The kinetic evolution of bicarbonate, carbonic acid and carbonates is presented in Figure 5.4(a), (b) and (c), respectively. The decrease of pH in the UK, Norwegian and Slovenian water is due to the conversion of the carbonates into bicarbonate and carbonic acid. Despite bicarbonates being the dominant form in the solution ($pKa\,(CO_3^{2-}/HCO_3^-) = 10.32$), there is however, a small concentration of carbonate present. The free hydrogen ions created through plasma exposure (R. 1.) and hydronium ions introduced by NO_2 dissolution (R. 9.) shift the equilibrium of the carbonic compounds in the water. The carbonates are therefore converted into bicarbonate following the reaction:

$$CO_3^{2-} + H^+ \rightarrow HCO_3^- \quad (R \cdot 12.)$$
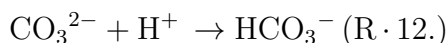
When the pH reaches the second value of the acidic constant (pKa $(HCO_3{}^{2-}/H_2CO_3 =$
6.37), the bicarbonates are transformed into carbonic acid (R. 13.). The remaining
carbonate present in the water is converted into carbonic acid (R. 14.) as the solution
becomes more acidic.

$$HCO_3{}^- + H^+ \rightarrow H_2CO_3 \ (R \cdot 13.)$$

$$CO_3{}^{2-} + 2\,H^+ \rightarrow H_2CO_3 \ (R \cdot 14.)$$
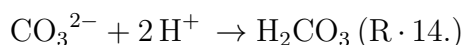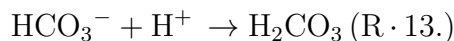
Reactions 13 & 14 can also be used to explain why water from France and Palestine
are resistant to plasma induced acidification. Their initial concentration of carbon-
ates and bicarbonates is significantly higher, thus enhancing their buffering capacity
and explaining the reduction of nitrous acid through the scavenging of hydronium
ions formed in reaction 9.
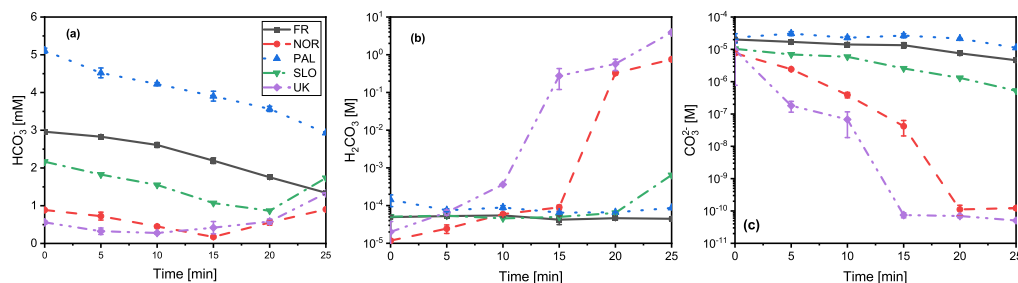
Figure 5.4: Kinetic evolution of: (a) bicarbonate, (b) carbonic acid, and (c) carbon-
ate concentration.

5.3.4 Buffer capacity of the treated waters

The buffer capacity or index is defined as the concentration of acid or base to add in
order to modify the pH of an aqueous solution. In potable water, the buffer capacity

is expressed as:

$$\beta = (\ln_{10}) K_{a1} [H^+] C_T \times \frac{K_{a1} K_{a2} + 4 K_{a2} [H^+] + [H^+]^2}{(K_{a1} K_{a2} + K_{a1} [H^+] + [H^+]^2)^2} \tag{5.1}$$

With $C_T = [H_2CO_3] + [HCO_3^-] + [CO_3^{2-}]$ the concentration of dissolved inorganic
carbon and, $K_{a1} = Ka_{[H2CO3]/[HCO3^-]}$ and $K_{a2} = Ka_{[HCO3^-]/[CO3^2-]}$ their respective
acidic constant [175].
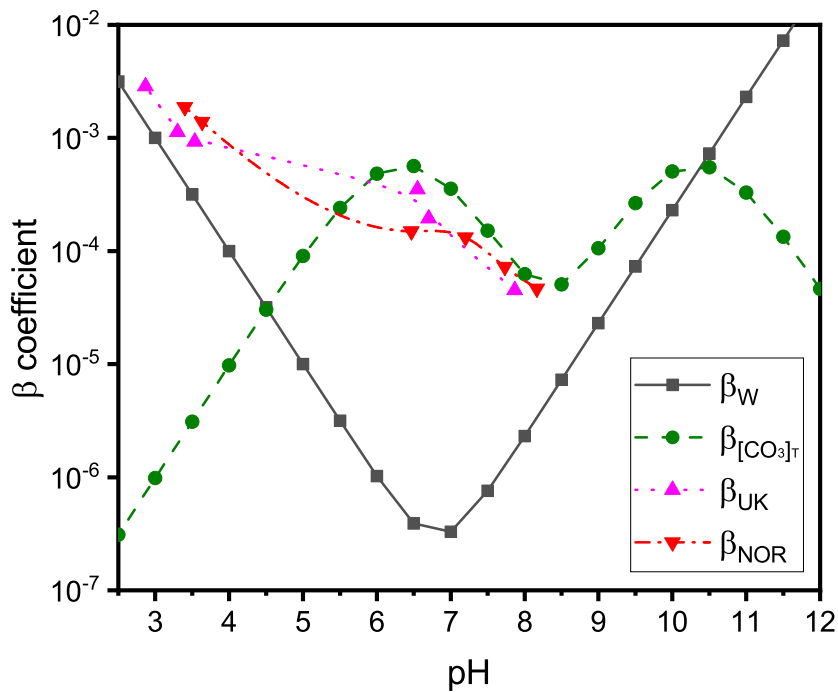
Figure 5.5: Buffer capacity β for the waters from UK and Norway and comparison
with $\beta_{[CO3]_T}$ and β_W.

The contributions of the water dissociation (β_W) and carbonate buffer system $\beta_{[CO3]_T}$
are shown in Figure 5.5. The β coefficient obtained for the samples from the UK and

Norway are also plotted for comparison with the chemical model. Waters from the
UK and Norway were the most affected by the plasma acidification, as the dissolved
carbonated species are converted in order to maintain the stability of the buffer
system (R. 12 – 14). As shown in the Figure, both waters follow the same trend
as the chemical model reaching a maximum when $pH = pKa_{[H2CO3]/[HCO3^{2-}]}$; water
from Norway has a lower maximum peak than the model which can be explained
by the initial low concentration of carbonic compounds present in solution. When
the pH decreases, the buffering system becomes unstable and β is dominated by the
contribution brought by (β_W). Both samples from the UK and Norway showed a
decrease in pH during plasma exposure and converge following (β_W). Consequently,
the free hydrogen ions (R. 1.) and hydronium ions (R. 9.) introduced to the system
are primarily responsible for the acidification of the water samples. Furthermore,
the calculation of the buffer coefficient for those samples indicates clearly that the
carbonic compounds are primarily responsible for the water buffering capacity to
the plasma exposure. The possible contribution brought by the dissolved cations
(e.g., Ca^+, Mg^{2+}, Na^+) is minimal. The β coefficient for water samples obtained
in France, Palestine and Slovenia were also compared to the chemical model (data
not shown). In all cases, their β coefficient remained stable ($\beta = 10\,e^{-4}, pH = 8\pm$
0.1) with a slightly increase for the water from Slovenia in agreement with its pH
($\beta = 10\,e^{-3}, pH = 6.7\pm 0.1$).

5.3.5   Formation of hydrogen peroxide and chlorine oxide

The formation of hydrogen peroxide in PAW has been reported previously and is considered an important component that contributes significantly to the oxidative potential of the solution [176]. In previous studies of noble gas plasma interaction with water, H_2O_2 formation in the liquid phase has been attributed to the interaction of OH at the liquid interface [177]. In the air-fed SBD configuration used in this study, OH radicals cannot reach the liquid interface, as confirmed by the work done by M. I. Hasan & J. L. Walsh in [151]. Consequently, the primary H_2O_2 production pathway is inhibited; an alternate pathway follows the recombination of hydroxyl radicals created in the plasma phase, $OH^\bullet + OH^\bullet \rightarrow H_2O_2$ (R.15.), and the subsequent diffusion of H_2O_2 to the liquid interface and its solvation following Henry's law. Notably, in all treated samples in this investigation, no H_2O_2 was detected using the standard colorimetric detection method with a $TiOSO_4$ reagent.

From an application perspective, the interaction between plasma generated reactive species in PAW and chlorine added by some water suppliers remains a key question. The influence of plasma exposure on Chlorine was investigated by Haghigat et al. and it was observed that Cl^- can scavenge $OH^\bullet$ to form $ClOH^{\bullet-}$; yet the product formed was unstable and rapidly decomposed (R. 17.). Under acidic conditions, the formation of $Cl_2^{\bullet-}$ from $ClOH^{\bullet-}$ (R. 18.) is favoured which recombines to form Cl^- and HOCl (R. 19.):

$$OH^{\bullet} + Cl^{-} \longleftrightarrow ClOH^{\bullet -} \quad (R \cdot 16.)$$

$$ClOH^{\bullet -} + Cl^{-} \longleftrightarrow Cl_2^{\bullet -} + OH^{-} \quad (R \cdot 17.)$$

$$Cl_2^{\bullet -} + OH^{\bullet} \longleftrightarrow Cl^{-} \quad (R \cdot 18.)$$
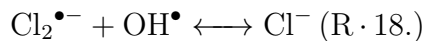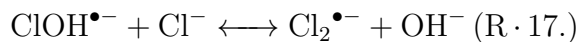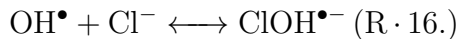
However, a significant concentration of chlorine is required (> 50 mg.L^{-1}) to form HOCl, which is not typical in potable water. With the samples considered in this study estimated to contain between 0.2 to 1 mg.L^{-1}, as described in section 5.2.5 [178].

5.3.6 Impact of water origin on PAW antimicrobial efficacy

To determine the impact of water origin on the antimicrobial properties of PAW, water samples from the UK (soft water) and Palestine (hard water) were selected as they showed the largest difference in composition. Two bacterial cultures were selected, *E. coli* and *S. aureus*, as representative Gram-negative and Gram-positive species. Several reports have shown Gram-positive species to be more resistant to plasma treatments [179], [180], which is mainly attributed to the presence of a thick peptidoglycan layer in their cell wall. The antibacterial efficacy of the various PAW samples is shown in Figure 5.6. To underline the dependency of the water origin, filtered water was plasma activated for 10 and 20 minutes, reaching a pH of 3.5 ± 0.1 and 2.8 ± 0.2, [NO$_2^-$] of 18.8 ± 3.0 and 60.0 ± 4.2 µM, [HNO$_2$] of 15.7 ± 4.6 and 298.7 ± 14.7 µM, respectively. As expected, plasma activated filtered water showed the greatest overall antibacterial activity, reaching the limit of detection (LOD) for

three out of four conditions tested. Water from the UK was less effective but was
still capable of reaching the LOD for both bacterial species following a 20 minute
exposure. In contrast, the Palestinian water showed no significant inactivation for
any condition tested.
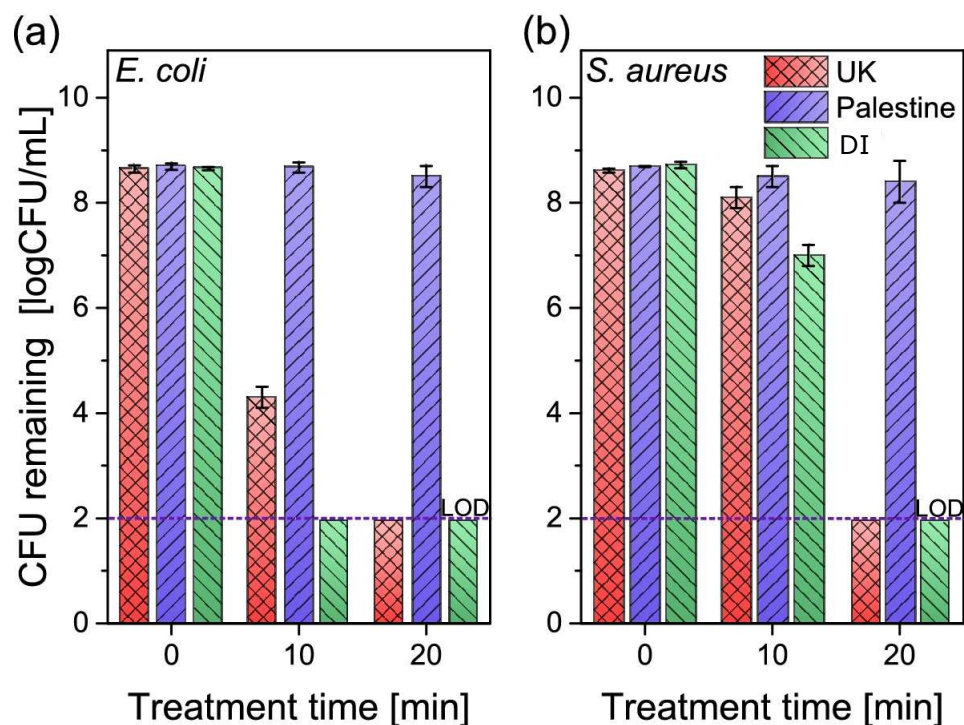
Figure 5.6: Impact of water origin on PAW inactivation of: (a) *E. coli* and (b) *S. aureus*.

Taking into account the chemistry of the plasma activated water samples (Figure 5.3 and 5.4), their antibacterial activity can be clearly linked by the dissolution of nitrogen oxide into the water (R. 9.), leading to the formation of nitrous acid by recombination of the nitrites with hydronium ions (R. 11.). After a plasma exposure of 10 and 20 min, both UK and Palestinian waters had a similar concentration of nitrites and nitrates, the main difference between them is their concentration of nitrous acid which, as explained in section 5.3.2, is known to be a potent antibacterial compound in plasma activated water. These results demonstrate that the antimicrobial efficacy of PAW is extremely sensitive to the initial composition of the water source used, with potable water sources from different geographical locations showing vastly different levels of antimicrobial activity. This finding has significant ramifications for the scale up and industrial application of PAW technology, where additional monitoring and filtration steps may be required to ensure consistency, traceability and efficacy.

5.4 Conclusion

In this study, five potable water samples were obtained from different geographical locations. Their initial composition was analysed, and the evolution of pH, nitrate, nitrite, nitrous acid and carbonate compounds was evaluated during exposure to an identical air plasma treatment. It was found that water from the UK and Norway showed the most significant decrease in pH (from 8 to below 3) associated with the highest concentration of nitrous acid (respectively 14.5 ± 3.7 and 13.4 ± 2.0 µM),

while the pH of water from Palestine and France remained relatively unchanged. The concentration of nitrates appeared to be independent of the pH and the initial concentration of bicarbonates present.

As PAW technology is currently under intensive investigation for use as a novel antimicrobial, the impact of water origin on the antimicrobial potential of PAW was investigated. Based on the chemical characterisation of the potable water samples, water sourced from the UK and Palestine was activated and assessed against both gram-positive and gram-negative bacterial species. It was demonstrated that PAW created from UK water was an extremely effective antimicrobial agent; whereas PAW created from Palestinian water showed very little antimicrobial activity. The implications of these results are significant for the future development of PAW technology. If the technology is to be widely adopted in areas such as food security and healthcare, then efficiency, repeatability and traceability are of paramount importance. This study demonstrates that the inevitable wide variation in the composition of potable water from different geographic locations has a dramatic impact on the overall effectiveness of PAW. Given this, it is essential that steps be taken to analyse and possibly adjust the composition of any water source prior to plasma activation in order to guarantee the repeatability and ultimately, the safety, of the process.

Chapter 6

Generation of large volumes of PAW: scale-up using venturi

6.1 Introduction

This chapter presents the work done as part of the project to design a reactor capable of generating high volumes of PAW (1 L.min^{-1}). A plethora of reactors were designed by the community, however most reactors are able to produce few milliliters to a maximum of hundreds milliliters of PAW. In chapter 2, this problematic was reported and observed to be mainly due to the small surface-to-volume ratio obtained for theses configurations. Recently, groups within the PAW community explored ways to enhance the generation of PAW through cavitation process.

Knowing the objectives of Nofima, the work presented in this chapter was designed as a proof of concept with investigation on the chemistry of the PAW obtained. The cavitation process itself is not investigated as considered outside the scopes of the thesis. However, the theory and designs of such devices can be found in the book written by Reader-Harris, "Orifice Plates and Venturi Tubes" [181]. The chapter

is organised as follows: (1) a description of the experimental conditions, and the diagnostics tools employed to characterise both bubble size and PAW. (2) The main results obtained for the generation of PAW through the system; with discussion on the size of the bubble and the possible influences due to either the air/water intake or plasma. The chemistry of the PAW is also reported as well as a comparison between different plasma reactors. (3) conclusion on the study and the feasibility of the device with remarks on future investigation.

6.2   Materials and methods

The theory used in this work to generate cavitation was found in the book written by Franc and Michel, "Fundamental of Cavitation" [182]. Most cavitation processes are based on Venturi tubes, this work does not make exception and the design can be found in section 3.1.3 of chapter 3. The venturi was coupled to an annular DBD and powered with similar power supply as already reported in chapter 4 and 5. The relevant background theory and data interpretation are presented in chapter 2.

Figure 6.1 reports the key dimensions, input/output water flow and air input of the final design of the Venturi tube employed in this study.
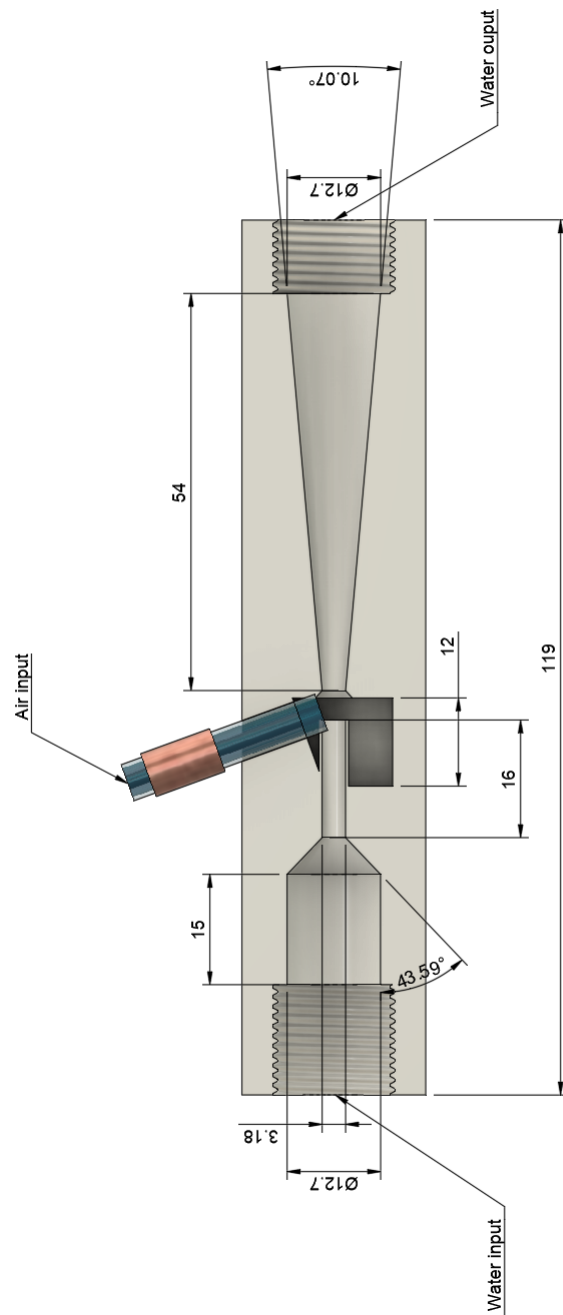
Figure 6.1: Schematic of the Venturi tube with key dimensions (values are in mm)

6.2.1 Experimental conditions

Aside of the design of the Venturi tube, two plasma reactors were employed in this study. The first consists of a quartz tube with a total length of 50 mm, an external diameter of 5 mm and internal diameter of 4 mm. A copper tape (30 × 5 mm) was placed at 10 mm from one of the extremity in order to form a ring which was connected to the power supply. On the other end of the tube, a wire was inserted and connected to the ground. The second plasma device, based on a surface barrier discharge, followed the same description as detailed in section 3.1.1 of chapter 3. Briefly, the SBD consisted on a quartz plate covered by a copper tape acting as the powered electrode and a grounded mesh was placed on the opposite side of the quartz plate. Both plasma devices were ran at both low and high mode similar to what has been done in chapter 4 and 5. The working power were set at 6 W and 10 W with a frequency of 33 kHz for the DBD, where the SBD was set at either 12 W or 30 W at a frequency of 28 kHz. Figure 6.2, shows a picture of the system in its initial setup.
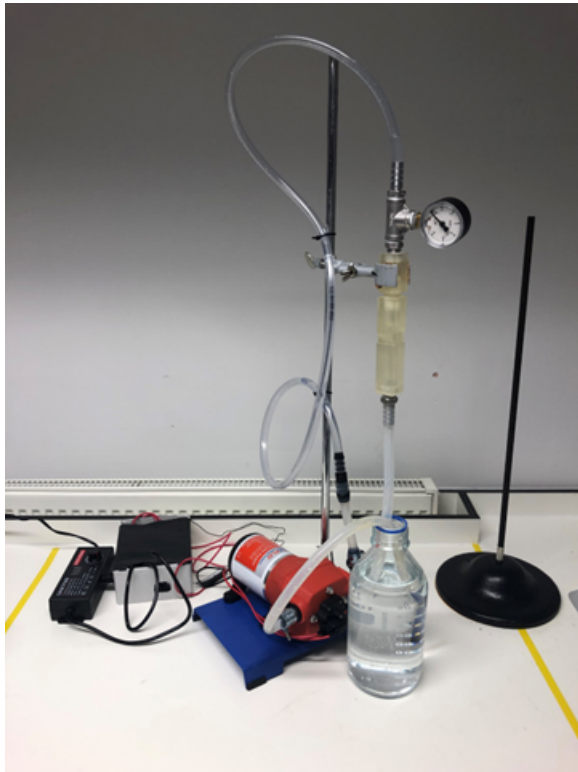
Figure 6.2: Picture of the system designed for this experiment.

From the Figure, the Venturi was connected to an external pump (Seaflo pressure
pump 41 Series, 12 V, 3.3 GPM/35 PSI) with a pressure gauge placed on the input
section of the tube. The outside of the tube was connected to a glass bottle containing
1 L of purified water. The system was also extended with an another Venturi tube
and mounted either in serial or parallel, see Figure 6.3.
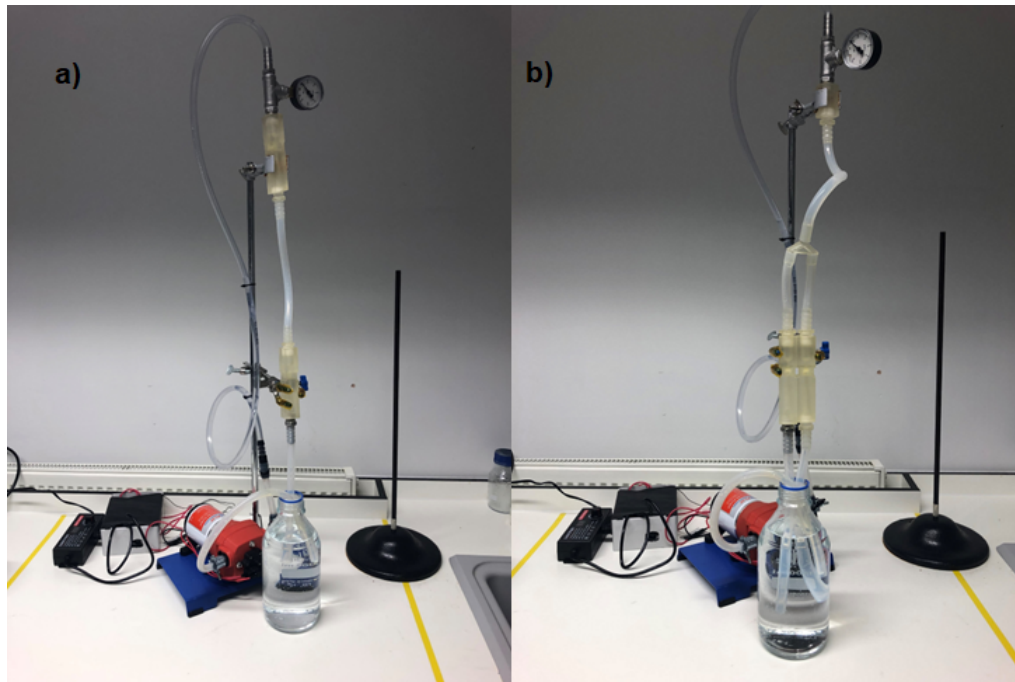
Figure 6.3: Configuration of the venturi set as a) in serial, and b) in parallel.

For all experiment, the water was treated for a maximum period of 30 minutes.

6.2.2   Tracking of the bubbles generated

A high-speed camera (Meros High Speed Digital Microscope) connected to an external computer was utilised to follow the formation of the bubbles in the Venturi. An LED backlighting with a diffuser was set up to record the process with 1024 * 1024 pixels resolution at 4100 frames per second.

6.2.3 Chemical analysis of the PAW

The chemical protocols can be found in chapter 3, section 3.3. For all experiment,
the blank was made using distilled water prepared beforehand in the same context
as detailed in chapter 4.

6.3 Results and discussions

6.3.1 Investigation on the distribution of the bubble size

The investigation regarding the size of the bubbles was done using the single Venturi
version of the system (section 6.2.1, the system was ran at different flow/pressure
conditions ranging from 2.5 L.min^{-1} at 0.2 bar to a maximum of 9 L.min^{-1} at 1.2
bar. The bubbles were recorded for three different cases: a) no intake air, b) air
intake and, c) plasma intake. Figure 6.4 reports the size of the bubble found for
those conditions.
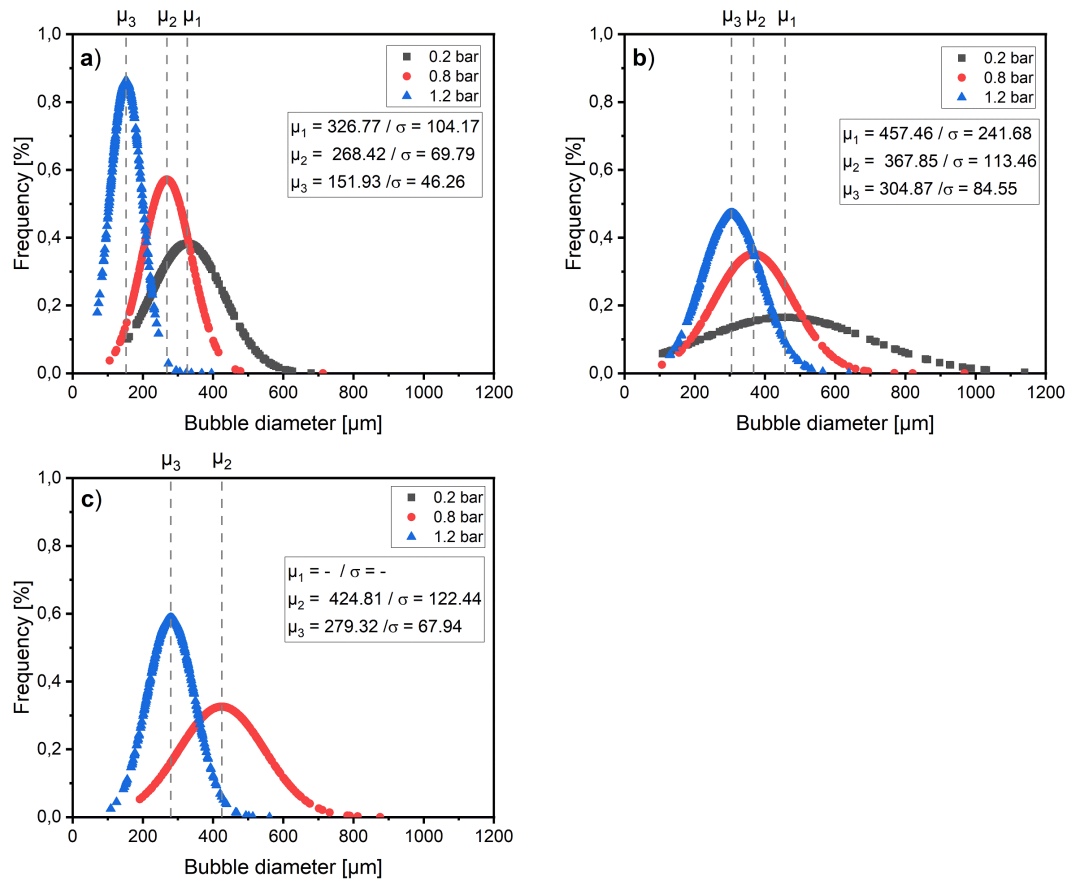
Figure 6.4: Comparison of the bubble size found for a) no air, b) with air intake,
and c) plasma intake.

In absence of intake air, the size of the bubble are dependent on the input pressure
and flow from the water pump. As shown in Figure 6.4 a), the mean size of the
bubble varies from 326.77 $\pm$ 104.17 µm at 0.2 bar to 151.93 $\pm$ 46.56 µm at 1.2
bar. In this scenario, the bubbles are only affected by the geometry of the Venturi

allowing the formation of microbubbles and reducing their mean size in agreement
with the rise of the water flow rate. In b), the aperture of the Venturi was left open
so the air can be sucked inside the tube. The air induce turbulences which will have
a negative impact on the mean size of the bubbles (respectively 457.46 ± 241.68 µm
at 0.2 bar, 367.85 ± 113.46 µm at 0.8 bar, and 304.87 ± 84.55 µm at 1.2 bar). When
the plasma is switched on as shown in c), the bubbles are found to have relatively
the same size as reported in b) with 424.81 ± 122.44 at 0.8 bar and 279.32 ± 67.94
µm at 1.2 bar. For the pressure of 0.2 bar, the size of the bubble were too big and
chaotic to be measured. As already reported in several studies, the efficiency of the
cavitating Venturi tubes depends on the cavitation phenomenon and its interaction
with turbulent flow, thus linked to the geometry of the tube [183], [184] and [185]. By
increasing the inlet flow rate, it appears that the device is suitable for the production
of relatively uniform microbubbles when set at a pressure of 1.2 bar; this trend was
also observed in similar work done by Gao et al. [186].

6.3.2 Efficiency on the generation of PAW through the Venturi system

6.3.2.1 Kinetic evolution of the main species through a single Venturi tube

To ensure a good activation of the water exposed, the main long lived species present
in the PAW were measured while performing the experiment and reported in Figure
6.5.

Figure 6.5: Kinetic evolution of a) the pH, b) nitrites concentration, c) nitrates concentration and d) nitrous acid concentration.

As expected and already demonstrated in chapters 4 and 5, the pH decreases consequently with exposure time going from a initial pH of 6.1 ± 0.3 to a minimum of respectively 3.7 ± 0.1 for a power of 9 W, and 3.6 ± 0.2 for a power of 12 W. This decrease can easily be associated with similar observation from the previous chapter and is mainly due to the dissolution of nitrogen oxide formed in the plasma and dissolved in the water bulk. However, the concentration of the nitrites appears to be different compared to the previous results obtained and the trend classically

found in literature as reported by Maheux et al. [171]. This could be due by the short residency time of the nitrogen oxide formed in the tube. As said previously, the air plasma is sucked into the Venturi at a flow rate up to 1.5 L.min^{-1}, at this flow rate most species formed in the tube are directly transferred into the microbubbles dissolving during the cavitation process. Concerning the concentration of nitrates, its rise appears to be delayed and to increase after a treatment time of 15 min for the 12 W to reach a maximum of 99.4 $\pm$ 7 µM; and after 20 min for the 9 W case with a maximum concentration of 107.4 $\pm$ 10 µM. This can be explained by the low formation of gaseous NO_3 within the plasma and its dissolution in the water bulk; furthermore the concentration of O_3 remains relatively low within the water bulk (maximum of 3 ppm after 30 min of treatment). As previously reported in chapter 5, O_3 is responsible of the possible conversion of NO_2^- into NO_3^- (see reaction R.10 of the same chapter). Finally, d) reports the concentration of nitrous acid measured during plasma exposure. Comparatively to the results obtained in the previous chapter, nitrous acid is formed by recombination of NO_2^- with hydronium ions. Knowing that the pKa of the couple $HNO_2/NO_2^- = 3.39$, the concentration of HNO_2 rises accordingly with the pH after 25 minutes of treatment reaching a maximum of 65.3 $\pm$ 5 µM for 9 W and 105.9 $\pm$ 10 µM for the 12 W after 30 minutes.

6.3.2.2 Comparison on the efficiency to generate PAW using serial or parallel configurations

As demonstrated in the previous section, the single Venturi tube appears to be able to modify the chemistry of the water to form PAW. This section aims to further

investigate this potential by reducing the treatment time in adding another Venturi tube, in this case the second tube will be either mount in serial or in parallel. In both cases, the annular DBD employed were powered from the same input power source at a power of 12 W.

Figure 6.6, reports the kinetic evolution of the main species analysed in the PAW after a treatment of 10 and 30 minutes for the different configurations. In a) the kinetic evolution of the pH is shown; for both serial and parallel configuration the pH reaches identical valued with a minimum obtained after an treatment of 30 min (respectively 3.1 ± 0.1 for the serial and 3.0 ± 0.1 for the parallel). This trend confirm that the secondary Venturi allow further acidification of the water due to the dissolution NO_2 into water, as expected the concentration of nitrites (reported in b) on the same Figure) is higher for both setups with a maximum obtained after 30 minutes. Similarly to the single Venturi, the concentration of nitrates reported in d) is delayed and reached a maximum after 30 minutes with concentrations up to 0.24 ± 0.10 mM for the serial and 0.3 ± 0.15 mM for the parallel.
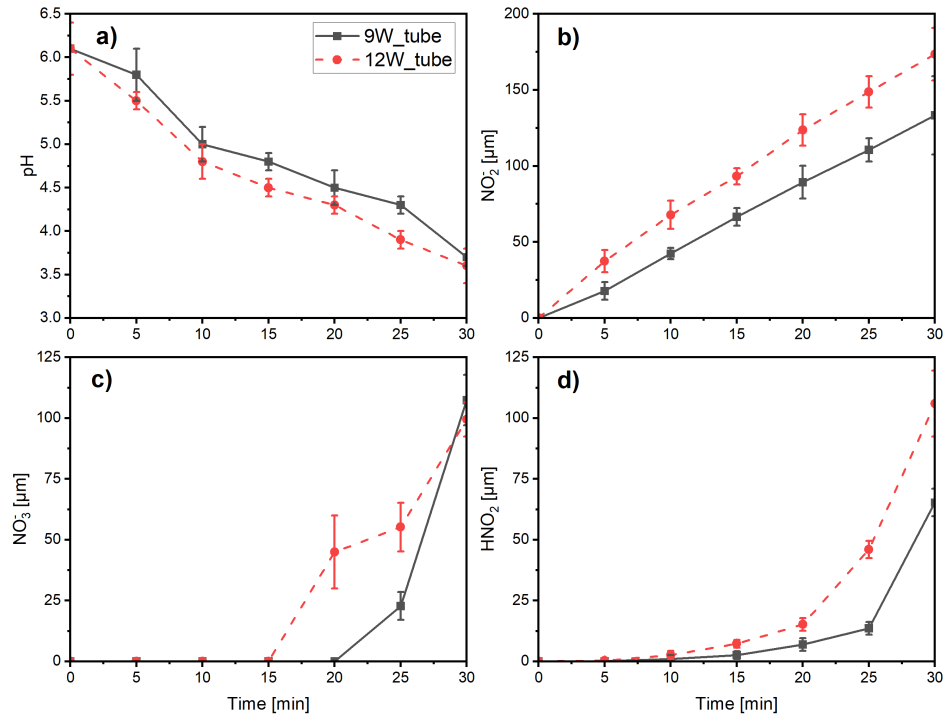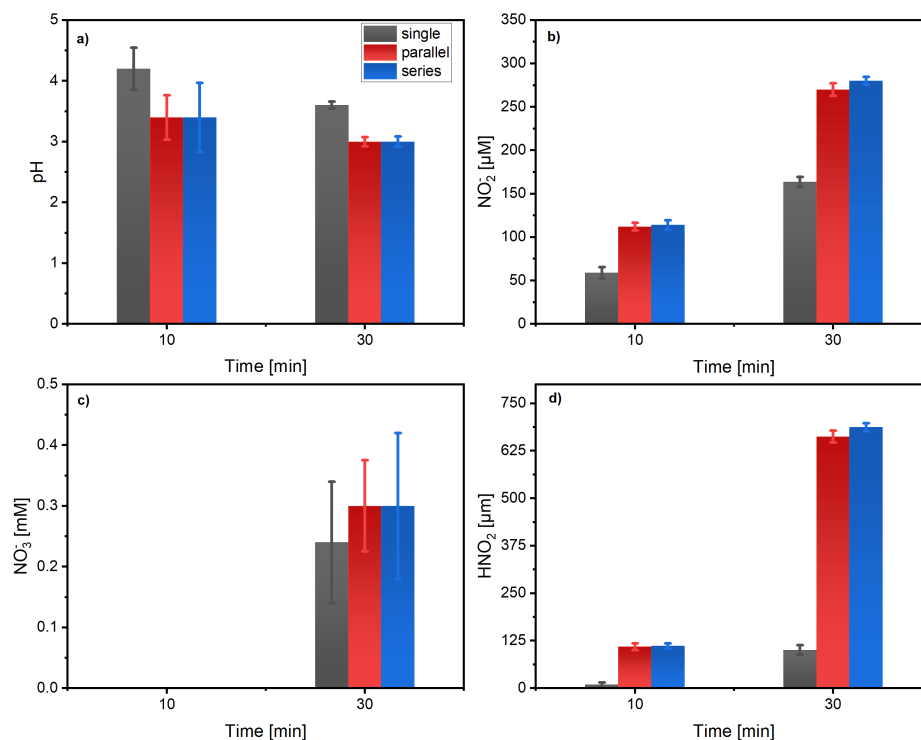
Figure 6.6: Kinetic evolution of a) pH, b) nitrites concentration, c) nitrates concentration and d) nitrous acid concentration for single, serial and parallel configurations

As the pH of the solution is lower, the concentration of nitrous acid obtained for both device is higher compared to the single Venturi with concentration up to 650 µM. The results obtained indicate that the input power plays a minimal role; whereas the addition of another Venturi tube appears to a major role in enhancing the PAW chemistry. Finally, the configuration type (serial vs parallel) plays a minor effect on the efficiency of the generation as the PAW formed show similar trends.

6.3.3 Comparison between two plasma reactors on the PAW chemistry

As seen previously, the serial or parallel configurations does not reduce the treatment time but promote the final chemistry of the PAW. This section aims to explore the efficiency of the activation when using different plasma reactors. Figure 6.7 details the evolution of the main species analysed in the PAW formed.
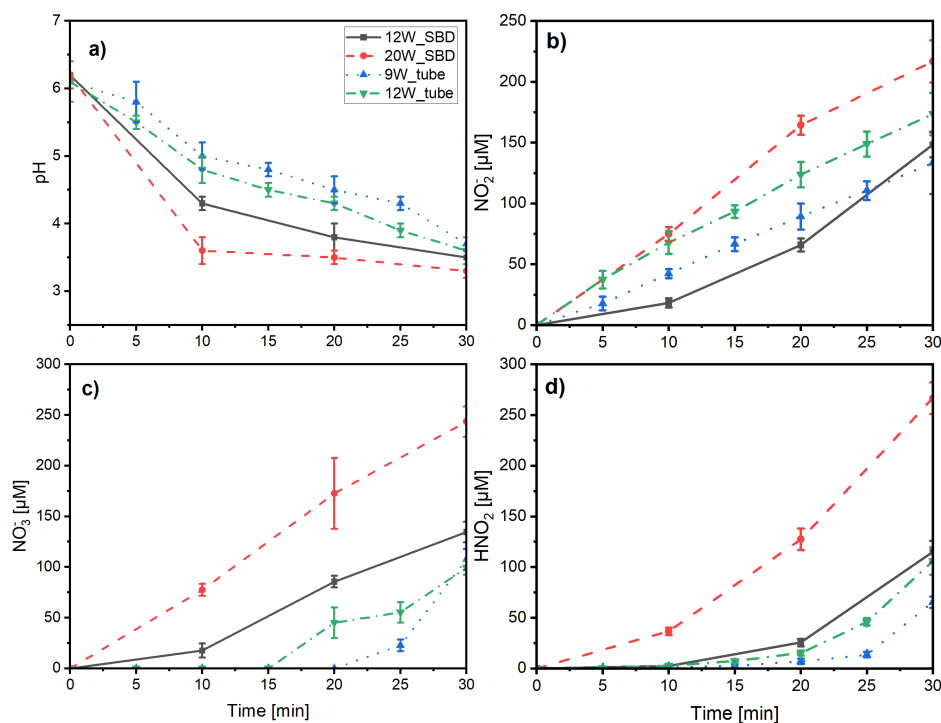
Figure 6.7: Kinetic evolution of the a) pH, b) concentration of nitrites, c) concentration of nitrates, and d) concentration of nitrous acid for the different plasma reactors

Figure 6.7 a) reports the value of the pH for both reactors during the experiment, as expected the pH decrease for all reactors with a significant advantage for the SBD either working at 12 or 20 W. The SBD at 20 W appears to be clearly efficient in this regard by reaching a pH of 3.6 ± 0.2 after only a treatment time of 10 minutes for 1 L of water treated. Concerning the concentration of NO_2^-, the SBD at 12 W appears to be less efficient to generate NO_2^- compare to the others configurations. The SBD at 20 W follows the same trend as previously reported for the tube DBD in section 6.3.2.1; with a identical rise for the first 10 minutes of treatment, then a significant increase to reach a maximum of 216.7 ± 17.3 µM after 30 minutes. However, the common trend found in literature for the concentration of NO_2^- seems to not match with this experiment. The faster decrease of pH and higher concentration of nitrites can be easily explained by the dimension of the SBD reactor compare to the tube DBD; the plasma formed will have a larger surface, thus generating higher concentration of species within it. Regarding the trend, it the previous section it was reported that flow rate could reached up to 1.5 $L.min^{-1}$; at this flow rate the residency of the species is short enough to encounter the conversion of gaseous NO_2 into other forms. In chapter 4 and 5, it was reported that SBD operating at high power where producing higher concentration of NOx due to the ozone quenching. However, even after 30 min ozone was found at concentrations up to 4 ppm indicating that the quenching did not occurred. This could explained the relatively low concentration of NO_3^- when compared to the PAW obtained in those chapters.

6.4 Conclusion

In this study, a plasma-Venturi system was developed and tested for its potential to produce PAW in higher volumes compared to SBDs with adequate chemistry. In the optimum conditions, the system was able to produce 1 L of PAW in 10 min with comparable chemistry to the one produced in chapter 4 and 5. The system shown capabilities to produce cavitation which allow a high surface-to-volume ratio and thus, faster dissolution of the species of interest within the water bulk. The design match with other work done in this area with formation of microbubbles having similar order of magnitude when looking at their diameter (around 300 µm when the plasma is on); those microbubbles appear to play a crucial role for the generation of high volume of PAW. Additionally, another Venturi tube was also mounted on serial or parallel and compared to the single configuration. It was demonstrated that the secondary system was not able to reduce the treatment time, but allowed a higher dissolution of the species of interest. Thus, increasing the potential of the PAW for application for bacterial inactivation. By increasing the dimension of the plasma reactor, the treatment time was clearly reduced with significant results in terms of chemistry after only 10 minutes. At this treatment time, the pH and concentration of nitrites and nitrous acid in the PAW were found to be compatible for bacterial inactivation when comparing with results obtained in chapter 4 and 5.

Further investigation could be done using computation to confirm the hypothesis regarding the concentration of NO_3^-; results obtained here were found to be promising to develop a system with characteristics matching industrial requirement.

Chapter 7

Conclusion and future work

7.1 Summary and main conclusions

The research in this work concerned the potential of PAW for bacterial inactivation and was designed into three main topics: a study comparing two approaches to generate PAW using either direct or indirect plasma treatment reported in chapter 4, an investigation on the initial properties of five tap waters and their impact on the chemistry of the PAW obtained in chapter 5, and a proof of concept to develop a plasma reactor able to produce high-volumes of PAW in chapter 6.

The first part of the research aimed to assess which plasma treatment was the most efficient to generate PAW with sufficient chemical properties for bio-decontamination. To assess this work, two plasma reactors were designed in which the plasma was either in contact with the water samples or formed remotely over the solution surface. The configurations consisted into a DBD with streamers forming from the bottom of the electrode and interacting with the water surface; the second reactors concerned a SBD which was placed above the Petri dish. Both reactors were found capable to

generate PAW with slight differences on the quality of the activation depending on the reactor used. However, due to the difference in term of plasma-liquid interaction, the final chemistry of the PAW contained slight variations. OES measurement of the DBD showed the presence of nitrogen oxide combined with oxygen species such as OH and O_3, resulting in a PAW with high concentration of nitrites, nitrates and hydrogen peroxide. Unfortunately, only one power setup could be explored due to the limitation of the device. With the SBD setup, two power modes were selected and tested either at low or high power. Comparatively, it was found that the SBD at higher power was able to produce higher concentration of NOx; meaning that the reactor was working mainly in a RNS mode rather than ROS. In the literature, studies reported that the quenching of O_3 was responsible to enhance the generation of nitrogen species, this characteristic was confirmed during this work. When looking at the PAW chemistry, the indirect reactor was found to decrease further the pH compared to the direct. This could be linked to the plasma surface generated during the process; in the case of the SBD, the plasma covers a larger area leading to a higher concentration of species. Same logic could be applied regarding the concentration of nitrites and nitrates which were found in higher than the DBD. However, the latter was found more efficient to produce H_2O_2. From the literature, H_2O_2 is known to be formed through recombination of the $OH^{\bullet}$ within the gas phase. Additionally, electrons formed during the process could also be transferred into the water bulk leading to an electrolysis of the water sample. For the DBD, both path are possible due to the plasma-liquid interaction which could explain the concentration of H_2O_2. Whereas, due to the regime of the SBD the formation of OH is reduced and the

electrolysis is completely absent. Regarding the bacterial inactivation, both PAW formed were found efficient against the bacteria strain tested with a clear advantage for the indirect treatment. In all experiment, the bacteria was incubated with the PAW for period ranging from 15 to 120 min. The direct treatment was unable to achieve complete inactivation with the best scenario obtained for an incubation of 120 minutes, with a log reduction of 4 ± 0.2 log for 8- and 16-min treated PAW. In the case of the indirect treatment, 4- and 8-min treatment were found unable to achieve complete inactivation with a maximum obtained after 120 minutes of incubation, respectively 6 ± 0.1 log and 3.8 ± 0.1 log reduction. For the 16-min treated PAW, complete inactivation was achieved after 30 minutes of incubation.

The conclusion from the results in chapter 4 suggested that the PAW containing strong concentration of nitrous acid combined with a low pH was more efficient compared to strong concentration of hydrogen peroxide. Furthermore, the results regarding the gas and liquid chemistry were found to be in agreement with the main mechanisms described in plasma-liquid interactions. These results helped also in the future design of the reactors for the work achieved notably in chapter 5.

The second part of the research focused on the activation of five tap waters and see how their initial chemistry will impact the efficiency of the activation. Waters from France, Norway, Palestine, Slovenia and United Kingdom were selected and treated with a SBD for period ranging from 0 to 30 minutes. It was found that the waters contained different level of dissolved bicarbonates which had an impact on the acidification of the solution. Comparatively, the waters from France and Palestine were found to have the highest concentration of HCO_3^- where waters from

the UK and Norway were the lowest. Bicarbonate is known to play a role as buffer in biological system, hydronium ions present in the solution will recombined with HCO_3^- and CO_3^{2-} to encounter the effect of the acidification. Further investigation on the buffer capacity of the water treated shown that only the bicarbonate were found responsible for the water buffering capacity to plasma exposure, and showing that dissolved cations effect was minimal. Thus, the pH of the PAW formed remained unchanged for the water from France and Palestine at 8 ± 0.1; where the water from Norway and UK decreased from 8.1 ± 0.1 to 3 ± 0.2 after 30 minutes. The water from Slovenia followed similar trend as the water from France and Palestine starting with a pH at 8.1 ± 0.1 and started to decrease after 10 minutes treatment to reach a minimum of 6.7 ± 0.1 after 30 minutes. Regarding the concentration of nitrites, all waters treated presented the same trend as reported by the community with an increase of the concentration during the first minutes of activation followed by a decrease occurring after 20 minutes treatment. The maximum concentration was reached by the water from Palestine at 24.1 ± 4.8 µM, whereas the water from UK had the lowest concentration at 10.2 ± 3.0 µM after a plasma treatment of 20 minutes. The decrease of the nitrites concentration was found to be linked to the conversion of NO_2^- into NO_3^- due by oxidoreduction with dissolved O_3 and formation of nitrous acid under acidic conditions. All waters shown an identical increase of the concentration of nitrates with a maximum reached at 3.1 ± 0.3 mM after 30 minutes exposure. In term of bio-decontamination, two waters were selected showing the largest discrepancy in intial composition, treated and tested against Gram-positive/negative strains. The waters were treated for either 10 or 20 minutes

then incubated for period of 24 h at 37 °C, the UK-PAW formed appeared to be the most efficient reaching complete inactivation after a treatment time of 20 min.

The results obtained in chapter 5 show that the initial chemistry of the water treated have various response towards plasma exposure. Waters with high concentration of HCO_3^- appeared to encounter the acidification due to their buffer capacity. Regarding the concentration of nitrites and nitrates, both were found to follow similar trends as observed in chapter 4 and in literature. The implications of these results are significant for the future development of PAW technology. If the technology is to be widely adopted in areas such as food security and healthcare, then efficiency, repeatability and traceability are of paramount importance. This study demonstrates that the inevitable wide variation in the composition of potable water from different geographic locations has a dramatic impact on the overall effectiveness of PAW. Given this, it is essential that steps be taken to analyse and possibly adjust the composition of any water source prior to plasma activation in order to guarantee the repeatability and ultimately, the safety, of the process.

The main outcome from the research in chapter 6 consisted in a working plasma device able to generate high-volumes of PAW. One limitation of plasma activated water technology is the low mass transfer of chemical species of interest into the water bulk; cavitation processes are known to increase this interaction by increasing the surface-to-volume ratio. The device developed in this chapter appeared to be able to generate cavitation with bubbles with diameters in range of 300 µm in the optimum conditions. As expected, variation with the water input flow rate and pressure will have a direct impact on the bubble generation and the efficiency of

the activation. Additionnaly, it was shown that combination with another Venturi tube in serial or parallel, could increase further the concentration of the species of interest in the PAW. Finally, when combined with other reactors, the quality of the activation was highly enhanced leading to a shorter time required for the treatment. Overall, those results are promising for possible integration of the technology into industrial settings.

7.2 Future work

Several suggestions for future work directly related to the research presented here are discussed below:

- The power supply employed here was based on continuous sinusoidal wave generator, the study could be extended by using nanosecond-pulsed generator. Neretti et al., reported that nanosecond-pulsed waveform have great benefit for the generation of a more stable glow discharge with higher energy efficiency compared to sinusoidal waveform. The PAW obtained shown higher concentration of ozone and hydrogen peroxide which could be interesting for biological applications [187]. Additionally, Laurita et al., reported the formation of peroxynitrite which is known to have a huge potential for decontamination [188].

- Another point could be investigated in identifying a way to mitigate against nitrates and nitrites. As an example, the temperature of the electrode could be controlled to either favour an ROS or RNS mode. This could have directly an impact on the plasma species formed and their interaction with the water

bulk leading to a different final chemistry of the PAW.

- Regarding the chemistry of the PAW, mostly the long lived species were characterised in this study with the assumption that short-lived plasma species may recombine during the process. Investigating the aqueous short-lived species could potential bring positive outcomes on the general knowledge of the plasma-liquid interactions. Notably, recent studies reported the possible role that per-oxynitrites could play combined with the presence of superoxide $O_2^{\bullet-}$ [189], [190], [191].

- Chapter 6 in this research reported a working plasma device for the generation of high-volumes of PAW. Similar reactors were developed by the community [192], [193], [194]. However, the settings of these experiment are still restrain into laboratories and further investigation are required to faster the integration of the technology into industry.

- With further development in PAW technology and possible implementation into industry, analysis on its long-term effects and possible interactions with human health should be considered.

Appendix A

Description of the numerical model

A coupled set of 1D convection-diffusion-reaction equations were solved, in space and time, for the densities of 53 species. These include electrons, positive and negative ions, excited state neutral species and neutral reactive species, interacting through 624 reactions. A complete list of the species and reactions considered in this model was previously reported by Sakiyama et al., [115]. For the purpose of the model, the air background was assumed to consist of 79 % N_2, 20 % O_2 and 1 % H_2O. Where the discharge was assumed to be driven by a Gaussian pulse of electric field with a duration of few nanoseconds, which mimic the lifetime of a filamentary discharge occurring in a SBD at atmospheric pressure in air. The field was converted to a mean electron energy through the local field approximation [195]. The densities of the reactive species were calculated as a function of distance in regards to the generating electrode; the model was solved for all species, with the assumption that the discharge was ignited in the first 40 µm representing the plasma region of the discharge. At the end of each period of the applied waveform, the average power was calculated and the magnitude of the electric field was modified to adjust the average power in the next period. This was done in order to match with the experiment.

The procedure was repeated until the variation of the average power was between the simulation and the experiment was less than 5 %. If five consecutive periods of the applied waveform satisfied this condition, the generation and loss rates of neutral species were averaged over the last period of the waveform. In the second step, the model was solved only for the long-lived species until the species reached the surface of the water, adopting the time-averaged generation and loss rates obtained from the first step. Thus, allowing for the effect of short-lived species, such as electrons and ions, to influence the chemistry of the neutral species without needing to resolve every period of the applied waveform.

Appendix B

Measurement of the concentration of ammonia and ammonium

Concentration of ammonia NH_3 and ammonium NH_4^+ was determined by spectrophotometry using Nessler's reagent as reactant (Sigma-Aldrich Ltd, CAS 7783-33-7) in basic solution. 2 mL of the reagent is added to 50 mL of PAW; after an incubation period of 10 min, the reaction produce an orange product detectable at 400 nm. Both ammonia and ammonia react with Nessler reagent, the concentration measured by absorption is defined as:

$$[C_{total}] = [NH_3] + [NH_4^+]$$

Knowing that $[NH_4^+]/[NH_3]$ form a conjugate acid-base pair ($pKa_5 = 9.25$), the concentration of each compound can be expressed individually following their pKa and C_{total}:

APPENDIX B. MEASUREMENT OF THE CONCENTRATION OF AMMONIA AND AMMONIUM

$$[NH_4{}^+] = \frac{[C_{total}]}{1 + 10^{pH-pKa_5}} \tag{B.1}$$

$$[NH_3] = \frac{[C_{total}] \times 10^{pH-pKa_5}}{1 + 10^{pH-pKa_5}} \tag{B.2}$$

For each concentration, the uncertainties are as following:

$$\Delta[NH_4{}^+] = \left| \frac{1}{1 + 10^{pH-pKa_5}} \right| \Delta[C_{total}] + \left| \frac{-[C_{total}] \times \ln(10) \times 10^{pH-pKa_5}}{(1 + 10^{pH-pKa_5})^2} \right| \Delta pH \tag{B.3}$$

$$\Delta[NH_3] = \left| \frac{10^{pH-pKa_5}}{1 + 10^{pH-pKa_5}} \right| \Delta[C_{total}] + \left| \frac{[C_{total}] \times \ln(10) \times 10^{pH-pKa_5}}{(1 + 10^{pH-pKa_5})^2} \right| \Delta pH \tag{B.4}$$

Bibliography

[1] Irving Langmuir. Electric discharges in gases at low pressures. *Journal of the Franklin Institute*, 214(3):275–298, 1932.

[2] Fatemeh Rezaei, Patrick Vanraes, Anton Nikiforov, Rino Morent, and Nathalie De Geyter. Applications of plasma-liquid systems: A review. *Materials*, 12 (17):2751, 2019.

[3] Alexander Fridman, Alexander Fridman, Lawrence A. Kennedy, and Lawrence A. Kennedy. *Plasma Physics and Engineering*. CRC Press, 2004.

[4] Michael A. Lieberman and Allan J. Lichtenberg. *Principles of plasma discharges and materials processing*. John Wiley & Sons, 2005.

[5] François Rossi, Ondrej Kylián, Hubert Rauscher, Douglas Gilliland, and Lucel Sirghi. Use of a low-pressure plasma discharge for the decontamination and sterilization of medical devices. *Pure and Applied Chemistry*, 80(9):1939–1951, 2008.

[6] Katharina Stapelmann, Marcel Fiebrandt, Marina Raguse, Peter Awakowicz, Günther Reitz, and Ralf Moeller. Utilization of low-pressure plasma to inactivate bacterial spores on stainless steel screws. *Astrobiology*, 13(7):597–606, 2013.

[7] Healthcare associated infections (hai): point prevalence survey, england, 2016. URL https://www.gov.uk/government/publications/healthcare-associated-infections-hcai-point-prevalence-survey-england.

[8] Carl Suetens, Katrien Latour, Tommi Kärki, Enrico Ricchizzi, Pete Kinross, Maria Luisa Moro, Béatrice Jans, Susan Hopkins, Sonja Hansen, Outi Lyytikäinen, et al. Prevalence of healthcare-associated infections, estimated incidence and composite antimicrobial resistance index in acute care hospitals and long-term care facilities: results from two european point prevalence surveys, 2016 to 2017. *Eurosurveillance*, 23(46):1800516, 2018.

[9] Julian F Guest, Tomas Keating, Dinah Gould, and Neil Wigglesworth. Modelling the annual nhs costs and outcomes attributable to healthcare-associated infections in england. *BMJ open*, 10(1):e033367, 2020.

[10] William A Rutala and David J Weber. Disinfection, sterilization, and control of hospital waste. *Mandell, Douglas, and Bennett's principles and practice of infectious diseases*, page 3294, 2015.

[11] Earl H Spaulding. Chemical disinfection of medical and surgical materials. *Disinfection, sterilization and prevention*, pages 517–531, 1968.

[12] Consultation on the future regulation of medical devices in the united kingdom, 2021. URL https://www.gov.uk/government/consultations/consultation-on-the-future-regulation-of-medical-devices-in-the-united-kingo

[13] Roberto Vivas, Ana Andréa Teixeira Barbosa, Silvio Santana Dolabela, and

Sona Jain. Multidrug-resistant bacteria and alternative methods to control them: an overview. *Microbial Drug Resistance*, 25(6):890–908, 2019.

[14] Jeetendra Gurung, Annie Bakorlin Khyriem, Amit Banik, Wihiwot Valarie Lyngdoh, Basabdatta Choudhury, and Prithwis Bhattacharyya. Association of biofilm production with multidrug resistance among clinical isolates of acinetobacter baumannii and pseudomonas aeruginosa from intensive care unit. *Indian journal of critical care medicine: peer-reviewed, official publication of Indian Society of Critical Care Medicine*, 17(4):214, 2013.

[15] Xinyu Song, Pengyan Liu, Xiaohu Liu, Yanan Wang, Huichao Wei, Jingwen Zhang, Liangmin Yu, Xuefeng Yan, and Zhiyu He. Dealing with mdr bacteria and biofilm in the post-antibiotic era: Application of antimicrobial peptides-based nano-formulation. *Materials Science and Engineering: C*, 128:112318, 2021.

[16] Julia Kovaleva, Frans TM Peters, Henny C van der Mei, and John E Degener. Transmission of infection by flexible gastrointestinal endoscopy and bronchoscopy. *Clinical microbiology reviews*, 26(2):231–254, 2013.

[17] Birgit Thiede and Axel Kramer. Evaluation of reprocessing medical devices in 14 german regional hospitals and at 27 medical practitioners 'offices within the european context–consequences for european harmonization. *GMS Hygiene and Infection Control*, 8(2), 2013.

[18] Sara Larsen, Rasmus Vinther Russell, Lotte Klinten Ockert, Stephen Spanos, Helena Strømstad Travis, Lars Holger Ehlers, and Anders Mærkedahl. Rate

and impact of duodenoscope contamination: a systematic review and meta-analysis. *EClinicalMedicine*, 25:100451, 2020.

[19] Jonathan Josephs-Spaulding and Om V Singh. Medical device sterilization and reprocessing in the era of multidrug-resistant (mdr) bacteria: issues and regulatory concepts. *Frontiers in Medical Technology*, 2:587352, 2021.

[20] Neil J Rowan and John G Laffey. Unlocking the surge in demand for personal and protective equipment (ppe) and improvised face coverings arising from coronavirus disease (covid-19) pandemic–implications for efficacy, re-use and sustainable waste management. *Science of the Total Environment*, 752:142259, 2021.

[21] Mubarak Taiwo Mubarak, Ilker Ozsahin, and Dilber Uzun Ozsahin. Evaluation of sterilization methods for medical devices. In *2019 Advances in Science and Engineering Technology International Conferences (ASET)*, pages 1–4. IEEE, 2019.

[22] Iwona Łopianiak and Beata A Butruk-Raszeja. Evaluation of sterilization/disinfection methods of fibrous polyurethane scaffolds designed for tissue engineering applications. *International Journal of Molecular Sciences*, 21(21): 8092, 2020.

[23] Brian McEvoy and Neil J Rowan. Terminal sterilization of medical devices using vaporized hydrogen peroxide: a review of current methods and emerging opportunities. *Journal of applied microbiology*, 127(5):1403–1420, 2019.

[24] Meihan Tao, Tianrang Ao, Xiaoyan Mao, Xinzhu Yan, Rabia Javed, Weijian Hou, Yang Wang, Cong Sun, Shuang Lin, and Tianhao Yu. Sterilization and disinfection methods for decellularized matrix materials: Review, consideration and proposal. *Bioactive Materials*, 6(9):2927–2945, 2021.

[25] Alexandra Peters, Rafael Palomo, Hervé Ney, Nasim Lotfinejad, Walter Zingg, Pierre Parneix, and Didier Pittet. The covid-19 pandemic and n95 masks: reusability and decontamination methods. *Antimicrobial Resistance & Infection Control*, 10(1):1–16, 2021.

[26] Jakob Munk Mouritsen, L Ehlers, Julia Kovaleva, I Ahmad, and K El-Boghdadly. A systematic review and cost effectiveness analysis of reusable vs. single-use flexible bronchoscopes. *Anaesthesia*, 75(4):529–540, 2020.

[27] Huizhen Yang, Huidong Chen, Baoan Gao, Weining Xiong, Xiaoju Zhang, D Kyle Hogarth, Jiayuan Sun, Mingyao Ke, and Felix JF Herth. Expert panel consensus statement on the applications and precaution strategies of bronchoscopy in patients with covid-19. *Endoscopic Ultrasound*, 9(4):211, 2020.

[28] Michael A Pritchett, Catherine L Oberg, Adam Belanger, Jose De Cardenas, George Cheng, Gustavo Cumbo Nacheli, Carlos Franco-Paredes, Jaspal Singh, Jennifer Toth, Michael Zgoda, et al. Society for advanced bronchoscopy consensus statement and guidelines for bronchoscopy and airway management amid the covid-19 pandemic. *Journal of Thoracic Disease*, 12(5):1781, 2020.

[29] Federica Furfaro, Lucine Vuitton, Gionata Fiorino, Stephane Koch, Mariangela Allocca, Daniela Gilardi, Alessandra Zilli, Ferdinando D'Amico, Simona

Radice, Jean-Baptiste Chevaux, et al. Sfed recommendations for ibd endoscopy during covid-19 pandemic: Italian and french experience. *Nature Reviews Gastroenterology & Hepatology*, 17(8):507–516, 2020.

[30] Marietta Iacucci, Rosanna Cannatelli, Nunzia Labarile, Ren Mao, Remo Panaccione, Silvio Danese, Gursimran S Kochhar, Subrata Ghosh, and Bo Shen. Endoscopy in inflammatory bowel diseases during the covid-19 pandemic and post-pandemic period. *The Lancet Gastroenterology & Hepatology*, 5(6):598–606, 2020.

[31] Antimicrobial resistance. fact sheet no, 194, 2019. URL https://www.who.int/about/licensing.

[32] Fred Fung, Huei-Shyong Wang, and Suresh Menon. Food safety in the 21st century. *Biomedical journal*, 41(2):88–95, 2018.

[33] Food safety, 2022. URL https://www.who.int/news-room/fact-sheets/detail/food-safety.

[34] C Edwards. *Environmental pollution by pesticides*, volume 3. Springer Science & Business Media, 2013.

[35] Irfan A Rather, Wee Yin Koh, Woon K Paek, and Jeongheui Lim. The sources of chemical contaminants in food and their health implications. *Frontiers in pharmacology*, 8:830, 2017.

[36] Thomas Bintsis. Foodborne pathogens. *AIMS microbiology*, 3(3):529, 2017.

[37] Jolanta Fenik, Maciej Tankiewicz, and Marek Biziuk. Properties and determination of pesticides in fruits and vegetables. *TrAC Trends in Analytical Chemistry*, 30(6):814–826, 2011.

[38] Peter Fantke, Rainer Friedrich, and Olivier Jolliet. Health impact and damage cost assessment of pesticides in europe. *Environment international*, 49:9–17, 2012.

[39] Petronela Cozma, Laura Carmen Apostol, Raluca Maria Hlihor, Isabela Maria Simion, and Maria Gavrilescu. Overview of human health hazards posed by pesticides in plant products. In *2017 E-Health and Bioengineering Conference (EHB)*, pages 293–296. IEEE, 2017.

[40] Luis Carrasco Cabrera and Paula Medina Pastor. The 2019 european union report on pesticide residues in food. *EFSA Journal*, 2021.

[41] Andrew Bamidele Falowo and Oluwakamisi Festus Akimoladun. Veterinary drug residues in meat and meat products: Occurrence, detection and implications. *Veterinary Medicine and Pharmaceuticals*, 3:194, 2019.

[42] Bronhilda Lemalue Ngangom, Stella Shinwin Ateim Tamunjoh, Fekam Fabrice Boyom, et al. Antibiotic residues in food animals: Public health concern. *Acta Ecologica Sinica*, 39(5):411–415, 2019.

[43] Islam Md Meftaul, Kadiyala Venkateswarlu, Rajarathnam Dharmarajan, Prasath Annamalai, Md Asaduzzaman, Aney Parven, and Mallavarapu Megharaj. Controversies over human health and ecological impacts of

glyphosate: Is it to be banned in modern agriculture? *Environmental Pollution*, 263:114372, 2020.

[44] Paraskevi Kalofiri, Giorgos Balias, and Fotios Tekos. The eu endocrine disruptors' regulation and the glyphosate controversy. *Toxicology Reports*, 8:1193–1199, 2021.

[45] Heeyoung Lee and Yohan Yoon. Etiological agents implicated in foodborne illness world wide. *Food Science of Animal Resources*, 41(1):1, 2021.

[46] Verônica Simões De Borba, Marcy Heli Paiva Rodrigues, and Eliana Badiale-Furlong. Impact of biological contamination of rice on food safety. *Food Reviews International*, 36(8):745–760, 2020.

[47] EFSA Panel on Biological Hazards (BIOHAZ). Risks for public health related to the presence of bacillus cereus and other bacillus spp. including bacillus thuringiensis in foodstuffs. *EFSA Journal*, 14(7):e04524, 2016.

[48] Chiara Trevisan, Paul R Torgerson, and Lucy J Robertson. Foodborne parasites in europe: present status and future trends. *Trends in parasitology*, 35 (9):695–703, 2019.

[49] DJH Martin, Stephen Paul Denyer, G McDonnell, and J-Y Maillard. Resistance and cross-resistance to oxidising agents of bacterial isolates from endoscope washer disinfectors. *Journal of Hospital Infection*, 69(4):377–383, 2008.

[50] Michelle M Nerandzic, Jennifer L Cadnum, Michael J Pultz, and Curtis J Donskey. Evaluation of an automated ultraviolet radiation device for decon-

tamination of clostridium difficile and other healthcare-associated pathogens in hospital rooms. *BMC infectious diseases*, 10(1):1–8, 2010.

[51] Lasse Per Petersson, Urs-Vito Albrecht, Ludwig Sedlacek, Stefanie Gemein, Jürgen Gebel, and Ralf-Peter Vonberg. Portable uv light as an alternative for decontamination. *American journal of infection control*, 42(12):1334–1336, 2014.

[52] Elisa Gayán, I Álvarez, and S Condón. Inactivation of bacterial spores by uv-c light. *Innovative Food Science & Emerging Technologies*, 19:140–145, 2013.

[53] JA Guerrero-Beltr· n and GV Barbosa-C· novas. Advantages and limitations on processing foods by uv light. *Food science and technology international*, 10 (3):137–147, 2004.

[54] Chand Wattal and JK Oberoi. Decontamination and sterilization procedures. In *Hospital Infection Prevention*, pages 103–120. Springer, 2014.

[55] Single-use medical devices: Implications and consequences of re-use, Jan 2021. URL https://www.gov.uk/government/publications/single-use-medical-devices-implications-and-consequences-of-re-use.

[56] Megan L. Casey, Brie Hawley, Nicole Edwards, Jean M. Cox-Ganser, and Kristin J. Cummings. Health problems and disinfectant product exposure among staff at a large multispecialty hospital. *American Journal of Infection Control*, 45(10):1133–1138, 2017.

[57] Dawood Ghafoor, Zafran Khan, Asaf Khan, Daniya Ualiyeva, and Nasib Zaman. Excessive use of disinfectants against covid-19 posing a potential threat to living beings. *Current Research in Toxicology*, 2:159–168, 2021.

[58] Parixit Prajapati, Heli Desai, and Chandni Chandarana. Hand sanitizers as a preventive measure in covid-19 pandemic, its characteristics, and harmful effects: A review. *Journal of the Egyptian Public Health Association*, 97(1), 2022.

[59] Adeel Mahmood, Maryam Eqan, Saher Pervez, Huda Ahmed Alghamdi, Amtul Bari Tabinda, Abdullah Yasar, Kathirvel Brindhadevi, and Arivalagan Pugazhendhi. Covid-19 and frequent use of hand sanitizers; human health and environmental hazards by exposure pathways. *Science of The Total Environment*, 742, 2020.

[60] Tekle Airgecho Lobie, Aklilu Abrham Roba, James Alexander Booth, Knut Ivan Kristiansen, Abraham Aseffa, Kirsten Skarstad, and Magnar Bjørås. Antimicrobial resistance: A challenge awaiting the post-covid-19 era. *International Journal of Infectious Diseases*, 111:322–325, 2021.

[61] Rosalee S. Hellberg and Eric Chu. Effects of climate change on the persistence and dispersal of foodborne bacterial pathogens in the outdoor environment: A review. *Critical Reviews in Microbiology*, 42(4):548–572, 2016.

[62] Edoardo Pozio. How globalization and climate change could affect foodborne parasites. *Experimental Parasitology*, 208:107807, 2020.

[63] Jennifer Sills, Ji Lu, and Jianhua Guo. Disinfection spreads antimicrobial resistance. *Science*, 371(6528):474–474, 2021.

[64] J. Van Impe, C. Smet, B. Tiwari, R. Greiner, S. Ojha, V. Stulić, T. Vukušić, and A. Režek Jambrak. State of the art of nonthermal and thermal processing for inactivation of micro-organisms. *Journal of Applied Microbiology*, 125(1): 16–35, 2018.

[65] Laetitia Picart-Palmade, Charles Cunault, Dominique Chevalier-Lucia, Marie-Pierre Belleville, and Sylvie Marchesseau. Potentialities and limits of some non-thermal technologies to improve sustainability of food processing. *Frontiers in Nutrition*, 5, 2019.

[66] H. Cavendish. *Experiments on Air: Papers Published in the Philosophical Transactions.* hansebooks, 1785. ISBN 9783742827227.

[67] PJ Bruggeman, Mark J Kushner, Bruce R Locke, Johannes GE Gardeniers, WG Graham, David B Graves, RCHM Hofman-Caris, Dragana Maric, Jonathan P Reid, Elisa Ceriani, et al. Plasma–liquid interactions: a review and roadmap. *Plasma sources science and technology*, 25(5):053002, 2016.

[68] Y. Yang, Y.I. Cho, and A. Fridman. *Plasma Discharge in Liquid: Water Treatment and Applications.* CRC Press, 2017. ISBN 9781439866245.

[69] H. Akiyama. Streamer discharges in liquids and their applications. *IEEE Transactions on Dielectrics and Electrical Insulation*, 7(5):646–653, 2000.

[70] I.V. Lisitsyn, H. Nomlyama, S. Katsuki, and H. Akiyama. Thermal processes in a streamer discharge in water. *IEEE Transactions on Dielectrics and Electrical Insulation*, 6(3):351–356, 1999.

[71] Igor V. Lisitsyn, Hiroaki Nomiyama, Sunao Katsuki, and Hidenori Akiyama. Streamer discharge reactor for water treatment by pulsed power. *Review of Scientific Instruments*, 70(8):3457–3462, 1999.

[72] Alexander Fridman. *Plasma decontamination of gases and liquids*, page 175–215. Cambridge University Press, 2012. doi: 10.1017/CBO9780511902598. 011.

[73] S. Katsuki, H. Akiyama, A. Abou-Ghazala, and K.H. Schoenbach. Parallel streamer discharges between wire and plane electrodes in water. *IEEE Transactions on Dielectrics and Electrical Insulation*, 9(4):498–506, 2002.

[74] James W. Robinson, Mooyoung Ham, and Ammon N. Balaster. Ultraviolet radiation from electrical discharges in water. *Journal of Applied Physics*, 44 (1):72–75, 1973.

[75] M. Sato, T. Ohgiyama, and J.S. Clements. Formation of chemical species and their effects on microorganisms using a pulsed high-voltage discharge in water. *IEEE Transactions on Industry Applications*, 32(1):106–112, 1996.

[76] B. R. Locke, M. Sato, P. Sunka, M. R. Hoffmann, and J.-S. Chang. Electrohydraulic discharge and nonthermal plasma for water treatment. *Industrial & Engineering Chemistry Research*, 45(3):882–905, 2006.

[77] P Sunka, V Babický, M Clupek, P Lukes, M Simek, J Schmidt, and M Cernák. Generation of chemically active species by electrical discharges in water. *Plasma Sources Science and Technology*, 8(2):258–265, 1999.

[78] Michael P. Brenner, Sascha Hilgenfeldt, and Detlef Lohse. Single-bubble sonoluminescence. *Rev. Mod. Phys.*, 74:425–484, 2002.

[79] A. Bataller, B. Kappus, C. Camara, and S. Putterman. Collision time measurements in a sonoluminescing microplasma with a large plasma parameter. *Phys. Rev. Lett.*, 113:024301, 2014.

[80] A. De Giacomo, M. Dell'Aglio, O. De Pascale, and M. Capitelli. From single pulse to double pulse ns-laser induced breakdown spectroscopy under water: Elemental analysis of aqueous solutions and submerged solid samples. *Spectrochimica Acta Part B: Atomic Spectroscopy*, 62(8):721–738, 2007.

[81] Peter Bruggeman, Leigh Graham, Joris Degroote, Jan Vierendeels, and Christophe Leys. Water surface deformation in strong electrical fields and its influence on electrical breakdown in a metal pin–water electrode system. *Journal of Physics D: Applied Physics*, 40(16):4779–4786, 2007.

[82] Peter Bruggeman, Peter Guns, Joris Degroote, Jan Vierendeels, and Christophe Leys. Influence of the water surface on the glow-to-spark transition in a metal-pin-to-water electrode system. *Plasma Sources Science and Technology*, 17(4):045014, 2008.

[83] Florian Judée, Stéphane Simon, Christophe Bailly, and Thierry Dufour.

Plasma-activation of tap water using dbd for agronomy applications: Identification and quantification of long lifetime chemical species and production/consumption mechanisms. *Water research*, 133:47–59, 2018.

[84] Bhagirath Ghimire, Endre J Szili, Bethany L Patenall, Pradeep Lamichhane, Nishtha Gaur, Alexander J Robson, Dhruv Trivedi, Naing T Thet, A Toby A Jenkins, Eun Ha Choi, and Robert D Short. Enhancement of hydrogen peroxide production from an atmospheric pressure argon plasma jet and implications to the antibacterial activity of plasma activated water. *Plasma Sources Science and Technology*, 30(3):035009, 2021.

[85] Ruonan Ma, Shuang Yu, Ying Tian, Kaile Wang, Chongde Sun, Xian Li, Jue Zhang, Kunsong Chen, and Jing Fang. Effect of non-thermal plasma-activated water on fruit decay and quality in postharvest chinese bayberries. *Food and Bioprocess Technology*, 9(11):1825–1834, 2016.

[86] Danil Dobrynin, Gregory Fridman, Yurii V. Mukhin, Meghan A. Wynosky-Dolfi, Judy Rieger, Richard F. Rest, Alexander F. Gutsol, and Alexander Fridman. Cold plasma inactivation of bacillus cereus and bacillus anthracis (anthrax) spores. *IEEE Transactions on Plasma Science*, 38(8):1878–1884, 2010.

[87] Li Guo, Zhiqian Yao, Lu Yang, Hao Zhang, Yu Qi, Lu Gou, Wang Xi, Dingxin Liu, Lei Zhang, Yilong Cheng, et al. Plasma-activated water: An alternative disinfectant for s protein inactivation to prevent sars-cov-2 infection. *Chemical Engineering Journal*, 421:127742, 2021.

[88] Jinzhang Gao, Xiaoyan Wang, Zhongai Hu, Hualing Deng, Jingguo Hou, Xi-aoquan Lu, and Jingwan Kang. Plasma degradation of dyes in water with contact glow discharge electrolysis. *Water Research*, 37(2):267–272, 2003.

[89] Susanta K Sen Gupta. Contact glow discharge electrolysis: a novel tool for manifold applications. *Plasma Chemistry and Plasma Processing*, 37(4):897–945, 2017.

[90] Peter Bruggeman, Eva Ribežl, Alan Maslani, Joris Degroote, Alexander Male-sevic, Robby Rego, Jan Vierendeels, and Christophe Leys. Characteristics of atmospheric pressure air discharges with a liquid cathode and a metal anode. *Plasma Sources Science and Technology*, 17(2):025012, 2008.

[91] Juan Pablo Trelles. Pattern formation and self-organization in plasmas inter-acting with surfaces. *Journal of Physics D: Applied Physics*, 49(39):393002, 2016.

[92] Patrick Vanraes and Annemie Bogaerts. The essential role of the plasma sheath in plasma–liquid interaction and its applications—a perspective. *Journal of Applied Physics*, 129(22):220901, 2021.

[93] Yu Zhang, Lijuan Liu, and Jiting Ouyang. On the negative corona and ionic wind over water electrode surface. *Journal of Electrostatics*, 72(1):76–81, 2014.

[94] Alexander Lindsay, Carly Anderson, Elmar Slikboer, Steven Shannon, and David Graves. Momentum, heat, and neutral mass transport in convective at-

mospheric pressure plasma-liquid systems and implications for aqueous targets. *Journal of Physics D: Applied Physics*, 48(42):424007, 2015.

[95] Vipa river-case study, 2021. URL http://www.bewaterproject.eu/case-studies/vipava-river-basin-slovenia.

[96] Youssef Morabit, Mohammad I Hasan, Richard D Whalley, Eric Robert, Martina Modic, and James L Walsh. A review of the gas and liquid phase interactions in low-temperature plasma jets used for biomedical applications. *The European Physical Journal D*, 75(1):1–26, 2021.

[97] H Lee, JY Park, Wonho Choe, and Sanghoo Park. Computational modelling of rons generation and its enhancement by uv photolysis in plasma-liquid system. In *2020 IEEE International Conference on Plasma Science (ICOPS)*, pages 611–611. IEEE, 2020.

[98] JA Silsby, S Simon, JL Walsh, and MI Hasan. The influence of gas–liquid interfacial transport theory on numerical modelling of plasma activation of water. *Plasma Chemistry and Plasma Processing*, 41(5):1363–1380, 2021.

[99] Stephane Simon, Breno Salgado, Mohammad I Hasan, Morten Sivertsvik, Estefania Noriega Fernández, and James L Walsh. Influence of potable water origin on the physicochemical and antimicrobial properties of plasma activated water. *Plasma Chemistry and Plasma Processing*, 42(2):377–393, 2022.

[100] HH Kim, Y Teramoto, N Negishi, A Ogata, JH Kim, B Pongrác, Z Machala,

and Alfonso M Gañán-Calvo. Polarity effect on the electrohydrodynamic (ehd) spray of water. *Journal of aerosol science*, 76:98–114, 2014.

[101] Zdenko Machala, Lenka Chládeková, and Michal Pelach. Plasma agents in bio-decontamination by dc discharges in atmospheric air. *Journal of Physics D: Applied Physics*, 43(22):222001, 2010.

[102] Anne Mai-Prochnow, Renwu Zhou, Tianqi Zhang, Kostya Ken Ostrikov, Sudarsan Mugunthan, Scott A Rice, and Patrick J Cullen. Interactions of plasma-activated water with biofilms: inactivation, dispersal effects and mechanisms of action. *npj Biofilms and Microbiomes*, 7(1):1–12, 2021.

[103] Renwu Zhou, Rusen Zhou, Peiyu Wang, Bingyu Luan, Xianhui Zhang, Zhi Fang, Yubin Xian, Xinpei Lu, Kostya Ken Ostrikov, and Kateryna Bazaka. Microplasma bubbles: reactive vehicles for biofilm dispersal. *ACS applied materials & interfaces*, 11(23):20660–20669, 2019.

[104] Alexander Wright, Hemaka Bandulasena, Christopher Ibenegbu, David Leak, Thomas Holmes, William Zimmerman, Alex Shaw, and Felipe Iza. Dielectric barrier discharge plasma microbubble reactor for pretreatment of lignocellulosic biomass. *AIChE Journal*, 64(11):3803–3816, 2018.

[105] Werner Siemens. Ueber die elektrostatische induction und die verzögerung des stroms in flaschendrähten. *Annalen der Physik*, 178(9):66–122, 1857.

[106] K Buss. Die elektrodenlose entladung nach messung mit dem kathodenoszillographen. *Archiv für Elektrotechnik*, 26(4):261–265, 1932.

[107] Hofer Klemenc, Hinterberger. No title. *Z. Electrochem*, 43:261–265, 1937.

[108] Ulrich Kogelschatz, Baldur Eliasson, and W Egli. Dielectric-barrier discharges. principle and applications. *Le Journal de Physique IV*, 7(C4):C4–47, 1997.

[109] Kurt H Becker, Ulrich Kogelschatz, KH Schoenbach, and RJ Barker. *Non-equilibrium air plasmas at atmospheric pressure*. CRC press, 2004.

[110] A Chirokov, A Gutsol, and A Fridman. Atmospheric pressure plasma of dielectric barrier discharges. *Pure and applied chemistry*, 77(2):487–495, 2005.

[111] Baldur Eliasson, M Hirth, and Ulrich Kogelschatz. Ozone synthesis from oxygen in dielectric barrier discharges. *Journal of Physics D: Applied Physics*, 20 (11):1421, 1987.

[112] Ulrich Kogelschatz. Dielectric-barrier discharges: their history, discharge physics, and industrial applications. *Plasma chemistry and plasma processing*, 23(1):1–46, 2003.

[113] Jochen Kriegseis. Performance characterization and quantification of dielectric barrier discharge plasma actuators. *Technische Universität*, 2011.

[114] Koen Van Laer and Annemie Bogaerts. Influence of gap size and dielectric constant of the packing material on the plasma behaviour in a packed bed dbd reactor: a fluid modelling study. *Plasma Processes and Polymers*, 14(4-5): 1600129, 2017.

[115] Yukinori Sakiyama, David B Graves, Hung-Wen Chang, Tetsuji Shimizu, and Gregor E Morfill. Plasma chemistry model of surface microdischarge in humid

air and dynamics of reactive neutral species. *Journal of Physics D: Applied Physics*, 45(42):425201, 2012.

[116] Matthew J Pavlovich, Douglas S Clark, and David B Graves. Quantification of air plasma chemistry for surface disinfection. *Plasma Sources Science and Technology*, 23(6):065036, 2014.

[117] Tetsuji Shimizu, Yukinori Sakiyama, David B Graves, Julia L Zimmermann, and Gregor E Morfill. The dynamics of ozone generation and mode transition in air surface micro-discharge plasma at atmospheric pressure. *New Journal of Physics*, 14(10):103028, 2012.

[118] Stanislav Pekárek and Jan Mikeš. Temperature-and airflow-related effects of ozone production by surface dielectric barrier discharge in air. *The European Physical Journal D*, 68(10):1–8, 2014.

[119] Seiji Samukawa, Masaru Hori, Shahid Rauf, Kunihide Tachibana, Peter Bruggeman, Gerrit Kroesen, J Christopher Whitehead, Anthony B Murphy, Alexander F Gutsol, Svetlana Starikovskaia, et al. The 2012 plasma roadmap. *Journal of Physics D: Applied Physics*, 45(25):253001, 2012.

[120] Carly E Anderson, Nico R Cha, Alexander D Lindsay, Douglas S Clark, and David B Graves. The role of interfacial reactions in determining plasma–liquid chemistry. *Plasma Chemistry and Plasma Processing*, 36(6):1393–1415, 2016.

[121] A Dascalu, V Pohoata, K Shimizu, and L Sirghi. Molecular species generated by surface dielectric barrier discharge micro-plasma in small chambers

enclosing atmospheric air and water samples. *Plasma Chemistry and Plasma Processing*, 41(1):389–408, 2021.

[122] Abdullah Al-Abduly and Paul Christensen. An in situ and downstream study of non-thermal plasma chemistry in an air fed dielectric barrier discharge (dbd). *Plasma Sources Science and Technology*, 24(6):065006, 2015.

[123] Gabi-Daniel Stancu, Farah Kaddouri, DA Lacoste, and CO Laux. Atmospheric pressure plasma diagnostics by oes, crds and talif. *Journal of Physics D: Applied Physics*, 43(12):124002, 2010.

[124] Sanxi Deng, Cheng Cheng, Guohua Ni, Yuedong Meng, and Hua Chen. Bacillus subtilis devitalization mechanism of atmosphere pressure plasma jet. *Current Applied Physics*, 10(4):1164–1168, 2010.

[125] Barbora Tarabová, Petr Lukeš, Mário Janda, Karol Hensel, Libuša Šikurová, and Zdenko Machala. Specificity of detection methods of nitrites and ozone in aqueous solutions activated by air plasma. *Plasma Processes and Polymers*, 15(6):1800030, 2018.

[126] D Kuvshinov, A Siswanto, J Lozano-Parada, and WB Zimmerman. Efficient compact micro dbd plasma reactor for ozone generation for industrial application in liquid and gas phase systems. *World Acad. Sci. Eng. Technol*, 8:80–83, 2014.

[127] Jun-Seok Oh, Hideki Yajima, Keiya Hashida, Tsunehisa Ono, Tatsuo Ishijima, Izumi Serizawa, Hiroshi Furuta, and Akimitsu Hatta. In-situ uv absorption

spectroscopy for observing dissolved ozone in water. *Journal of Photopolymer Science and Technology*, 29(3):427–432, 2016.

[128] Kunihide Tachibana and Toshihiro Nakamura. Examination of uv-absorption spectroscopy for analysis of o3, no2-, and hno2 compositions and kinetics in plasma-activated water. *Japanese Journal of Applied Physics*, 59(5):056004, 2020.

[129] Barbora Tarabová, Petr Lukeš, Malte U Hammer, Helena Jablonowski, Thomas von Woedtke, Stephan Reuter, and Zdenko Machala. Fluorescence measurements of peroxynitrite/peroxynitrous acid in cold air plasma treated aqueous solutions. *Physical Chemistry Chemical Physics*, 21(17):8883–8896, 2019.

[130] Seiji Kanazawa, Hirokazu Kawano, Satoshi Watanabe, Takashi Furuki, Shuichi Akamine, Ryuta Ichiki, Toshikazu Ohkubo, Marek Kocik, and Jerzy Mizeraczyk. Observation of oh radicals produced by pulsed discharges on the surface of a liquid. *Plasma Sources Science and Technology*, 20(3):034010, 2011.

[131] Francesco Tampieri, Maria-Pau Ginebra, and Cristina Canal. Quantification of plasma-produced hydroxyl radicals in solution and their dependence on the ph. *Analytical chemistry*, 93(8):3666–3670, 2021.

[132] Akimitsu Hatta, Kotaro Ogawa, Jun-Seok Oh, and Hiroshi Furuta. Uv absorption spectroscopy analysis on water irradiated to atmospheric pressure plasma jet. In *2018 International Electrical Engineering Congress (iEECON)*, pages 1–3, 2018.

[133] Zhijie Liu, Chunxi Zhou, Dingxin Liu, Tongtong He, Li Guo, Dehui Xu, and Michael G Kong. Quantifying the concentration and penetration depth of long-lived rons in plasma-activated water by uv absorption spectroscopy. *AIP Advances*, 9(1):015014, 2019.

[134] William A Pryor. Oxy-radicals and related species: their formation, lifetimes, and reactions. *Annual review of Physiology*, 48(1):657–667, 1986.

[135] Edward G Janzen and Barry J Blackburn. Detection and identification of short-lived free radicals by an electron spin resonance trapping technique. *Journal of the American Chemical Society*, 90(21):5909–5910, 1968.

[136] Masato Kamibayashi, Shigeru Oowada, Hiroaki Kameda, Taiichi Okada, Osamu Inanami, Shunsaku Ohta, Toshihiko Ozawa, Keisuke Makino, and Yashige Kotake. Synthesis and characterization of a practically better depmpo-type spin trap, 5-(2, 2-dimethyl-1, 3-propoxy cyclophosphoryl)-5-methyl-1-pyrroline n-oxide (cypmpo). *Free radical research*, 40(11):1166–1172, 2006.

[137] Jin-Yi Han, Jin-Tae Hong, Sang-Yoon Nam, and Ki-Wan Oh. Evaluation of hydroxyl radical reduction activity of red ginseng extract using esr spectroscopy. *Journal of Biomedical Research*, 13(1):83–92, 2012.

[138] Helena Tresp, Malte U Hammer, J Winter, KD Weltmann, and S Reuter. Quantitative detection of plasma-generated radicals in liquids by electron paramagnetic resonance spectroscopy. *Journal of Physics D: Applied Physics*, 46 (43):435401, 2013.

[139] J. Rodier. *Analysis of Water*. A Halsted Press Book. Wiley, 1975. ISBN 9780470729342. URL https://books.google.co.uk/books?id=sZURAQAAIAAJ.

[140] Gheorghe G Bălan, Irina Roşca, Elena-Laura Ursu, Florica Doroftei, Andra-Cristina Bostănaru, Eugen Hnatiuc, Valentin Năstasă, Vasile Şandru, Gabriela Ştefănescu, Anca Trifan, et al. Plasma-activated water: A new and effective alternative for duodenoscope reprocessing. *Infection and drug resistance*, 11: 727, 2018.

[141] Noala Vicensoto Moreira Milhan, William Chiappim, Aline da Graça Sampaio, Mariana Raquel da Cruz Vegian, Rodrigo Sávio Pessoa, and Cristiane Yumi Koga-Ito. Applications of plasma-activated water in dentistry: A review. *International Journal of Molecular Sciences*, 23(8):4131, 2022.

[142] PS Ganesh Subramanian, Aditi Jain, Anand M Shivapuji, Nagalingam R Sundaresan, Srinivasaiah Dasappa, and Lakshminarayana Rao. Plasma-activated water from a dielectric barrier discharge plasma source for the selective treatment of cancer cells. *Plasma Processes and Polymers*, 17(8):1900260, 2020.

[143] Isam Osman, Aravind Ponukumati, Michael Vargas, Dipesh Bhakta, Berk Ozoglu, and Charles Bailey. Plasma-activated vapor for sanitization of hands. *Plasma Medicine*, 6(3-4), 2016.

[144] Xinyu Liao, Yuan Su, Donghong Liu, Shiguo Chen, Yaqin Hu, Xingqian Ye, Jun Wang, and Tian Ding. Application of atmospheric cold plasma-activated

water (paw) ice for preservation of shrimps (metapenaeus ensis). *Food Control*, 94:307–314, 2018.

[145] Aswathi Soni, Jonghyun Choi, and Gale Brightwell. Plasma-activated water (paw) as a disinfection technology for bacterial inactivation with a focus on fruit and vegetables. *Foods*, 10(1):166, 2021.

[146] Samuel Herianto, Chih-Yao Hou, Chia-Min Lin, and Hsiu-Ling Chen. Non-thermal plasma-activated water: A comprehensive review of this new tool for enhanced food safety and quality. *Comprehensive Reviews in Food Science and Food Safety*, 20(1):583–626, 2021.

[147] Natasa Hojnik, Martina Modic, Yuan Ni, Gregor Filipic, Uros Cvelbar, and James L Walsh. Effective fungal spore inactivation with an environmentally friendly approach based on atmospheric pressure air plasma. *Environmental science & technology*, 53(4):1893–1904, 2019.

[148] Rai Naveed Arshad, Zulkurnain Abdul-Malek, Abdullah Munir, Zolkafle Buntat, Mohd Hafizi Ahmad, Yanti M.M. Jusoh, Alaa El-Din Bekhit, Ume Roobab, Muhammad Faisal Manzoor, and Rana Muhammad Aadil. Electrical systems for pulsed electric field applications in the food industry: An engineering perspective. *Trends in Food Science & Technology*, 104:1–13, 2020.

[149] Beining Cassar, Joshua R.and Ouyang, Kathiravan Krishnamurthy, and Ali" Demirci. *Microbial Decontamination of Food by Light-Based Technologies: Ultraviolet (UV) Light, Pulsed UV Light (PUV), and UV Light-Emitting Diodes (UV-LED)*, pages 493–521. Springer International Publishing, 2020.

[150] D. M. Sango, D. Abela, A. McElhatton, and V.P. Valdramidis. Assisted ultrasound applications for the production of safe foods. *Journal of Applied Microbiology*, 116(5):1067–1083, 2014.

[151] MI Hasan and JL Walsh. Influence of gas flow velocity on the transport of chemical species in an atmospheric pressure air plasma discharge. *Applied Physics Letters*, 110(13):134102, 2017.

[152] Herbert S Harned, Benton B Owen, and CV King. The physical chemistry of electrolytic solutions. *Journal of The Electrochemical Society*, 106(1):15C, 1959.

[153] NN Misra, KM Keener, P Bourke, and PJ Cullen. Generation of in-package cold plasma and efficacy assessment using methylene blue. *Plasma Chemistry and Plasma Processing*, 35(6):1043–1056, 2015.

[154] Pankaj Attri, Yong Hee Kim, Dae Hoon Park, Ji Hoon Park, Young J Hong, Han Sup Uhm, Kyoung-Nam Kim, Alexander Fridman, and Eun Ha Choi. Generation mechanism of hydroxyl radical species and its lifetime prediction during the plasma-initiated ultraviolet (uv) photolysis. *Scientific reports*, 5(1): 1–8, 2015.

[155] J Tomeková, S Kyzek, V Medvecká, E Gálová, and A Zahoranová. Influence of cold atmospheric pressure plasma on pea seeds: Dna damage of seedlings and optical diagnostics of plasma. *Plasma Chemistry and Plasma Processing*, 40(6):1571–1584, 2020.

[156] Fawei Lin, Zhihua Wang, Qiang Ma, Yong He, Ronald Whiddon, Yanqun Zhu, and Jianzhong Liu. N2o5 formation mechanism during the ozone-based low-temperature oxidation deno x process. *Energy & Fuels*, 30(6):5101–5107, 2016.

[157] Sanghoo Park, Wonho Choe, and Cheorun Jo. Interplay among ozone and nitrogen oxides in air plasmas: Rapid change in plasma chemistry. *Chemical Engineering Journal*, 352:1014–1021, 2018.

[158] Brian McEvoy and Neil J Rowan. Terminal sterilization of medical devices using vaporized hydrogen peroxide: a review of current methods and emerging opportunities. *Journal of applied microbiology*, 127(5):1403–1420, 2019.

[159] Kun Liu, Shi-ting Liu, and Cong-fu Ran. The effect of air-water-plasma-jet-activated water on penicillium: The reaction of hno2 and h2o2 under acidic condition. *Frontiers in Physics*, 8:242, 2020.

[160] Z Machala, B Tarabová, D Sersenová, M Janda, and K Hensel. Chemical and antibacterial effects of plasma activated water: Correlation with gaseous and aqueous reactive oxygen and nitrogen species, plasma sources and air flow conditions. *Journal of Physics D: Applied Physics*, 52(3):034002, 2018.

[161] Toshihiro Takamatsu, Kodai Uehara, Yota Sasaki, Hidekazu Miyahara, Yuriko Matsumura, Atsuo Iwasawa, Norihiko Ito, Takeshi Azuma, Masahiro Kohno, and Akitoshi Okino. Investigation of reactive species using various gas plasmas. *Rsc Advances*, 4(75):39901–39905, 2014.

[162] Uta Schnabel, Mathias Andrasch, Jörg Stachowiak, Christoph Weit, Thomas

Weihe, Christian Schmidt, Peter Muranyi, Oliver Schlüter, and Jörg Ehlbeck. Sanitation of fresh-cut endive lettuce by plasma processed tap water (pptw)– up-scaling to industrial level. *Innovative Food Science & Emerging Technologies*, 53:45–55, 2019.

[163] Eau de paris, 2022. URL https://www.eaudeparis.fr/.

[164] Hvor kommer vannet fra?, May 2018. URL https://www.ivar.no/vannkilder/.

[165] Water resources in palestine, Apr 2021. URL https://water.fanack.com/palestine/water-resources/.

[166] United utilities, 2021. URL https://www.unitedutilities.com/help-and-support/your-water-supply/your-water/water-quality//water-quality-search-results/?postcodeField=L69%2B3GJ.

[167] Mark W. LeChevallier and Kwok-Keung Au. *Water treatment and pathogen control process efficiency in achieving safe drinking-water.* Published on behalf of the World Health Organization by IWA Pub., 2004.

[168] WHO. Chlorine in Drinking-water Background document for development of WHO Guidelines for Drinking-water Quality. Technical report, World Health Organisation, 2003.

[169] WHO. *Guidelines for drinking-water quality, 3rd edition: Volume 1.* WHO, 2008. ISBN 978 92 4 154761 1. URL https://www.who.int/water_sanitation_health/publications/gdwq3rev/en/.

[170] Yi-Ming Zhao, Apurva Patange, Da-Wen Sun, and Brijesh Tiwari. Plasma-activated water: Physicochemical properties, microbial inactivation mechanisms, factors influencing antimicrobial effectiveness, and applications in the food industry. *Comprehensive reviews in food science and food safety*, 19(6): 3951–3979, 2020.

[171] Simon Maheux, David Duday, Thierry Belmonte, Christian Penny, Henry-Michel Cauchie, Franck Clément, and Patrick Choquet. Formation of ammonium in saline solution treated by nanosecond pulsed cold atmospheric microplasma: a route to fast inactivation of e. coli bacteria. *RSC Advances*, 5 (52):42135–42140, 2015.

[172] Renwu Zhou, Rusen Zhou, Peiyu Wang, Yubin Xian, Anne Mai-Prochnow, Xinpei Lu, PJ Cullen, Kostya Ken Ostrikov, and Kateryna Bazaka. Plasma-activated water: Generation, origin of reactive species and biological applications. *Journal of Physics D: Applied Physics*, 53(30):303001, 2020.

[173] John H. Seinfeld and Spyros N. Pandis. *Atmospheric Chemistry and Physics: From Air Pollution to Climate Change, 3rd Edition*. Wiley, 3rd editio edition, 2016. ISBN 978-1-118-94740-1. URL https://www.wiley.com/en-gb/Atmospheric+Chemistry+and+Physics%3A+From+Air+Pollution+to+Climate+Change%2C+3rd+Edition-p-9781118947401.

[174] Matthew J Traylor, Matthew J Pavlovich, Sharmin Karim, Pritha Hait, Yukinori Sakiyama, Douglas S Clark, and David B Graves. Long-term antibacterial

efficacy of air plasma-activated water. *Journal of Physics D: Applied Physics*, 44(47):472001, 2011.

[175] Edward T Urbansky and Michael R Schock. Understanding, deriving, and computing buffer capacity. *Journal of chemical education*, 77(12):1640, 2000.

[176] Daniela Boehm, James Curtin, Patrick J Cullen, and Paula Bourke. Hydrogen peroxide and beyond-the potential of high-voltage plasma-activated liquids against cancerous cells. *Anti-Cancer Agents in Medicinal Chemistry (Formerly Current Medicinal Chemistry-Anti-Cancer Agents)*, 18(6):815–823, 2018.

[177] Jan Voráč, Petr Synek, Pavel Dvořák, and Tomáš Hoder. Time-and space-resolved lif measurement of the concentration of oh radicals generated by surface barrier discharge emerging from liquid water. *Plasma Sources Science and Technology*, 28(10):105008, 2019.

[178] Ghazaleh Haghighat, Amirreza Sohrabi, Parmiss Mojir Shaibani, CW Van Neste, Selvaraj Naicker, and Thomas Thundat. The role of chloride ions in plasma-activated water treatment processes. *Environmental Science: Water Research & Technology*, 3(1):156–168, 2017.

[179] Y-M Zhao, S Ojha, CM Burgess, D-W Sun, and BK Tiwari. Inactivation efficacy and mechanisms of plasma activated water on bacteria in planktonic state. *Journal of Applied Microbiology*, 129(5):1248–1260, 2020.

[180] Yi-Ming Zhao, Shikha Ojha, Catherine M Burgess, Da-Wen Sun, and Brijesh K Tiwari. Inactivation efficacy of plasma-activated water: influence of plasma

treatment time, exposure time and bacterial species. *International Journal of Food Science & Technology*, 56(2):721–732, 2021.

[181] M. Reader-Harris. *Orifice Plates and Venturi Tubes*. Experimental Fluid Mechanics. Springer International Publishing, 2015. ISBN 9783319168807. URL https://books.google.co.uk/books?id=d-rxCAAAQBAJ.

[182] Jean-Pierre Franc and Jean-Marie Michel. *Fundamentals of cavitation*, volume 76. Springer science & Business media, 2006.

[183] Seyed Mehdi Ashrafizadeh and Hojat Ghassemi. Experimental and numerical investigation on the performance of small-sized cavitating venturis. *Flow measurement and Instrumentation*, 42:6–15, 2015.

[184] JX Zhang. Analysis on the effect of venturi tube structural parameters on fluid flow. *AIP Advances*, 7(6):065315, 2017.

[185] Hongbo Shi, Mingda Li, Petr Nikrityuk, and Qingxia Liu. Experimental and numerical study of cavitation flows in venturi tubes: From cfd to an empirical model. *Chemical Engineering Science*, 207:672–687, 2019.

[186] Yawen Gao, Mingbo Li, Chao Sun, and Xuehua Zhang. Microbubble-enhanced water activation by cold plasma. *Chemical Engineering Journal*, 446:137318, 2022.

[187] G Neretti, M Taglioli, G Colonna, and CA Borghi. Characterization of a dielectric barrier discharge in contact with liquid and producing a plasma activated water. *Plasma Sources Science and Technology*, 26(1):015013, 2016.

[188] R Laurita, D Barbieri, M Gherardi, V Colombo, and P Lukes. Chemical analysis of reactive species and antimicrobial activity of water treated by nanosecond pulsed dbd air plasma. *Clinical Plasma Medicine*, 3(2):53–61, 2015.

[189] Renwu Zhou, Rusen Zhou, Karthika Prasad, Zhi Fang, Robert Speight, Kateryna Bazaka, and Kostya Ken Ostrikov. Cold atmospheric plasma activated water as a prospective disinfectant: The crucial role of peroxynitrite. *Green Chemistry*, 20(23):5276–5284, 2018.

[190] Barbora Tarabová, Petr Lukeš, Malte U Hammer, Helena Jablonowski, Thomas von Woedtke, Stephan Reuter, and Zdenko Machala. Fluorescence measurements of peroxynitrite/peroxynitrous acid in cold air plasma treated aqueous solutions. *Physical Chemistry Chemical Physics*, 21(17):8883–8896, 2019.

[191] Rohit Thirumdas, Anjinelyulu Kothakota, Uday Annapure, Kaliramesh Siliveru, Renald Blundell, Ruben Gatt, and Vasilis P Valdramidis. Plasma activated water (paw): Chemistry, physico-chemical properties, applications in food and agriculture. *Trends in food science & technology*, 77:21–31, 2018.

[192] Satoshi Ihara, Hiroki Nishiyama, Takashi Matsunaga, Yuuki Yoshida, Yuka Tokuyama, and Hiroaki Terato. Improving the efficiency of a water-treatment system based on water cavitation and plasma using a nozzle-less reactor. *AIP Advances*, 9(4):045005, 2019.

[193] Jan Čech, Pavel St'ahel, Jozef Ráhel', Lubomír Prokeš, Pavel Rudolf, Eliška Maršálková, and Blahoslav Maršálek. Mass production of plasma activated

water: case studies of its biocidal effect on algae and cyanobacteria. *Water*, 12 (11):3167, 2020.

[194] Yawen Gao, Keziah Francis, and Xuehua Zhang. Review on formation of cold plasma activated water (paw) and the applications in food and agriculture. *Food Research International*, page 111246, 2022.

[195] MI Hasan and JL Walsh. Numerical investigation of the spatiotemporal distribution of chemical species in an atmospheric surface barrier-discharge. *Journal of Applied Physics*, 119(20):203302, 2016.